INTERPRETATION OF EFFECTS OF DRIVEN PILE INSTALLATION IN BAY MUD

by

Chung Yee Kwok

B. Eng. Civil and Structural Engineering
The University of Sheffield, 2001

SUBMITTED TO THE DEPARTMENT OF CIVIL AND ENVIRONMENTAL ENGINEERING IN PARTIAL FULFILLMENT OF THE REQUIREMENTS FOR THE DEGREE OF

MASTER OF ENGINEERING IN CIVIL AND ENVIRONMENTAL ENGINEERING
AT THE
MASSACHUSETTS INSTITUTE OF TECHNOLOGY

JUNE 2002

© 2002, Chung Yee Kwok. All rights reserved.

The author hereby grants to MIT permission to reproduce and to distribute publicly paper and electronic copies of this thesis document in whole or in part.

Signature of Author:_____
Chung Yee Kwok
Department of Civil and Environmental Engineering
May 28, 2002

Certified by:_____
Andrew J. Whittle
Professor of Civil and Environmental Engineering
Thesis Supervisor

Accepted by:_____
Oral Buyukozturk
Chairman, Departmental Committee on Graduate Students

MASSACHUSETTS INSTITUTE OF TECHNOLOGY
JUN 3 2002
LIBRARIES

BARKER

INTERPRETATION OF EFFECTS OF DRIVEN PILE INSTALLATION IN BAY MUD

by

Chung Yee Kwok

Submitted to the Department of Civil and Environmental Engineering on May 28, 2002
in partial fulfillment of the requirements for the degree of
Master of Engineering in Civil and Environmental Engineering

ABSTRACT

The process of pile driving causes large changes in stresses and properties within the surrounding soil. Field measurements of radial displacements, pore pressures and shear wave velocities have recently been presented by Hunt (Ph.D., UC. Berkeley, 2000) at selected locations around the shaft of a full scale, 61cm diameter, 35m long closed-ended pile driven in San Francisco Bay Mud. Hunt reports these data immediately after pile installation and at selected time intervals throughout the consolidation phase (lasting approximately 250 days) when installation-induced excess pore pressures dissipate. Further changes in shear wave velocity were recorded up to 2 years after pile installation.

This thesis presents predictions of clay behavior due to pile driving using a package of analysis methods develop previously at MIT. These simulations are based on Strain Path analyses of undrained pile installation, MIT-E3 modeling of clay behavior and non-linear finite element analyses of radial consolidation around the pile shaft. Site specific model input parameters were selected from laboratory tests presented by Hunt (and other available sources) and assume normalized properties for the Bay Mud. Predictions of pore pressure dissipation are in very good agreement with measured data for piezometers installed at three depths and at radial locations, r/R = 3-5. Discrepancies between predicted and measured data for devices at r/R = 7-8 may reflect limitations in predictions of the initial field of installation-induced excess pore pressures. The analyses also predict quite well the radial displacements that occur both during installation (outward – cavity expansion) and consolidation (inward – radial return). However, neither the current analyses nor previous cavity expansion models is able to explain the large net increase in shear wave velocity in the clay reported by Hunt.

Thesis Supervisor: Andrew J. Whittle

Title: Professor of Civil and Environmental Engineering

ACKNOWLEDGEMENTS

There area so many people whom I would like to thank. The M.Eng. program is such a challenging program and would be impossible without the support, assistance and understanding of others.

First of all, I would like to thank my supervisor, Prof. Andrew Whittle: Thank you for your time, effort and help you put into my thesis. Especially I would like to thank you for helping me to select the MIT-E3 parameters. Thank you so much.

Thank you Prof. Jerome Connor: for being my academic advisor and giving me lots of invaluable advises. Thank you Dr. Eric Adams: for putting the M.Eng program, for all your assistance, care and leadership. Thanks to all the other staff in the CEE department: Without anyone of you, this year would not be made possible.

Thank you, the M. Eng. Class of 2002: We had a tough year but we made it thorough together. My fellow Geotect, Charisis and Aw: Thanks for always being willing to answer my questions.

Finally, I would like to thank my parents: Mama and Papa: Thanks for your endless support, love, care and encouragement in the past 22 years, especially during my time at MIT. Thank you for supporting me for finishing my goals and dreams.

TABLE OF CONTENTS

1 INTRODUCTION 1

1.1 Background and Problem Statement 1

1.2 Current Solutions and Existed Studies 2

1.3 Research Objectives and Scope 3

1.4 Research Approach 3

1.5 Thesis Organization 4

2 ANALYSIS OF EFFECTS OF PILE INSTALLATION 5

2.1 Strain Path Method 5

2.1.1 Fundamental concepts 5

2.1.2 Theoretical Description 8

2.2 MIT-E3 Model (Whittle et al.) 12

2.3 Finite Element Model 16

2.4 Cavity Expansion Method 17

2.4.1 Fundamental concepts 17

2.4.2 Theoretical Description 19

2.5 Comparison of CEM and SPM 21

3 FIELD PERFORMANCE OF A PILE INSTALLED IN BAY MUD 23

3.1 Field Work 23

3.1.1 Site 24

3.1.2 Geology 26

3.1.3 Subsurface conditions 26

3.1.4 Soil Boring 27

3.1.5 Instrumentation 29

3.1.6 Pore Pressure 30

3.1.7 Lateral Deformations 34

3.1.8 Shear Wave Velocities 38

3.2 Laboratory Work 40

3.2.1 Index properties 40

3.2.2 Constant rate of strain consolidation testing 41
3.2.3 Triaxial radial consolidation testing 43
3.2.4 Triaxial strength testing 45
3.2.5 Direct simple shear 48
4 PREDICTION OF PILE BEHAVIOR IN BAY MUD 50
4.1 Background 50
4.2 Selection of MIT-E3 Model Parameters 52
4.3 MIT-E3 model predictions 55
4.4 Hydraulic Conductivity 59
4.5 Predictions of Pile Performance 61
4.5.1 Predictions of Pile Installation 61
4.5.2 Prediction of Set-Up 62
4.5.3 Stress changes during installation and consolidation 64
4.5.4 Strain and return deflection after consolidation 68
4.5.5 Prediction of consolidation at different distance to the pile 72
5 INTERPRETATIONS OF HUNTS DATA 74
5.1 Comparison of pore water pressure 74
5.2 Comparison of dissipation of excess pore pressure 75
5.3 Comparison of Return Deflection 78
5.4 Comparison of Shear Wave Velocity 79
5.5 Comparison of Strain Path Method Predictions with Cavity Expansion Method 80
6 SUMMARY CONCLUSIONS AND RECOMMENDATIONS 89
7 REFERENCES 92

TABLE OF FIGURES

Figure 2-1 Shear strain of a closed ended pile during pile installation.....7

Figure 2-2 Grid deformation due to simple pile penetration with Strain Path Method (Baligh, 1985).....9

Figure 2-3 Application of Strain Path Method to deep penetration in clays.....11

Figure 2-4 Expansion of a cavity.....18

Figure 2-5 Cylindrical cavity expansion schematic.....20

Figure 2-6 Grid deformation due to cylindrical cavity expansion.....21

Figure 3-1 Site Location – corner of Evans Ave. & Selby Street, San Francisco, CA.....24

Figure 3-2 Map of the site at Islais Creek.....25

Figure 3-3 Generalized soil profile (from CALTRANS and DFI, 1993).....27

Figure 3-4 Borehole layout relative to pile location (Hunt 2000).....28

Figure 3-5 Summary of cone penetration testing (Hunt 2000).....28

Figure 3-6 Pore pressure measurements 2 hours after pile installation.....31

Figure 3-7 Summary of pore pressure program.....32

Figure 3-8 Dissipation of excess pore pressure.....33

Figure 3-9 Plan view of boreholes relative to radial path from pile.....35

Figure 3-10 Initial deflections after pile installation.....36

Figure 3-11 Time history of radial deflection induced by consolidation.....37

Figure 3-12 Change in shear-wave velocity profile as a function of time.....39

Figure 3-13 Summary of index tests results (Hunt et al 2000).....41

Figure 3-14 Constant rate of strain consolidation test on pre-pile specimens.....42

Figure 3-15 Constant rate of strain consolidation test on post-pile specimens.....42

Figure 3-16 Results form triaxial radial isotropic consolidation tests.....44

Figure 3-17 Stress-strain curves, pore pressure generation and stress paths for anisotropically consolidated triaxial tests to pre-pile in situ stress..... 46

Figure 3-18 Stress-strain curves, pore pressure generation and stress paths for anisotropically consolidated triaxial tests to three times pre-pile in situ stress (SHANSEP type)..... 47

Figure 3-19 Shear stress-strain curves and pore pressure generated during monotonic direct simple tests.....49

Figure 4-1 Flow chart of the proposed analysis.....51

Figure 4-2 MIT-E3 model prediction of stress path for CK_0UC test on normally consolidated Buy Mud.....55

Figure 4-3 MIT-E3 model prediction of normalized deviatoric stress versus axial strain for CK_0UC test on normally consolidated Buy Mud 56

Figure 4-4 MIT-E3 model prediction1 of normalized deviatoric stress versus axial strain for CK_0UC test on normally consolidated Buy Mud.....56

Figure 4-5 Predicted Shear Stress versus shear strain.....57

Figure 4-6 Predicted pore pressure versus shear strain.....58

Figure 4-7 Predicted dissipation of pore pressure.....59

Figure 4-8 SCPTU-2 Dissipation tests.....60

Figure 4-9 SPM computed stress after pile installation.....62

Figure 4-10 SPM computed stress after consolidation.....63

Figure 4-11 Effective radial stresses during post-pile consolidation.....64

Figure 4-12 Effective tangential stresses during post-pile consolidation.....65

Figure 4-13 Effective vertical stresses during post-pile consolidation.....65

Figure 4-14 Change of stresses and pore pressure during consolidation.....66

Figure 4-15 Change of soil behavior and pore pressure during consolidation.....67

Figure 4-16 SPM radial strain after pile installation for R = 30.5cm.....68

Figure 4-17 SPM radial displacement after pile installation for R = 30.5cm.....69

Figure 4-18 State of strain at the end of consolidation.....70

Figure 4-19 Consolidation return deflection at depth 12.8m.....71

Figure 4-20 Predicted percent of normalized excess pore pressure versus time factor for boreholes B-1 to B-5.....72

Figure 4-21 Predicted normalized excess pore pressure versus time factor for boreholes B-1 to B5.....73

Figure 4-22 Predicted normalized effective radial stress versus time factor for boreholes B-1 to B-5.....73

Figure 5-1 Comparison of predicted and measured excess pore water pressure after pile installation.....74

Figure 5-2 Percent of excess pore pressure dissipated for depth 8.5m.....76

Figure 5-3 Percent of excess pore pressure dissipated for depth 12.8m.....76

Figure 5-4 Percent of excess pore pressure dissipated for depth 23.8m.....77

Figure 5-5 Consolidation return deflection around the pile shaft.....78

Figure 5-6 Distribution of excess pore pressures around pile shafts.....81

Figure 5-7 SPM computed stresses after pile installation.....83

Figure 5-8 CEM computed stresses after pile installation.....83

Figure 5-9 Changes in horizontal effective stress during consolidation at pile shaft.....85

Figure 5-10 SPM computed stresses after consolidation.....87

Figure 5-11 CEM computed stresses after consolidation 87

Figure 5-12 Radial displacements from pile installation and subsequent consolidation...88

TABLE OF TABLES

Table 2-1 Summary of input parameters with the corresponding physical contribution for MIT-E3 soil model.....14

Table 2-2 Summary of input parameters for MIT-E3 categorized into two groups.....15

Table 4-1 MIT-E3 parameters..... 54

1 INTRODUCTION

1.1 BACKGROUND AND PROBLEM STATEMENT

Pile driving in saturated low permeability clay is an undrained phenomenon. The process of pile driving is an inherent destructive process. Large changes in total stress are imposed on the soil and excess pore pressures are generated as the clay is pushed around the pile tip and expanded outwards. During pile installation, the soil around the pile undergoes large plastic shear deformations and remolding with corresponding reduction in the effective soil shear strength and initial pile shaft capacity. After the completion of pile driving, soil reconsolidation occurs in cohesive soils, manifested by the dissipation of excess pore pressure at the soil-pile interface zone and is usually accompanied by an increase effective stress levels and shaft capacity (pile set-up).

The performance of driven pile foundations is actually dependent on these processes and hence, reliable predictions of capacity must account for changes in soil stresses and properties caused by the installation process. Much prior research work has been carried out for offshore foundations where pile set-up can play a critical role in scheduling the installation of the superstructure (most significant for tension leg platforms). Much less work has been carried out for onshore applications. Hence, this thesis will investigate the effect of driven pile installation on onshore land.

1.2 CURRENT SOLUTIONS AND EXISTED STUDIES

A large research effort over the last 50 years has been put at quantification of the effects of pile installation on the properties of soft cohesive soils. Most of this work was motivated primarily by the need to predict axial pile capacity and shaft capacity for offshore platforms (e.g. Whittle et al. 1992) and major bridges under monotonic and cyclic loading (e.g., O'Neill 2001). As a result, extensive field and laboratory instrumentation of model or full-scale piles have focused on the characterization of ''quasi-static'' stress–strain–strength relationships of the soil surrounding the pile as a function of time after pile installation. Although most of the research has concentrated on

shear strength characteristics and their relation to pore pressure generation and dissipation (e.g., Roy et al. 1981; Bond and Jardine 1991), other researchers have measured lateral and vertical deformation (e.g., Cooke and Price 1973; Randolph et al. 1979), compressibility (e.g., Airhart et al. 1969; Bozozuk et al. 1978), surface heave (e.g., Hagerty and Peck 1971; Bozozuk et al. 1978) and load transfer (e.g., Reese and Seed 1955).

Numerous field and laboratory research projects have examined loading conditions, total soil stresses, and excess pore pressures during and following pile installation. Recently, a large number of seismic retrofitting projects for bridges in California have revealed the need for well-documented field tests evaluating the effect of pile installation on the static and dynamic properties of soft clays. For example, Hunt (2000) presents results of field measurements of pore pressures and soil properties around a single 3.05m diameter pile driven 36.6m into a relatively uniform deposit of San Francisco Bay Mud.

With respect to the methodology that required predicting the effect of pile installation, Cylindrical Expansion Method (CEM) has been first developed by Randolph in (1979) to investigate the deformation pattern around closed- and open-ended piles jacked into clay. Later another more sophisticated method called Strain Path Method (SPM), which is similar to CEM, was developed by Baligh (1985). Hence, by applying the data provided by Hunts into the CEM and SPM, the effect of pile installation can be investigated in a simple way.

1.3 RESEARCH OBJECTIVES AND SCOPE

A large body of research has been performed by MIT to analyze the effective stress for predicting the performance of driven piles in clays. This work has included the development of the Strain Path Method (SPM) which describes the mechanics of the pile installation process and the effective stress soil models (MIT-E3) which can describe realistically the constitutive behavior of K_0-consolidated clays. The SPM has been evaluated through comparisons with field measurements from the Piezo-Lateral Stress (PSLS) cell and instrumented model piles (Whittle & Baligh, 1988).

This thesis will use those recent theoretical methods developed at MIT to re-interpret well documented test data on the effects of driven pile installation in San Francisco Bay Mud. All data are based on Hunt's thesis. The predictions will be compared versus the measured field results to show the suitability of the numerical framework developed by MIT.

This thesis mainly focuses on closed-ended piles. Apart from being more fully understand the changes occurring in the soil around a large diameter closed-ended steel pile, the main goal is to assess the applicability of the approach in order to help foundation design. As due to the changes of soil properties during installation, a typical pile foundation design which is based on soil properties determined in the field before driving of piles may not be as accurate as we believe. Therefore, a more rational approach for pile foundation design should be developed. The ultimate goal is for future use to extrapolate local findings to other sites.

1.4 RESEARCH APPROACH

There are two basic approaches that can be taken in studying the influence of pile installation on the properties of the foundation soil.

1) Experimental measurements - to study/observe directly the physical processes, (in the field or in the lab), by collecting data and monitoring different phenomena occurring in the soil and on the pile. Pore pressure, lateral deformations and shear wave velocities have been measured. These measurements are essential in the calibration and validation of analytical techniques to predict changes in properties of the foundation soil.
2) Numerical simulations that attempt to reproduce or predict the experimental measurements. Theoretical frameworks offer the potential for predicting or extrapolating performance to other sites, soil properties etc.

This thesis considers both approaches. The thesis summarizes in-situ measurements around a closed–ended pile installed in San Francisco Bay Mud. (Hunt et al., 2000). The measurements included pore pressure, lateral deformation and shear wave velocities. With the comparison of the real data, reliability of the proposed analysis can be accessed. Laboratory testing performed by Hunt (2000) included the constant rate of strain (radial and vertical) consolidation tests and undrained triaxial compression shear tests. These data enable direct calibration of advanced soil models, such as MIT-E3 (Whittle et al., 1993) that can be used to predict pile performance.

Numerical simulations using the Strain Path Method (Baligh) in combination with the MIT-E3 soil model (Whittle) and non-linear finite element methods (Whittle) enable predictions of stresses and pore pressures caused by pile installation in San Francisco Bay Mud.

1.5 THESIS ORGANIZATION

The next chapter of this thesis will introduce the framework of the proposed analysis which includes the strain path method, MIT-E3 soil model and the finite element. One-dimensional Cavity expansion methods which were introduced to predict pile capacity by Randopll et .al (1997) will also be compared with two-dimensional SPPM prediction.

Since one of the main purpose of this thesis is to re-interpretate the effect of pile installation presented by Hunt (2000). A description of his work will be included in Chapter 3.

The new analysis proposed will be illustrated in Chapter 4. A flow chart clearly shows the sequence of works and the methods used. Results obtained from the proposed analysis will be shown. Some typical changes of pile behavior during the installation and set-up will be discussed.

Chapter 5 compares and evaluates the theoretical predictions with field measurements made by Hunt (2000).

2 ANALYSIS OF EFFECTS OF PILE INSTALLATION

In order to analyze the effect of pile installation, pile installation modeling is required to collaborate into numerical tools to generate predictions of stresses and deformations caused by pile installation. The most widely used methods are the Cavity Expansion Methods (CEM) and the Strain Path Method (SPM). This chapter presents a review of these two methods and a comparison between the two. In addition, since the stress-strain relationship of soil changes during pile installation and post-pile installation, a more advanced soil model, MIT-E3, is required to describe the complex change of the relationship. Therefore, with the use of the finite element program to adapt the pile installation modeling and the soil model, an analysis of effects of pile installation can be performed.

2.1 STRAIN PATH METHOD

2.1.1 Fundamental concepts

The Strain Path Method (SPM) is an approximate analytical framework for describing the mechanics of quasi-static, steady undrained deep penetration in saturated clay. Strictly speaking, the method consists of an approximate analytic technique to predict soil disturbances caused by installation of foundation elements at depth in the ground. Baligh (1985) introduced the Strain Path Method (SPM) as a framework for predicting ground movements caused by installation of piles in low permeability clays. SPM simulates soil disturbance effects associated with pile installation.

However, since soil disturbances are often of paramount importance, their estimates represent the first step in understanding, formulating and predicting the behavior of deep foundations. The geotechnical designer can utilize the method to identify problem areas, focus on important issues and ultimately make more realistic and informed predictions of deep foundation performance.

SPM assumes that

1. There is no migration of pore water during penetration and hence the soil is sheared in an undrained mode.
2. Pile driving can be modeled as a steady, deep penetration problem.
3. The deformations and strains can be estimated from the steady, irrotational flow of an incompressible, inviscid fluid around the pile. (Baligh 1980)

Due to the complexity of the problem, the analysis assumes that due to the severe kinematic constraints in deep penetration problems, strains and deformations in the soil are essentially independent of its shearing resistance. Strains and deformations can then be estimated, with reasonable accuracy, based only on kinemtatic considerations and boundary conditions. This means that these problems are essentially strain-controlled and implies that, even if relatively isotropy soil properties are utilized to estimate deformations and strains caused by penetration the errors introduced are expected to be reasonably small. The key assumption of the predictive analyses is that the capacity of driven, friction piles is controlled by changes in the effective stresses and soil properties that occur during successive phases in the life of pile.

Approximate stresses and pore pressures can then be computed by utilizing realistic soil behavior responses and by satisfying equilibrium conditions. Exact stresses and pore pressures would be obtained of and only if the estimated soil deformations were identical to those experienced in the actual problem. The latter depend on soil behavior and cannot be exactly known a priori.

Strain path analysis has been presented for closed and open-ended piles sampling tube: cone penetrometers and flat plate penetrometers such as the dilatometer and field vane. Following Baligh the shear strains caused by axisymmetric penetrometers can be conveniently characterized by 3 components $E_1 = \varepsilon_{zz}$, $E_2 = \frac{1}{\sqrt{3(\varepsilon_{rr} - \varepsilon_{\theta\theta})}}$ and

$E_3 = \frac{2}{\sqrt{3\varepsilon_{rz}}}$ which correspond to triaxial, presuremeter and direct simple shear modes respectively. Each of these components contributes equally to the overall magnitude of the shear strain described by the octahedral shear strain, $E = \frac{1}{\sqrt{2}}(\sqrt{E_1^2 + E_2^2 + E_3^2})$.

Figure 2-1 shows the contour of octahedral shear strain for a closed-ended pile of radius R with a rounded tip geometry (simple pile).

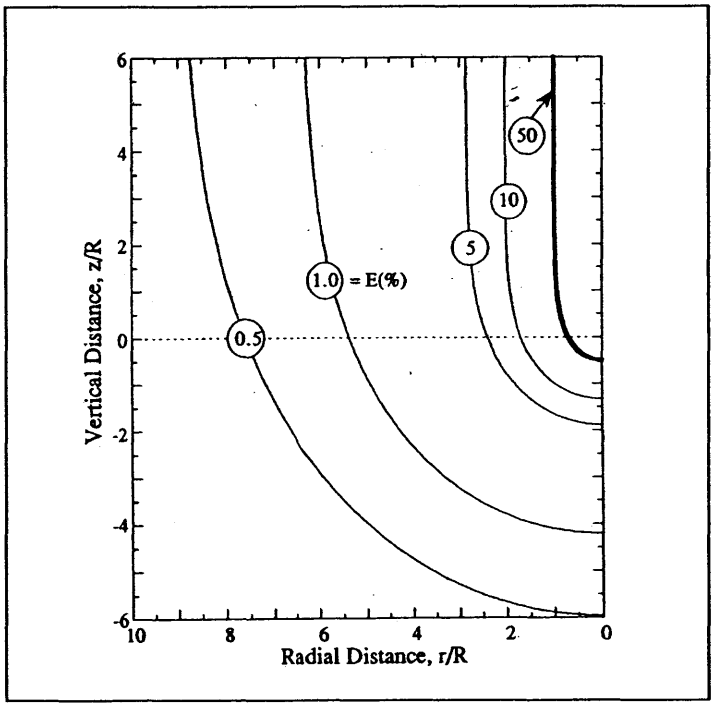

Figure 2-1 Shear strain of a closed ended pile during pile installation

Considering undrained shearing of the clay and neglecting viscoelastic effects, a steady mode of penetration can be assumed without loss of generality. Assuming that inertial effects can be neglected, the process of penetration is reduced to a flow problem where soil particles move along streamline around a fixed rigid body. A solution therefore consists of obtaining the deformations, strain, stresses and pore pressures at various soil elements along different streamlines.

The far field behavior is controlled by the volume of soil displaced during penetration. Closer to the shaft the strain distribution is closely related to the pile geometry. For a closed-ended pile there is an inner zone of soil which experienced much larger shear strain levels than can be imposed in conventional laboratory shear tests. The difference in near field strains can be linked to subsequent calculations of stresses during set-up.

The installation excess pore pressures around the pile shaft are computed from the effective stresses by satisfying conditions of radial equilibrium (Baligh, 1986). Further predictions of excess pore pressure distributions around the tip of the pile are difficult to achieve due to approximations used in the Strain Path Method.

2.1.2 Theoretical Description

Development of the simple pile equations of SPM begins with the equation for the radius of the cavity created by the spherical source at a time *t*:

$$R(t)=\left(\frac{3}{4\pi}\cdot V\cdot t\right)^{1/3}$$

where V is the volume rate of discharge from the source per unit time. In a cylindrical coordinate system, as shown on figure 2-2 (where θ, the rotation coordinate about the centerline, is not shown due to axisymmetry) the velocity components of any point of radius ρ are given by:

$$v_r^0=\frac{V}{4\pi}\cdot\frac{\sin\phi}{\rho^2} \quad \text{and} \quad v_z^0=\frac{V}{4\pi}\cdot\frac{\cos\phi}{\rho^2}\theta$$

$$\rho^2=r^2+z^2 \quad r=\rho\sin\phi \quad z=\rho\cos\phi \quad \phi=\arctan(r/z)$$

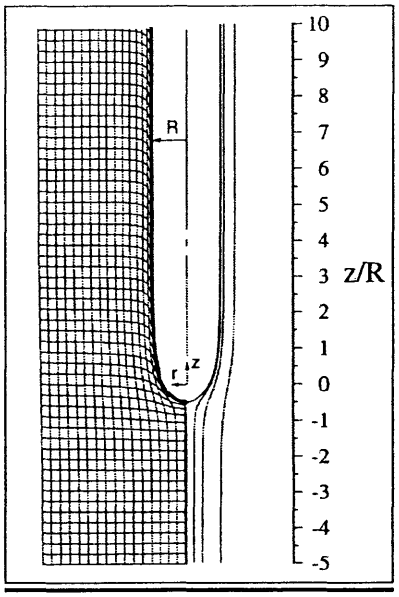

Figure 2-2 Grid deformation due to simple pile penetration with Strain Path Method (Baligh, 1985)

Advancement from this cavity expansion approach to that of the SPM simple pile is obtained by adding the uniform flow field of velocity U in the positive z direction. Velocities for the spherical source were indicated in equations below with a superscript "0". Velocities for the simple pile solution are shown below:

$$v_r = v_r^0 = \frac{V}{4\pi} \cdot \frac{\sin\phi}{\rho^2} \quad \text{and} \quad v_z = v_z^0 + U = \frac{V}{4\pi} \cdot \frac{\cos\phi}{\rho^2}\theta + U$$

In order to achieve a final radius R for the pile, V and U must be related according to the following equation:

$$R = \left(\frac{V}{\pi \cdot U} \right)^{1/2}$$

which leads to an essentially vertical shaft above $4R$ behind the pile tip located at $r = 0$ and $z = -R/2$. Once the velocities are defined the deformations can be obtained through numerical integration over time.

Derivatives of the velocity equations can be used to determine the four non-zero strain rate components (three normal and one shearing) of SPM as follows:

$$\dot{\varepsilon}_{rr} = -\frac{dv_r}{dr} = -\frac{UR^2}{4\rho^3}\cdot\left(\cos^2\phi - 2\sin^2\phi\right)$$

$$\dot{\varepsilon}_{zz} = -\frac{dv_z}{dz} = -\frac{UR^2}{4\rho^3}\cdot\left(\sin^2\phi - 2\cos^2\phi\right)$$

$$\dot{\varepsilon}_{\theta\theta} = -\frac{v_z}{r} = -\frac{UR^2}{4\rho^3}$$

$$\dot{\varepsilon}_{rz} = -\frac{1}{2}\left(\frac{dv_r}{dz} + \frac{dv_z}{dr}\right) = -\frac{UR^2}{4\rho^3}\cdot\left(-\frac{3}{2}\sin 2\phi\right)$$

These four strain rates can then be time integrated to obtain the strain field. Application of a suitable constitutive model allows the determination of stresses from the incremental strains. The assumption of an idealized deformation field (developed independently from the actual constitutive relationships of the soil) also implies that the resulting stresses do not fully satisfy the equilibrium conditions.

$$\frac{\partial \sigma_{ij}}{\partial x_j} = 0$$

Figure 2-3 describes the necessary steps to obtain solutions by means of the Strain Path Method.

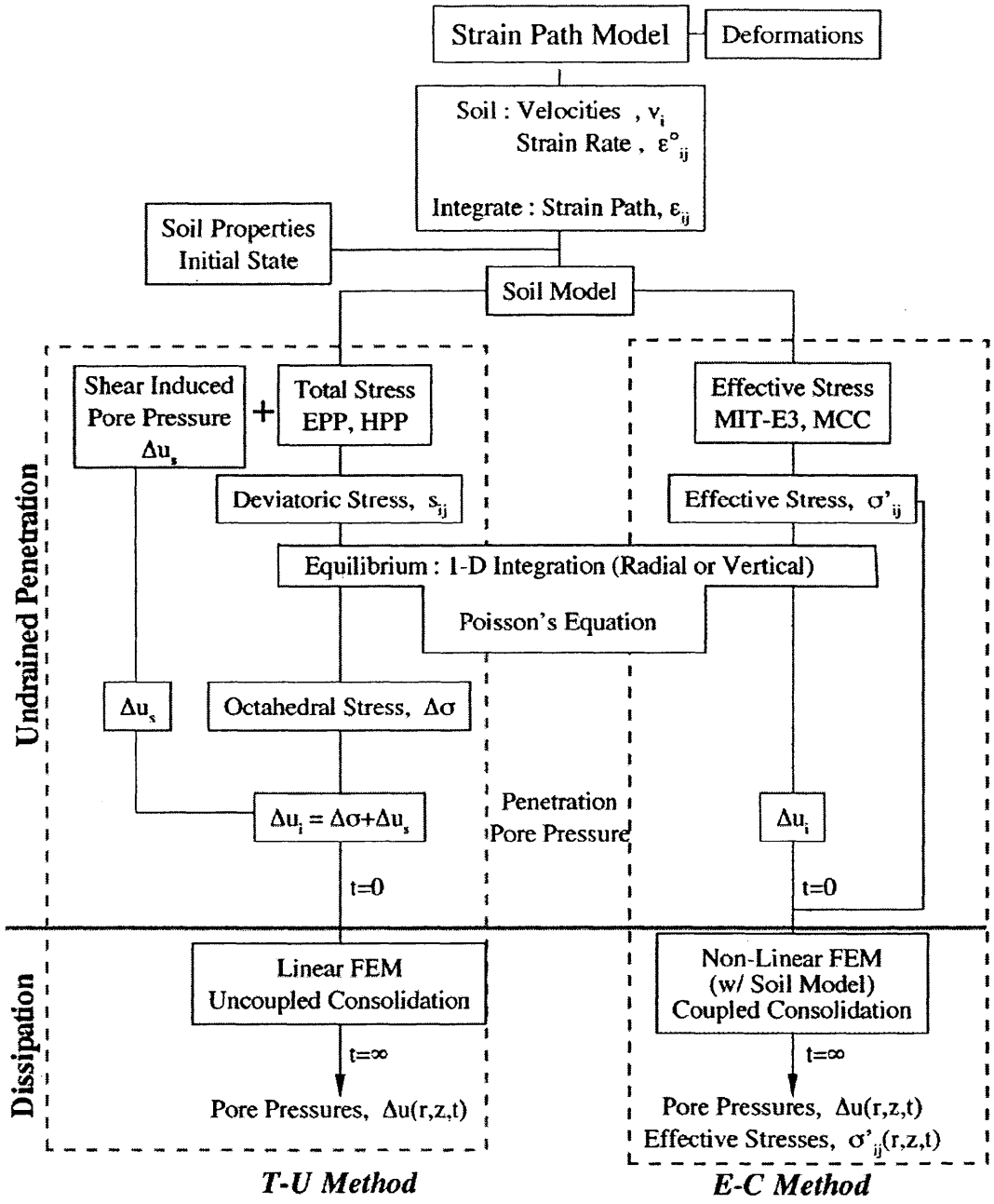

Figure 2-3 Application of Strain Path Method to deep penetration in clays

This thesis presents results of SPM predictions where stresses are solved by one-dimensional radial integration around the pile shaft. This gives a very good approximation for all points in the soil far above the pile tip.

2.2 MIT-E3 MODEL (Whittle et al.)

This soil model is used in conjunction with strain path method to estimate conditions during penetration. It is a constitutive soil model which describes the effective stress-strain behavior of normally and lightly overconsolidated clays (OCR=<4) through successive phases in the life of the pile.

MIT-E3 was originally developed to improve predictions of set-up. The MIT-E3 model describes a number of important aspects of soil behavior which have between observed in laboratory test on Ko-consolidation clays including

1) Small strain non-linearity following a reversal of load direction
2) Hysteretic behavior during unload-reload cycles of loading
3) Anisotropic stress-strain-strength properties associates with 1-D consolidation history and subsequent straining
4) Post-peck, strain softening in undrained shear tests in certain modes of shearing on normally and lightly overconsolidated clays
5) Occurrence of irrecoverable plastic strains during cyclic loading and shearing of overconsolidated clays.

The model formulation comprises 3 components

1) An elasto-plastic model for normally consolidated clays which describes anisotropic properties and strain softening behavior
2) Equations for the small strain non-linearity and hysteretic stress-strain response in unload-reload cycles
3) Bounding surface plasticity for irrecoverable, anisotropic and path dependent behavior of overconsolidated clays.

The model also has a number of limitations

1) it uses a rate dependent property of the soil skeleton and hence cannot model creep, relaxation or other strain rate dependent properties of the soil skeleton

2) it assumes normalized soil properties (eg. The strength and stiffness are proportional to the confining pressure at a given overconsolidation ratio OCR) and hence does not describe complex aspects of soil behavior associsted with cementation
3) its predictions become progressively less reliable for OCR > 4 to 8

Totally 15 input parameters are required for MIT-E3 soil model. Table 2-1 presents the summary of the input parameters with the corresponding physical contributions and the method of obtaining the parameters. The parameters can be categorized into two main groups 1) parameters that can be obtained form the laboratory tests directly 2) parameter that have to be obtained form parametric studies. Table 2-2 summarizes the input parameters categorized into these two groups.

Although the formulation of MIT-E3 is relatively complex, there is a standard procedure for selecting model input parameters. However, due to time limitations, the selection of parameters for Bay Mud have been done by Whittle. Most of the parameters are derived from laboratory tests which consist of 1-D consolidation test (to determine the pre-consolidation pressure σ'_p and hydraulic conductivity k) and at least 3 undrained triaxial shear test on specimens that are K_{0nc} consolidated using SHANSEP procedures. Further details of the parameters and evaluation of the soil model predictions will be discussed in Chapter 4.2.

Test Type	Parameters	Physical Contribution/Meaning
Consolidation tests (Oedometer or CRSC tests)	e_0	Void ratio at reference stress on virgin compression line
	λ	Compressibility of virgin consolidated clays
	C	Nonlinear volumetric swelling behavior
	N	Nonlinear volumetric swelling behavior
	H	Irrecoverable plastic strain
Consolidation tests with measurements of horizontal effective stress (K_0-oedometer or K_0-triaxial tests)	K_{0NC}	K_0 for virgin normally consolidated clays
	$2G/K$	Ratio of elastic shear to bulk modulus (Poisson's ratio for initial unload)
Undrained triaxial shear tests	ϕ'_{TC}	Critical state friction angles in triaxial compression (large strain failure criterion)
	ϕ'_{TE}	Critical state friction angles in triaxial extension (large strain failure criterion)
	c	Undrained shear strength (geometric of bounding surface)
	S_t	Amount of postpeak strain softening in undrained triaxial compression
	ω	Nonlinearity at small strains in undrained shear
	γ	Shear-induced pore pressure for OC clay
Resonant Column or Cross-hole shear wave velocity type tests	κ_0	Small strain compressibility at load reversal
Drained triaxial tests	ψ_0	Rate of evolution of anisotropy (rotation and changes in size of bounding surface)

Table 2-1 Summary of input parameters with the corresponding physical contribution for MIT-E3 soil model

Parameters		Physical Contribution/Meaning
Directly obtained from the appropriate tests	e_0	Void ratio at reference stress on virgin compression line
	λ	Compressibility of virgin consolidated clays
	K_{0NC}	K_0 for virgin normally consolidated clays
	$2G/K$	Ratio of elastic shear to bulk modulus (Poisson's ratio for initial unload)
	ϕ'_{TC}	Critical state friction angles in triaxial compression (large strain failure criterion)
	ϕ'_{TE}	Critical state friction angles in triaxial extension (large strain failure criterion)
	κ_0	Small strain compressibility at load reversal
Can be obtained from the appropriate parametric studies	C	Nonlinear volumetric swelling behavior
	n	Nonlinear volumetric swelling behavior
	h	Irrecoverable plastic strain
	c	Undrained shear strength (geometric of bounding surface)
	S_t	Amount of postpeak strain softening in undrained triaxial compression
	ω	Nonlinearity at small strains in undrained shear
	γ	Shear-induced pore pressure for OC clay
	ψ_0	Rate of evolution of anisotropy (rotation and changes in size of bounding surface)

Table 2-2 Summary of input parameters for MIT-E3 categorized into two groups

2.3 FINITE ELEMENT MODEL

A finite element model is required to adapt the pile installation modeling and the soil model in order to predict the effects of pile installation. Previous studies have shown that predictions of the change in radial effective stress acting on the pile shaft during construction are strongly affected by non-linearities of the soil. In contrast of the soil is linear, isotropic and elastic, the amount of decrease in excess pore pressure decrease is always balanced by an increase in radial effective stress such that at the end of consolidation $\sigma'_{rc} = \sigma'_{ri} + \Delta u_i$ where σ'_{ri} and Δu_i are the radial effective stress and pore pressure predicted at the shaft during installation. Comparison with the measured data shows that this leads to a significant overprediction of the set-up around the pile shaft in soft clay. Hence, a comprehensive analysis is required for non-linear consolidation in order to achieve reliable predictions.

In this finite element model, since the strain path method and the MIT-E3 model are incorporated into the model so that nonlinear stress-strain behavior of soil can be taken into account. The analysis assumes that the excess pore pressures dissipate radially around the shaft of a long pile. Pore water flow is described by Darcy's law in which the permeability of the soil is assumed to be homogeneous and constant throughout the layer. The inputs of model are the initial stresses and the pore pressure which are obtained from the strain path method and the constant permeability (k) of the soil.

Since the rate of dissipation of excess pre pressure changes with time after pile installation and hence the effective stress, a time factor should be defined to normalize the predictions of set-up times. The time factor (T) is presented as follows:

$$T = \frac{k\sigma'_p t}{\gamma_w R^2_{eq}}$$

where t is the time after pile installation

σ'_p is the in-situ pre-consolidation pressure stress

γ_w is the unit weight of water

k is the horizontal coefficient of the hydraulic conductivity

R_{eq} is the radius of the piezometer

Therefore, the time of full dissipation can be estimated if σ'_p, σ'_{v0} and k are known. Details of estimating the soil permeability k will be presented in Chapter 4.

2.4 CAVITY EXPANSION METHOD

2.4.1 Fundamental concepts

Cavity expansion theory has been widely used in the analysis of geotechnical problems. Different solutions have been developed mainly because of differences in the constitutive models used to describe the stress-strain behavior of the material enclosing the cavity.

Cavity Expansion Method (CEM) assumes the conditions of radial symmetry and thus restricts the dependence of field variable (i.e. displacement, strains, stresses and pore pressure) to the radial coordinate only. In CEM, the installation process is modeled as the expansion of a spherical or cylindrical cavity into an ideal medium of infinite extent. Spherical CEM has been used for predictions of bearing capacity of piles, as the act of pushing the tip of the pile into the soil below is somewhat analogous to the expansion of stresses around the shaft of the pile as once the tip of the pile is well below the region of interest, the radial deformations in the soil are assumed analogous to those around a cylinder of infinite length.

Definition of the problem

A cavity with an initial radius a_o and an initial internal pressure p_o in an unbounded three dimensional medium of modified Cam clay is expanded by a uniformly distributed internal pressure s_a. When the cavity expands from a_o to a, an element initially located at a radial distance r_o from the center of the cavity will move to a new position at a radial distance r from the center (Figure 2-4).

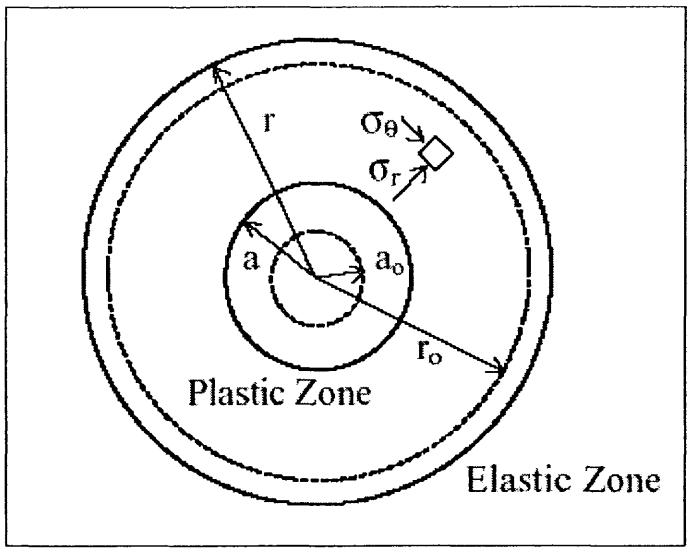

Figure 2-4 Expansion of a cavity

The condition of spherical symmetry holds in spherical cavity expansion, and the condition of axial symmetry holds in cylindrical cavity expansion. Plane strain condition is assumed for the cylindrical cavity in the vertical direction and the vertical stress s_z is equal to the mean of radial stress s_r and circumferential stress s_q in the undrained condition.

Elastic analysis

The solution for stresses and displacement can be easily obtained based on the assumption of small strain. In the undrained condition, the volume change is zero. The mean effective stress is constant in the elastic zone. Consequently, no excess pore pressure is generated in the elastic zone.

Plastic analysis

After the initial yielding at the cavity wall, a zone of soil extending from the cavity wall to a radial distance r_p will become plastic as the cavity pressure continues to increase. Combining the yielding condition and the elastic solution, the stresses and the displacement at the elastic-plastic boundary can be obtained.

The expansion of a spherical cavity in saturated, homogeneous, isotropic clays initially subjected to isotropic stresses represents a problem where solutions by the strain path methods are exact because soil strains are completely independent of material properties. On the other hand, in more realistic situations where the strains are slightly dependent on material properties, solutions based on simplified strain fields are approximate and the effective stresses computed by means of a given constitutive model will not satisfy all equilibrium requirements.

Soil deformations behind the tip of the pile bear absolutely no similarities to the spherical cavity solution. In fact, deformations around the pile shaft are also different from cylindrical cavity expansion predictions that ate presently the leading analytic tool used to study the shaft behavior of piles.

2.4.2 Theoretical Description

Figure 2-5 depicts the geometric considerations for cylindrical cavity expansion. An initial cavity of radius ρ_0 is expanded to a radius r_0. This causes an arbitrary circle of initial radius ρ to expand to a new radius r. With the assumptions of incompressibility and infinite radial extent, determining the new radius, r, is a simple matter of calculating the increment in area of the cavity, and applying that same increment in area to the arbitrary circle of initial radius ρ. The areas of the circle defined by all four radii are given by:

$$A_{\rho_0} = \pi\rho_0^2 \quad A_{r_0} = \pi r_0^2 \quad A_\rho = \pi\rho^2 \quad A_r = \pi r^2$$

the area of the expanded circle of radius r can be computed from

$$A_r = A_\rho + \left(A_{r_0} - A_{\rho_0}\right) = \pi\rho^2 + \left(\pi r_0^2 - \pi\rho_0^2\right) = \pi\left(\rho^2 + r_0^2 - \rho_0^2\right)$$

$$\pi r^2 = \pi\left(\rho^2 + r_0^2 - \rho_0^2\right)$$

which leads to an equation for the new radius, r, given any initial radius ρ:

$$r = \sqrt{\rho^2 + r_0^2 - \rho_0^2}$$

or a simpler form if the initial cavity radius, ρ_0, is zero:

$$r = \sqrt{\rho^2 + r_0^2}$$

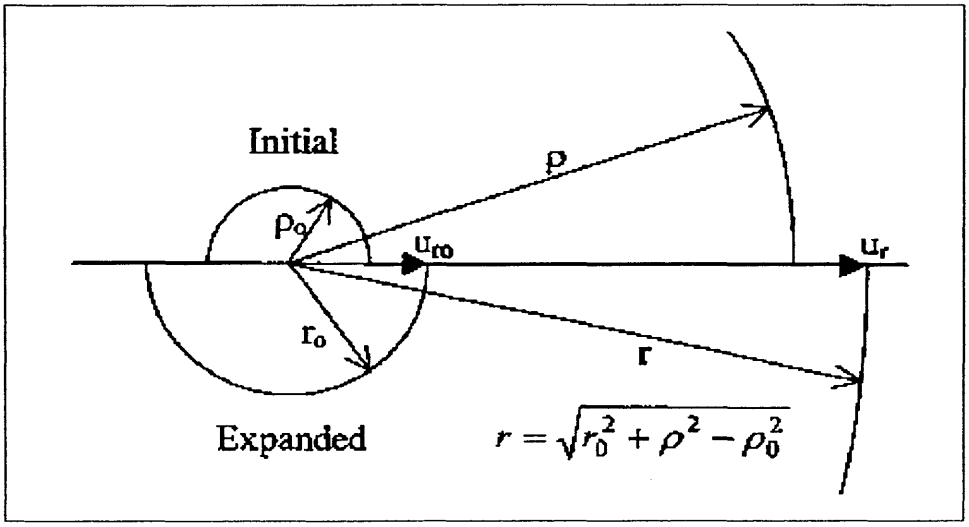

Figure 2-5 Cylindrical cavity expansion schematic

Figure 2-6 illustrates the deformations obtained by applying equation above to the nodes of a previously undeformed grid. As would be expected, deformations are highest close to the cavity wall, decreasing rapidly with distance.

The displacement of a point in the soil mass is given by:

$$u_r = r - \rho$$

The radial and tangential strains developed in cavity expansion are computed as:

$$\varepsilon_r = -\frac{du_r}{dr} = \frac{u_r}{r}; \varepsilon_\theta = -\frac{u_r}{r}$$

with sign convention considered positive in compression, and with the understanding that the final portion of the equation for radial strain (i.e. $\varepsilon_r = u_r/r$) arises from the assumption of incompressibility. Cylindrical cavity expansion is a plane strain theory, with no strain in vertical direction (i.e. $\varepsilon_z = 0$) and thus is applicable to conditions far from the ground surface.

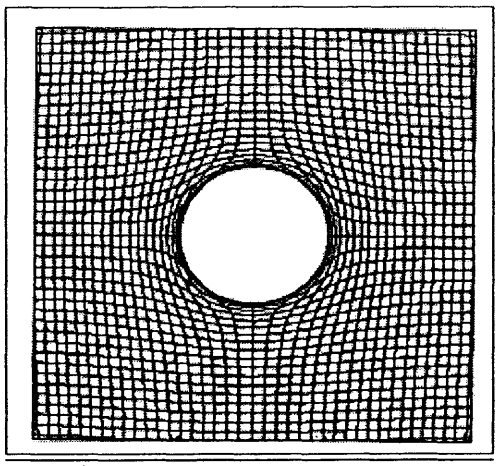

Figure 2-6 Grid deformation due to cylindrical cavity expansion

2.5 COMPARISON OF CEM AND SPM

As mentioned before, the two approaches for modeling pile installation are the strain path method (SPM) and the cavity expansion method (CEM). Both methods assume that the pile is being installed in an incompressible, homogeneous, isotropic material of infinite radial extent. However, based on other different assumptions made in each method, the two solutions are quite different where the cavity expansion significantly underpredicts deformations and strains.

Cylindrical cavity expansion assumes radials soil deformation in a cylindrical coordinate system. Similar to spherical cavity expansion, the premise of the stain path method is the expansion of a cavity within an idea, infinite, incompressible medium. Unlike cavity expansion the medium is modeled as fluid, and the expanding cavity is modeled as a spherical source discharging an incompressible material. The fluid medium is at the same time given a uniform velocity in the vertical direction past the spherical source and as the source material is carried by the flow field, the resultant streamlines describe a scenario very similar to the penetration of a pile or other penetrometer into an incompressible medium.

The stain path method can provide a more realistic framework for describing the mechanics of deep penetration by considering 2 dimensional deformations of soil elements while the cylindrical cavity expansion method only consider 1-dimensional deformation. The stain path method can account properly for the effects of non-linear and inelastic soil behavior. On the other hand, the assumptions of strain controlled behavior used in Strain Path Method greatly simplify the mechanics of penetration and avoid the complexity of large scale finite element computations.

Figure 2-3 and 2-6 present a comparison of the deformations induced in a uniformly spaced grid by cylindrical cavity expansion and the strain path method. CEM produces a purely radial expansion with the vertical gridlines closet to the pile surface being compressed significantly, with less effect at a larger distance. SPM produces this same essential condition, with the added downward deformation component seen most clearly in the soil adjacent to the pile.

3 FIELD PERFORMANCE OF A PILE INSTALLED IN BAY MUD

Hunt (2000) focuses on characterizing of the response of soft clay to the installation of a full scale (61 cm diameter, 35 m long) steel pipe pile that is driven closed-ended into a deep deposit of San Francisco Bay Mud. The scope of his work includes field measurements of pore water pressure, deformation and shear wave velocity and supporting laboratory tests of stress-strain properties of the clay surrounding the pile

3.1 FIELD WORK

Hunt's research included the following tasks:

1. Site selection
2. Site exploration and characterization
3. Installation of all instrumentation (piezometers and inclinometers)
4. Collection of soil samples for laboratory testing
5. Pre-pile measurement - Data collection (deformations, pore pressures and shear wave velocities)
6. Pile installation
7. Subsequent data collection for a period of up to two years
8. Collection of additional soil samples and shear wave velocity measurements within boreholes (8 and 31 months after installation) adjacent to pile wall.

The following sections present a summary of soil characterization, instrumentation as well as the program of field monitoring of excess pore pressures and lateral deformation following the driving of a full-scale closed-ended steel pipe pile into a deep deposit of Young Bay Mud.

3.1.1 Site

The project site is located on the San Francisco Peninsula in California, near areas of recently completed seismic retrofit work on the I-280 freeway. The project site, referred to as Islais Creek, is located at the intersection of Evans Avenue and Selby Street and is within the right of way of the freeway structure owned by the California Department of Transportation (CALTRANS).

Several sites have been explored for selection. This location was selected because of the benefit of the existing site data. Boring and cone penetration test (CPT) results were collected before.

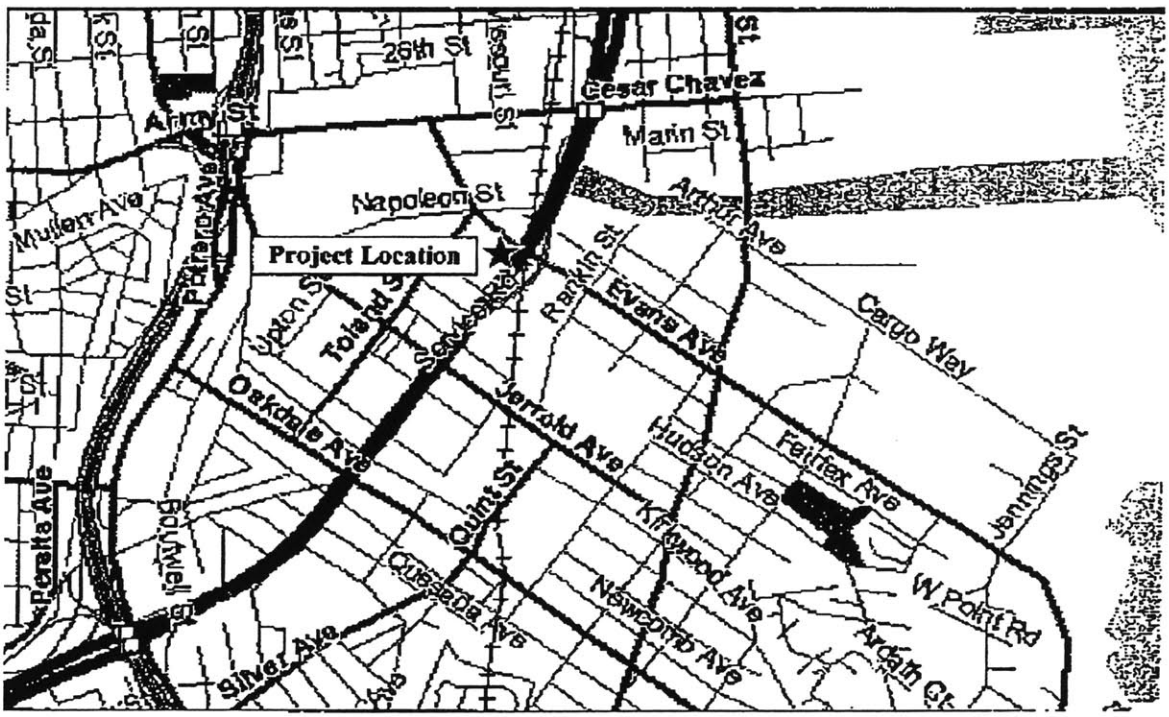

Figure 3-1 Site Location – corner of Evans Ave. & Selby Street, San Francisco, CA

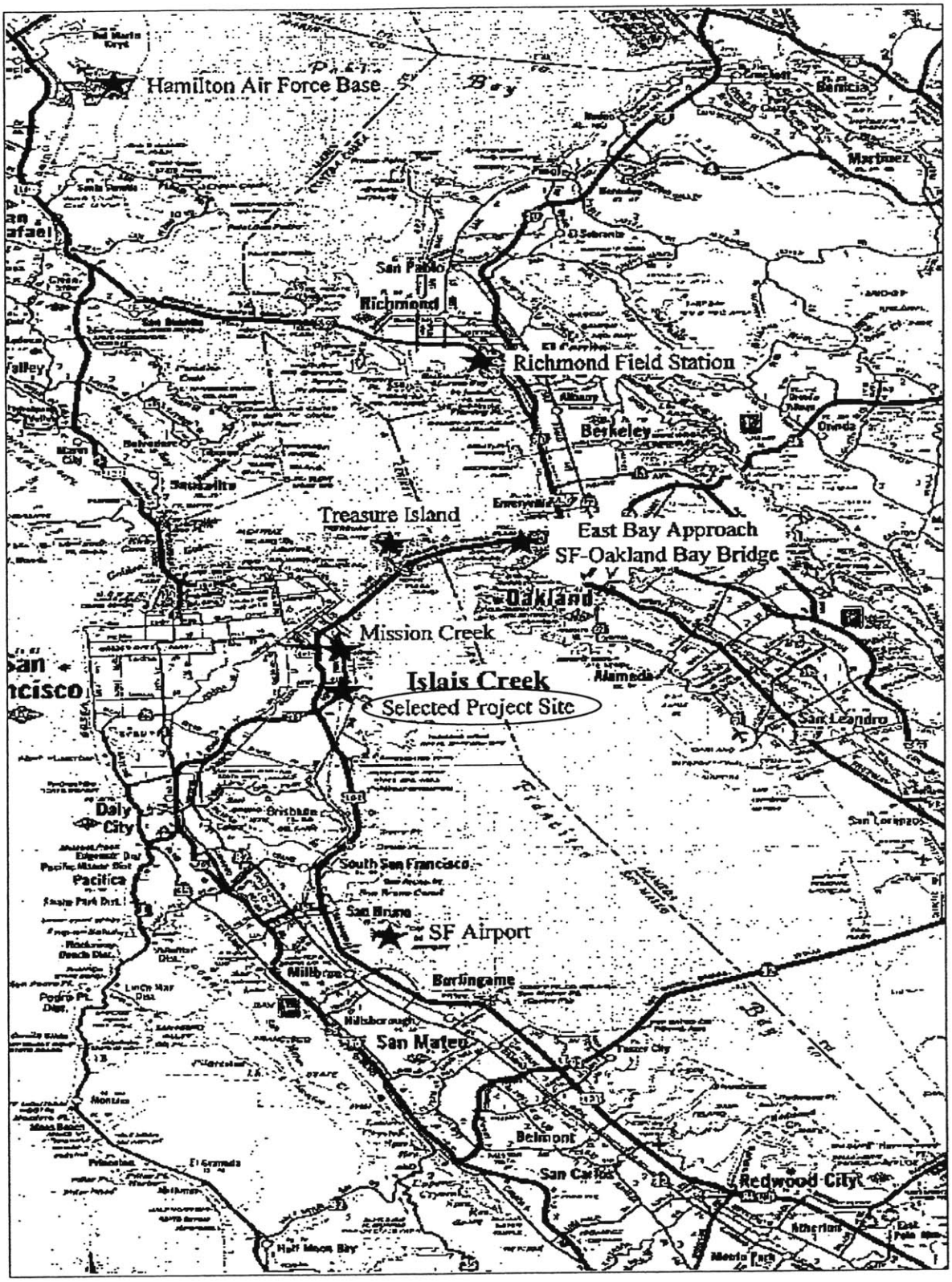

Figure 3-2 Map of the site at Islais Creek

3.1.2 Geology

In 1876, the Islais Creek Basin was a salt marsh, continuously inundated by high tides and with numerous stream channels running through it (Radbruch and Schlocker 1958). Bedrock consists of serpentines and Franciscan rocks of Jurassic and Cretaceous age of varying depths due to erosional channels from ancient streambeds. Overlying much of the bedrock, in particular near the present shoreline, there is a deposit of older Bay Clay (Old Bay Mud) with thicknesses greater than 15 m in some areas. Above the older bay clay layer (or the bedrock when there is no clay) lies a deposit up to 45-m-thick (although typically less than 15 m) of slightly clayey sand. The final natural deposit, overlying the sand layer or in some cases lying directly over bedrock is soft Holocene clay, commonly referred to as Young Bay Mud. According to Radbruch and Schlocker (1958), fill was placed throughout this area at various times from about 1890 to 1940 to raise the surface and allow for commercial development, and it was most likely completely filled between 1915 and 1940. The miscellaneous fill is composed alternately of dune sand, rock waste, miscellaneous debris (including concrete, wood, and brick), and organic waste.

3.1.3 Subsurface conditions

Boring from the site indicated approximately 6m of miscellaneous fill, underlain by 27m of Young Bay Mud, and followed by approximately 21m of dense sand before reaching bedrock. It showed that the Young Bay Mud is remarkably uniform.

There are five distinct layers apparent in the profiles. All borings as well as the CPT tests show the fill layer extending from the ground surface to a depth of approximately 3.5 m. Two Bay Mud layers are present beneath the fill, separated by a stiffer and significantly more permeable soil layer at a depth of approximately 15.5–17.5 m. This is likely the remnant of a meandering stream channel thousands of years old. Finally, a stiff sand layer appears at approximately 31 m in both profiles. The ground water table is encountered at a depth of 1.5–3 m throughout the site or taken as 2.14m as an average.

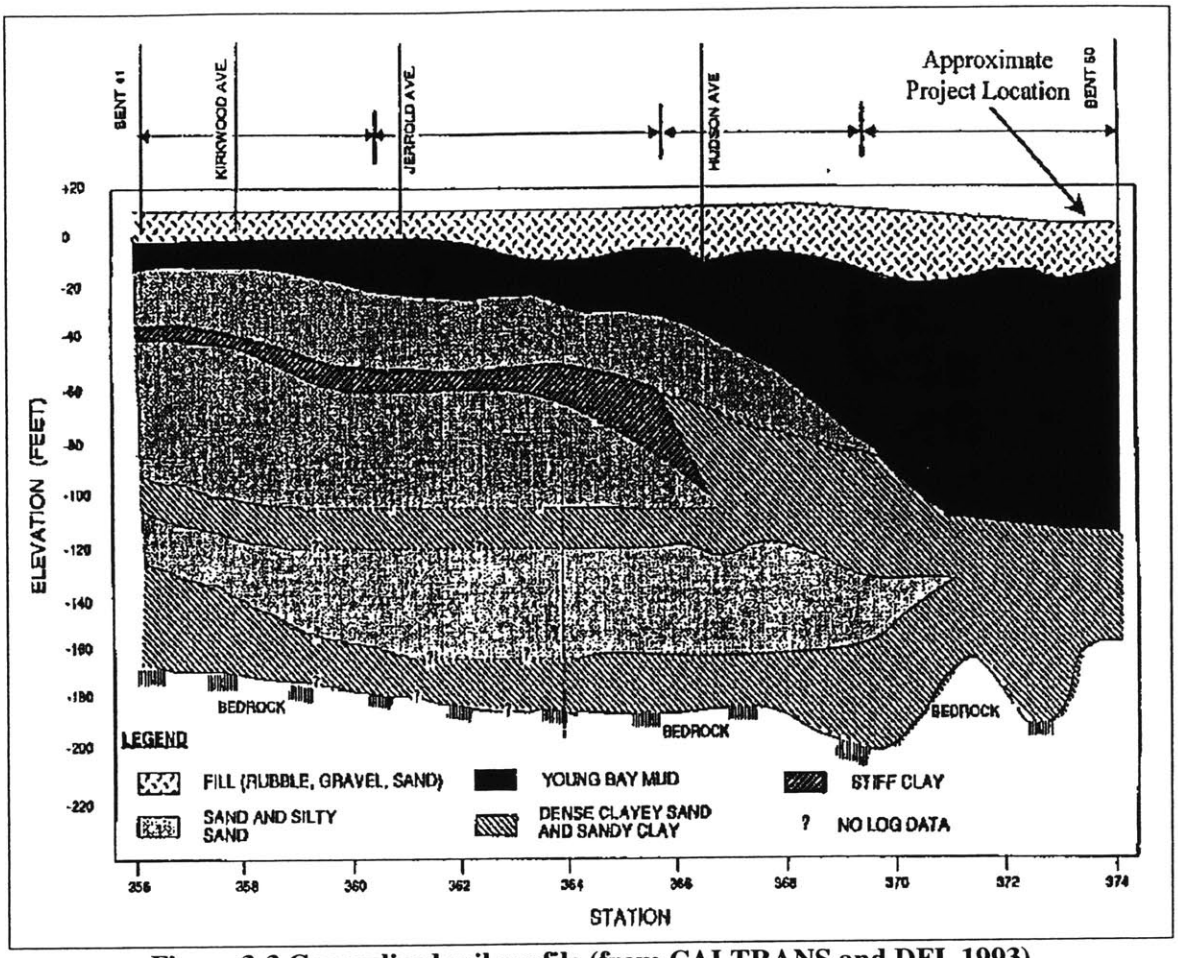

Figure 3-3 Generalized soil profile (from CALTRANS and DFI, 1993)

3.1.4 Soil Boring

Two seismic cone penetration tests with pore pressure measurements (SCPTU) and 8 soil borings were drilled to various depths for the purposes of collecting high-quality laboratory samples and installing field instrumentation at the site. Figure 3-4 shows the surface location of all borings and CPT soundings relative to the pile location. Borings 1–7 were drilled during installation of field instrumentation (i.e. piezometers and inclinometers), borings 9 and 10 were drilled 8 and 31 months after pile installation to obtain post-pile soil specimens and shear-wave velocity measurements adjacent to the pile. Boring 8 was a shallow boring through the fill layer without sample retrieval, followed by the jacking of a steel pipe (outside diameter of 10.16 cm) through the Young Bay Mud to a depth of 17.5 m for a shear-wave velocity feasibility study.

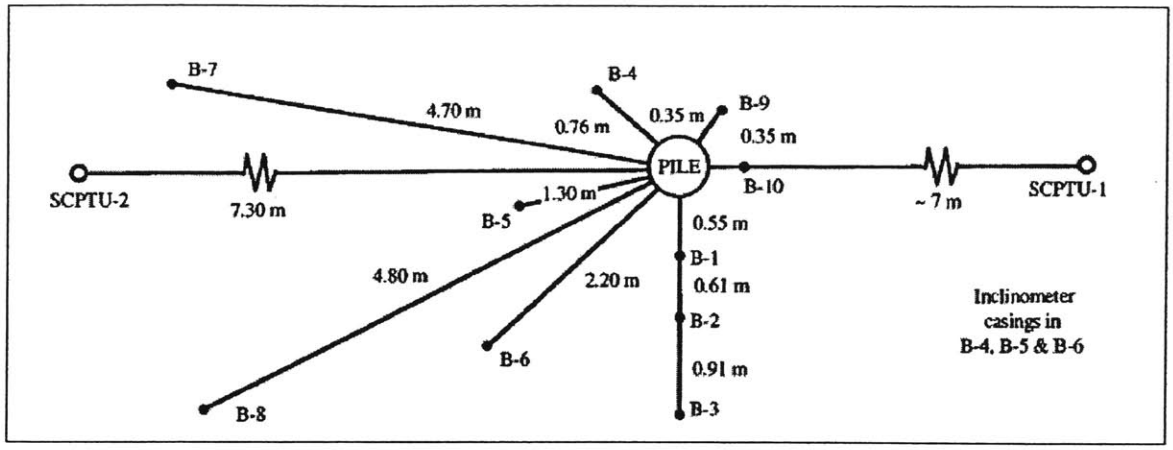

Figure 3-4 Borehole layout relative to pile location (Hunt 2000)

Figure 3–5 shows the combined penetration results of the two SCPTU tests performed at the site. The plots of corrected cone resistance (q_t), friction ratio (R_f), are derived parameters computed based on measured values of pore pressure behind the cone tip (u), cone resistance (q_c), and sleeve friction (f_s) as presented by Hunt et al. (2000).

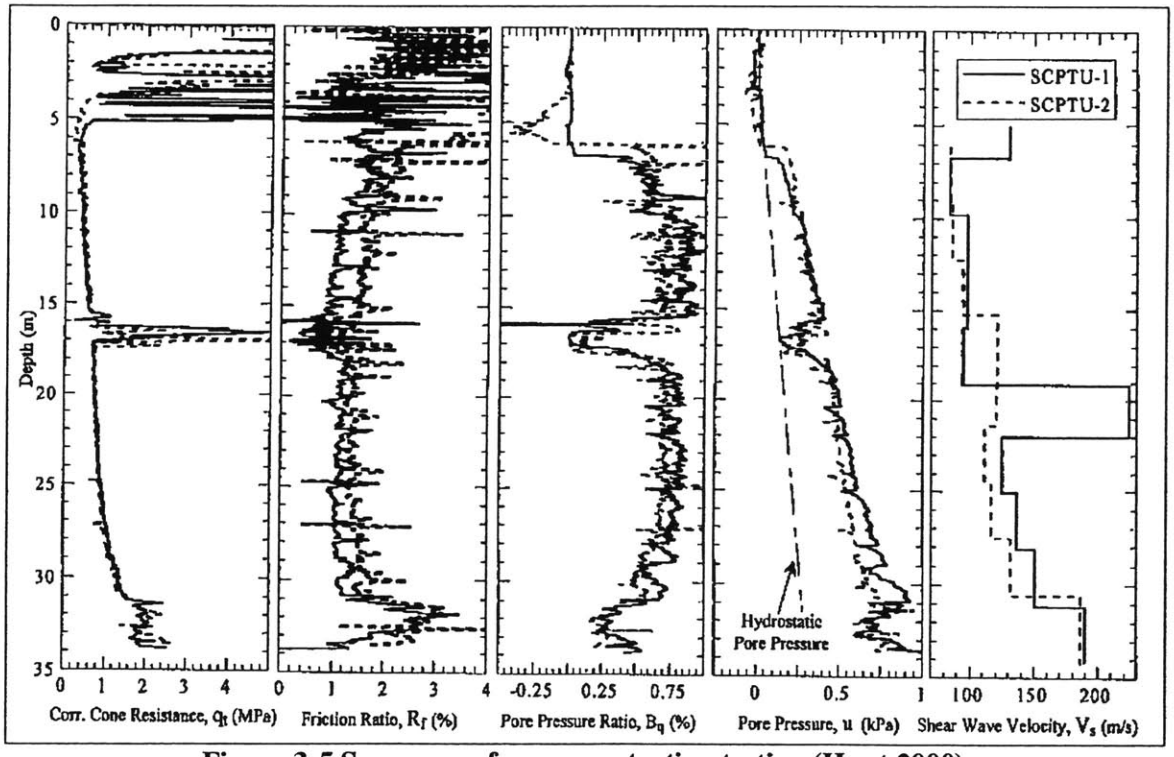

Figure 3-5 Summary of cone penetration testing (Hunt 2000)

3.1.5 Instrumentation

1) Piezometer Instrumentation

Three piezometer levels were selected: 8.5, 12.8, and 23.8 m. These depths were chosen to obtain information from both layers of Young Bay Mud and to stay sufficiently far from the sandy drainage layer so that the predominant drainage path would be radial. Nine 1-inch diameter pneumatic piezometers were installed over a grid representing three depths and three radial distances from the pile. In addition, another piezometer was placed sufficiently far from the pile to measure any seasonal fluctuations in the ground water table, and one was placed on the pile itself to measure pore pressures on the surface of the pile. Pneumatic devices were chosen over electrical ones for their robustness, as the piezometers closest to the pile had to survive large lateral displacements and pressures induced while the pile was being driven past them and had to provide reliable readings for at least one year. Borings 1, 2, and 3 each have two piezometers at nominal depths of 8.5 and 12.8 m (the deeper piezometer in boring 2 is at 12.65m). Borings 4, 5, and 6 have one piezometer each at 23.8 m, with inclinometer casing grouted in place above 22.4 m. Boring 7, at 7.7 pile diameters from the pile wall, contains one piezometer at a depth of 6.7 m. Each piezometer was placed inside a sand-filled canvas bag, and then within a 1 m sand cell, with a bentonite seal above to ensure localized measurements. The entire space between the two sand cells in borings 1, 2, and 3 was filled with a bentonite plug to prevent coupling of measurements.

2) Inclinometer Instrumentation

Three sets of inclinometer casings (85 mm outer dimension, 75 mm inner dimension) were installed at three radial distances from the pile, each to a depth of 23 m. Since borings 4, 5, and 6 contained a piezometer at 23.8 m, the base of the casing could not be locked into competent material and be isolated from pile penetration induced displacements. Instead, the tops of the casings were assumed to be locked within the very stiff 3–5 m of fill at the surface and were verified through accurate surface surveys. A period of two months after installation was allowed to enable the grout to set up and the pore pressures to come to equilibrium.

3.1.6 Pore Pressure

Pore pressure measurements provide insight into the state of stress within the post-pile soil, serve as an indicator of the lateral extent of the pile's influence on the surrounding soil. Besides, by monitoring pore pressure dissipation after pile installation, the measurements serve as partial indicator if the time required for soil recovery.

Measuring pore pressures in the soil around a pile is perhaps the simplest and most effective way of gauging the recovery of the soil from the effects of pile driving. A soft, nearly normally consolidated soil responds immediately to the driving with a significant increase in pore water pressure. Higher pore pressures lead to a reduction of effective stresses, and these, in combination with remolding of the soil adjacent to the pile, can lead to drastic reductions in the strength of the soil immediately after pile installation. Depending on the permeability of the soil and the presence of preferential drainage paths, these increased pore pressures dissipate in the following weeks, months, and in some cases years, allowing the soil to consolidate and regain much, if not all, of the strength.

For this project, knowledge of the pore pressures was used as a guide for when to measure shear wave velocities, which was anticipated to be intimately linked with both the corresponding changes in effective stresses and the densification of soil due to consolidation.

Dissipation tests were performed in the upper and lower clay layers during the SCPTU-2 sounding to estimate the required time for pore pressure dissipation following pile driving. Pore pressures measured in all ten piezometers prior to pile installation were very consistent and the average value is shown on Figure 3-6. After two years of measurements, the pore pressures returned to approximately the same values measured previous to the installation of the pile.

Figure 3-6 shows measured pore pressures immediately after pile driving, As can be seen, higher excess pore pressures occur near the pile and decrease with increasing distance from the pile wall.

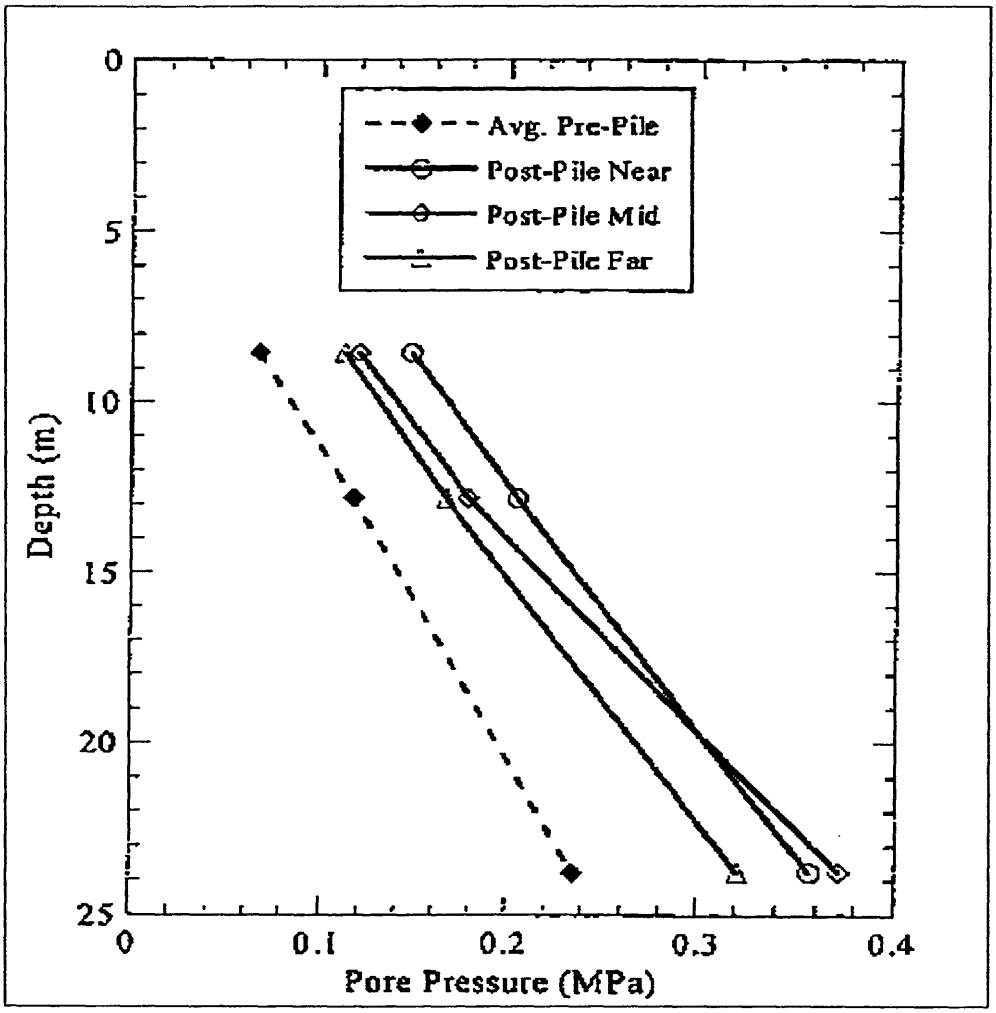

Figure 3-6 Pore pressure measurements 2 hours after pile installation

Measured values of pore pressure are presented in Figure 3-7 relative to the number of days elapsed since pile driving. All piezometers seem to show an exponential decay of excess pore pressure as a function of time, and at the same time show a vertical gradient throughout the entire process of consolidation.

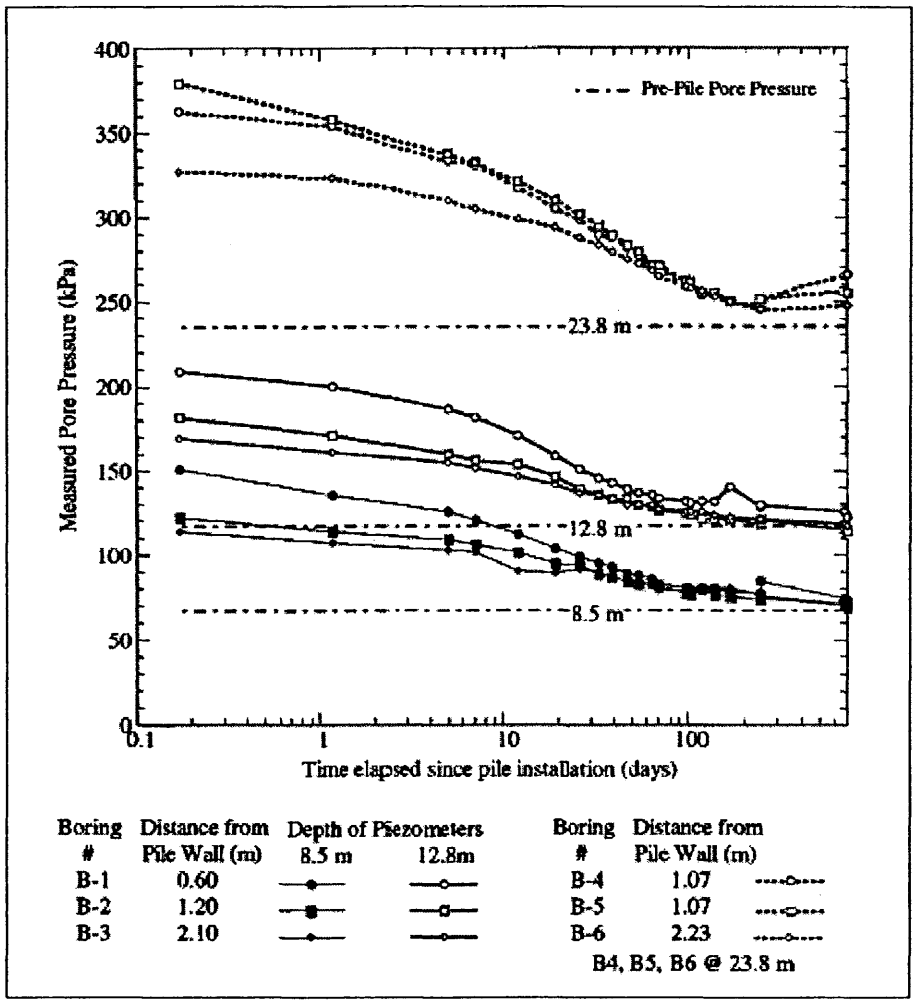

Figure 3-7 Summary of pore pressure program

Figure 3-8 shows the normalized pore pressure ratio ($\Delta u/\Delta u_i$) dissipation curves for each instrumented depth. It shows that the far piezometers in all three cases display the slowest dissipation times. This can be
explained by the radial dissipation path away from the pile, in which flow of pore water from the near piezometers must pass by the far piezometers, thus adding to the pore pressure they have to dissipate.

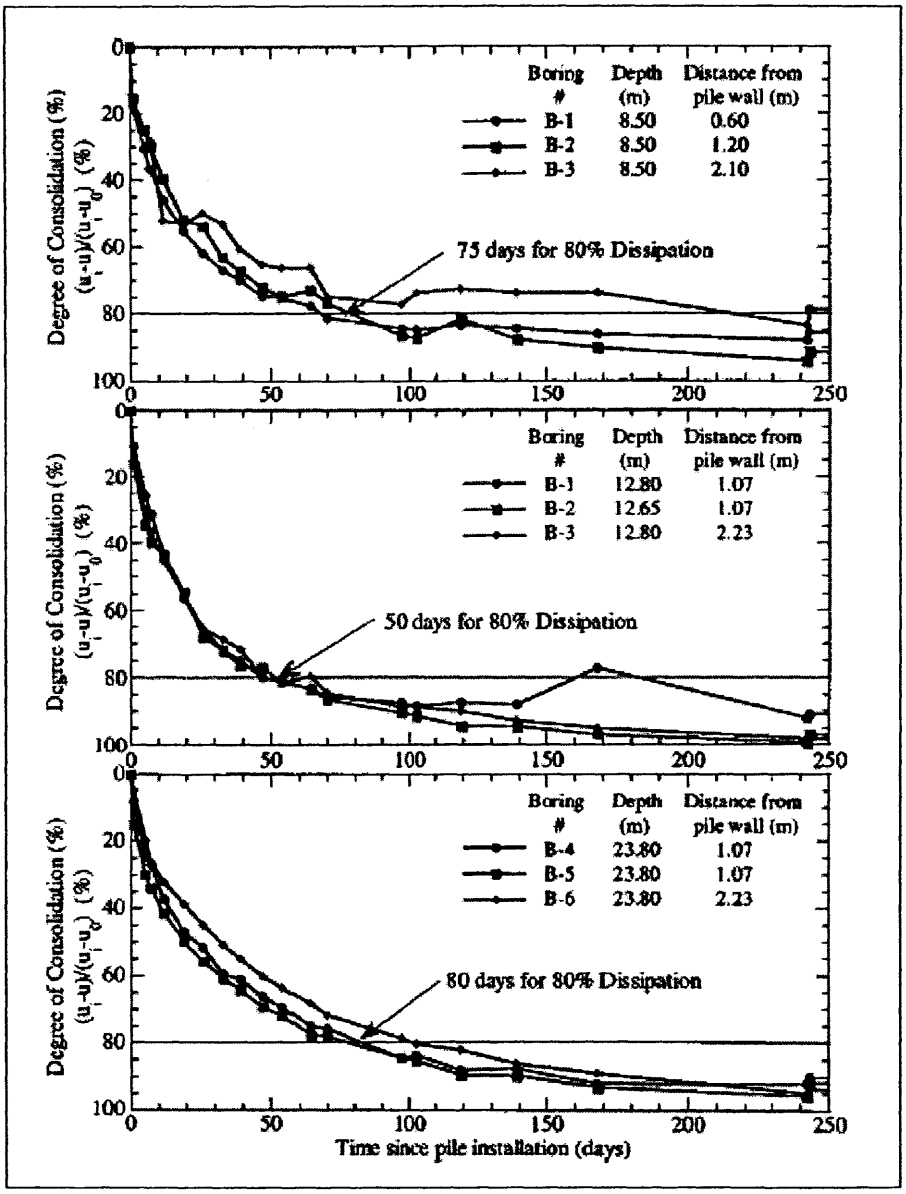

Figure 3-8 Dissipation of excess pore pressure

3.1.7 Lateral Deformations

Deformation measurements give an additional indication of the extent of the pile's influence, and more importantly, allow for calibration of the measured responses with numerical simulations of pile installation, which rely on assumptions regarding the strain induced by pile penetration. In addition, measuring lateral deformations would provide information on the consolidation process as the generated excess pore pressures dissipated.

With the measure of the significant lateral deformations occurring within the soil surrounding a driven pile, comparisons can be made with theoretical predictions which could support the widely held assumption that driving a pile through normally consolidated clay is an undrained phenomenon. In addition, measuring return deformations towards the pile during pore pressure dissipation would serve as an indicator of the radial consolidation occurring over time after pile driving. In this section, all the major results obtained from Hunt will be discussed.

Hunt has used several ways to represent the deflections measured in inclinometers. They are measurements along A-axis, B-axis and angular deformations. Measurements along the perpendicular A- and B-axis grooves within the casing provide a traditional set of deformation readings. The A axis was aligned along an approximated radial path to the center of the pile at the ground surface. A coordinate system is shown schematically in Figure 3-9. It is important to note that the cased boreholes are not absolutely vertical. While drilling for B-4 began significantly closer to the pile than B-5, drift of the drilling head over the 24 m travel depth led to deviations less than 1–2% from the intended vertical alignment. This brought the bottom of B-5, and thus its piezometer, slightly closer to the pile wall than the bottom piezometer in B-4.

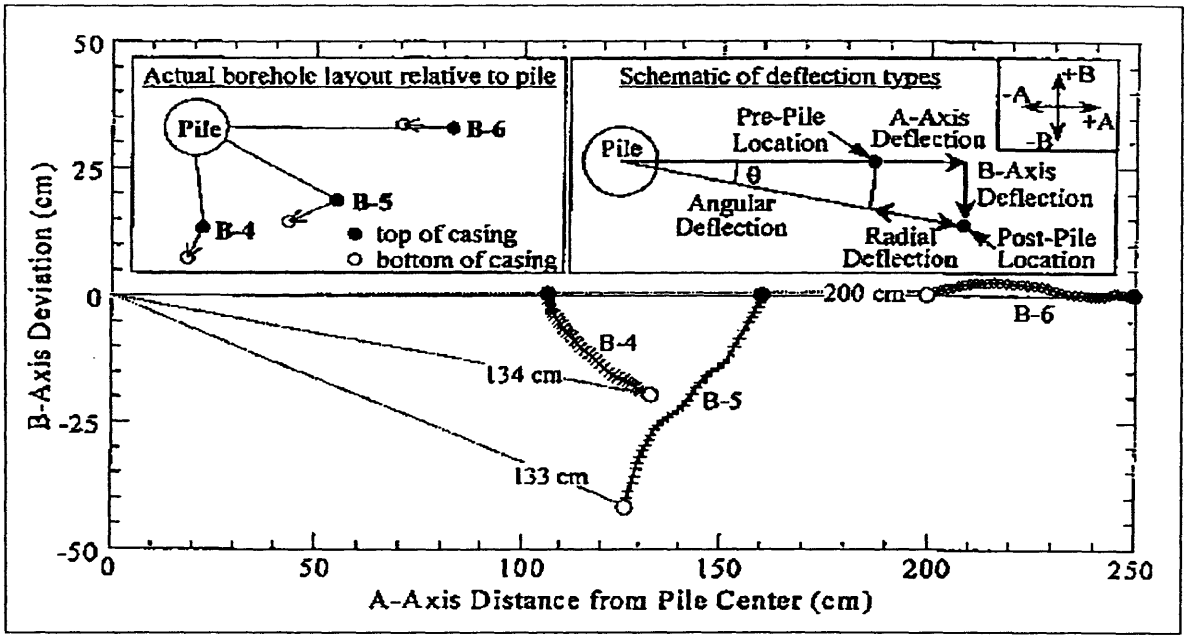

Figure 3-9 Plan view of boreholes relative to radial path from pile

Deflections are measured one day (~16 h) after pile installation along both the A and radial axes and the results are shown in Figure 3-10. It shows positive A-axis and radial deflections which indicate that all inclinometers were, as expected, displaced outwards due to pile installation. Measured B-axis and angular deflections were found to be negligible which means that the deformation is dominated by radial expansion of the soil. From the measurement, it indicates that all inclinometers were, as expected, displaced outwards due to pile installation. Radial expansion of the soil was demonstrated by the nearly identical values of A-axis and radial deflections. In addition, there is angular deflection. However, under ideal condition, there should be no rotation.

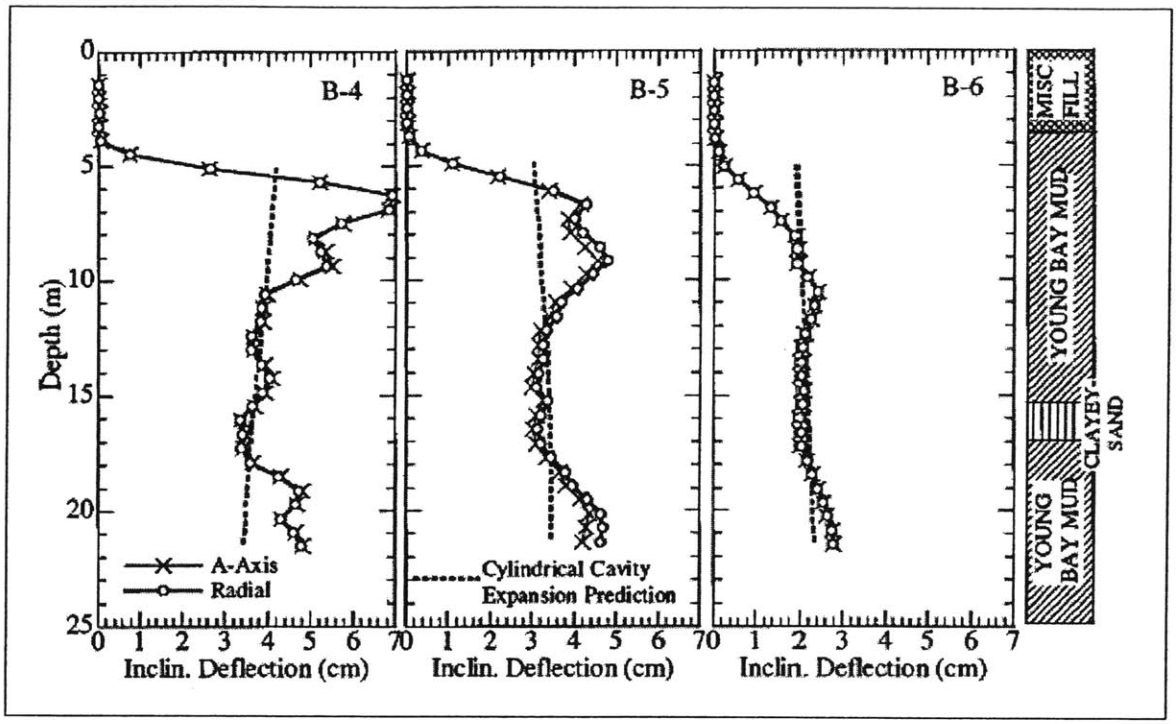

Figure 3-10 Initial deflections after pile installation

Figure 3-11 shows the radial inclinometer deflections in each borehole over time. As the excess pore pressures dissipate, some radial consolidation is taking place and is reflected in the deformation of the inclinometer casings towards the pile over time as shown by the incremental deformations from 1 day to 47 days and 1 day to 678 days. It is quite apparent that the radial consolidation occurring within the soil as the pore pressures dissipate, it is pulling the casings back towards the pile over time.

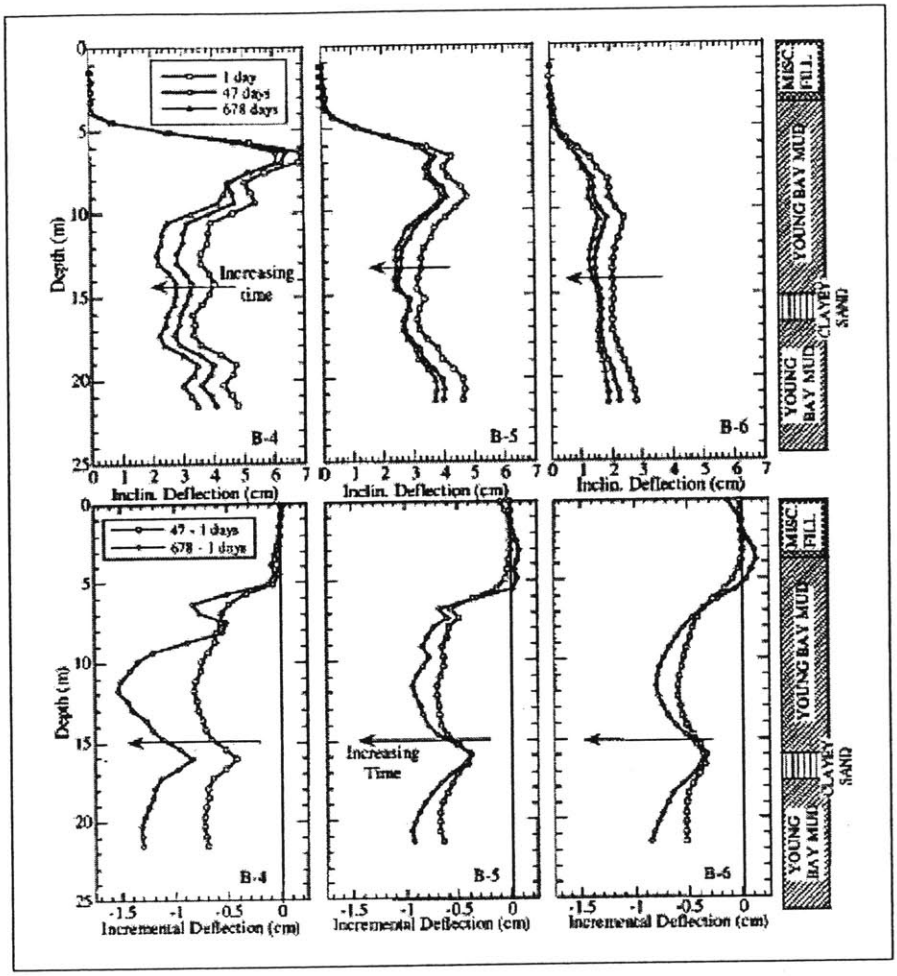

Figure 3-11 Time history of radial deflection induced by consolidation

The inclinometers show a consistent decrease in deflection as a function of distance from the pile. It is assumed that there is approximately 70% pore pressure dissipation at 47 days and pore pressures are assumed to be fully dissipated at 678 days. All boreholes show essentially little or small additional deformation at depths corresponding to the sandy layer as the rate of consolidation is higher at that layer.

A small deformation in the top 6–7 m for all boreholes was registered at 678 days (1–3 mm) and is partially attributed to the unexpected use of the site for storage of large diameter steel pipe piles approximately 650 days after pile installation which may have produced some near surface deformation.

3.1.8 Shear Wave Velocities

Shear wave velocities provide a measure of the stiffness of the surrounding soil, and are important both for their influence on the near-field soil-pile interaction and in the larger scale seismic site response. It is the key component of the research.

Measurement of shear velocities was vital for several reasons. First, it can be tied in with measured pore pressures as both are related to the state of stresses in the ground, and should provide an addition measure for the recovery of the soil after pile installation. Second, shear wave velocity (v_s), or alternately shear modulus are essential for any site response analysis.

The field technique used for measuring the shear wave velocity of soils is the OYO suspension logging method. The values are obtained by establishing a reference shear wave arrival time at shallow depth and then tracking the increase in travel time between the reference and the shear waves at subsequent depths. By dividing the difference in arrival time between the difference in the travel path from the source to the receiver produces the average shear wave velocity in the soil.

Figure 3-12 shows a summary of shear-wave velocity measurements as a function of time after pile installation (Hunt 2000). All three borings (B-4, B-5, and B-6) show an initial decrease in shear wave velocity at 5 days after pile installation. It is quite possible that shear wave velocities in the vicinity of the pile dropped almost to zero immediately after driving as velocities are stress dependent and effective stress are likely to be very low. In all cases, the sandy-clay layer from 15.5 to 17 m showed the largest increase in shear wave velocity following pile installation. In contrast to the measurements obtained in B-4 through B-6, B-9 shows much smaller shear-wave velocity, which can be partially attributed to the fact that the soil in the immediate vicinity of the pile was significantly remolded by the driving process. Thus, potential increases in velocity from an increase in density and stress were offset by the destruction of the clay structure and any bonds that had developed over its post-depositional history. The soils at greater distance were

expanded outward and densified upon consolidating, but were not sufficiently remolded to break down their structure, thus displaying an overall increase in shear wave velocity.

It has been found that there is an initial decrease in velocity followed by gradual increases over time. For the effects of distance from the pile, it can be theorized that the soil within approximately 1 diameter of the pile wall was heavily remolded due to pile installation, while outside of this region the soil was displaced outwards and subsequently consolidated.

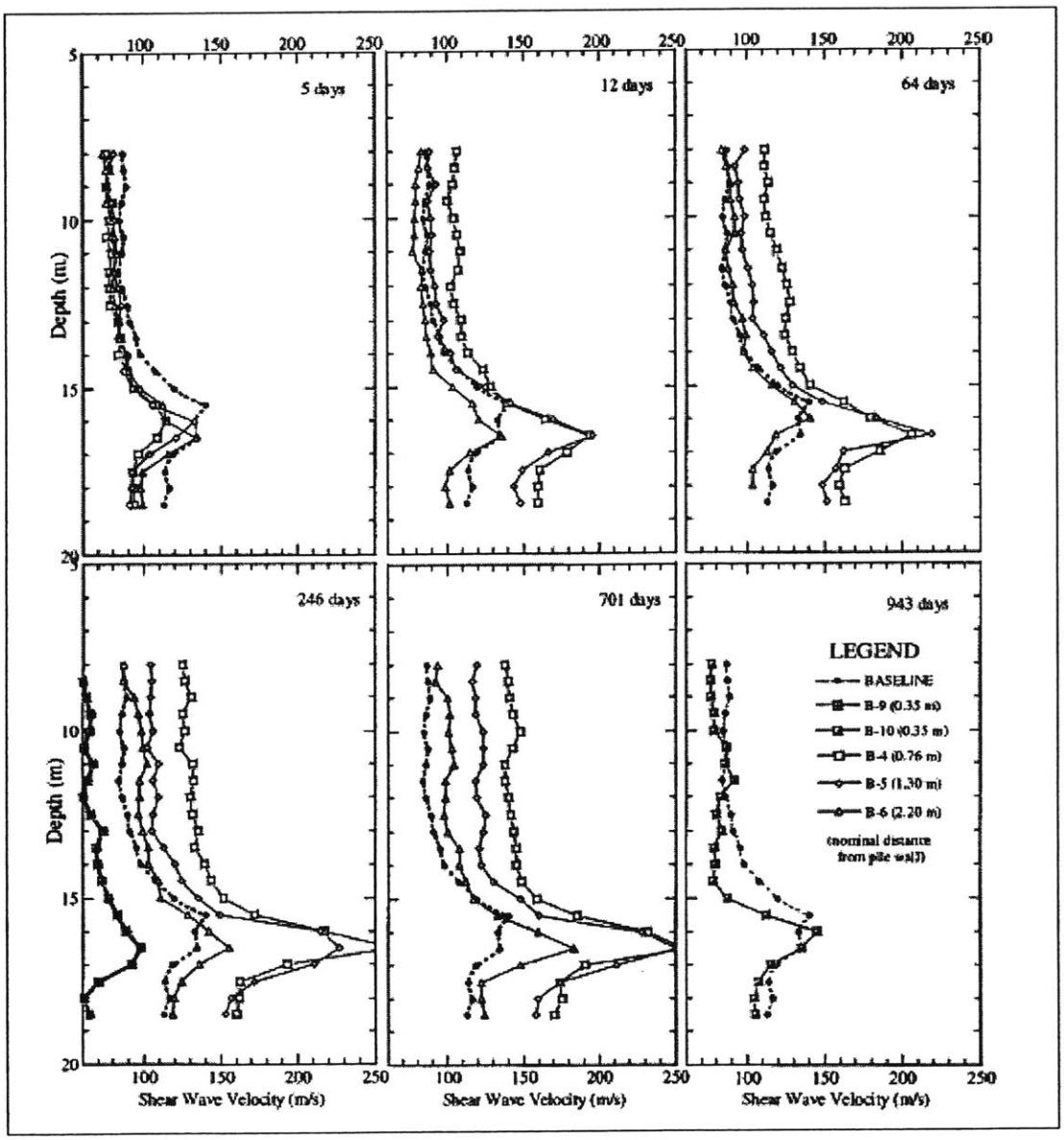

Figure 3-12 Change in shear-wave velocity profile as a function of time

3.2 LABORATORY WORK

Laboratory work involves comparison and interpretation of the behavior if pre- and post-pile specimens through water, density, consolidation, triaxial and simple shear testing. These comparisons provide insight into the mechanisms at work within the soil during and after pile installation. Additionally they provide a framework for some assessment of the adequacy of current design methods, which are based on pre-pile testing results.

The remolding of the clay caused by pile installation does not produce a completely random orientation of particles, but rather a "systematic distortion of the soil's fabric" (Jardine, 1991). This is a key concept and will be used subsequently in comparing measured post-pile versus pre-pile behavior in consolidation tests, triaxial strength tests and simple shear test.

The aim of this part is to investigate the effect of pile installation on the orientation of soil layering near the pile wall.

3.2.1 Index properties

Results indicate a soil profile with decreasing water content, plasticity index, specific gravity, and void ratio with increasing depth. The corresponding unit weights increase with depths, as the deeper samples are at lower water content and void ratio.

Index tests conducted in the laboratory included total unit weight, water content, and Atterberg limits, and they are summarized in Figure 3-13. The average total unit weight for the overall clay layer is 15 kN/m$_3$. The plasticity index (PI) for the clay ranges from approximately 35 to 45%, with a low value of 20% occurring at 13 m due to the presence of sand lenses. Water content is very close to the liquid limit in the clay above 17 m (ranging from 60 to 80%), dropping below in the lower portion of the deposit and suggest a lightly overconsolidated soil profile (e.g., Brittsan and Speer 1993).

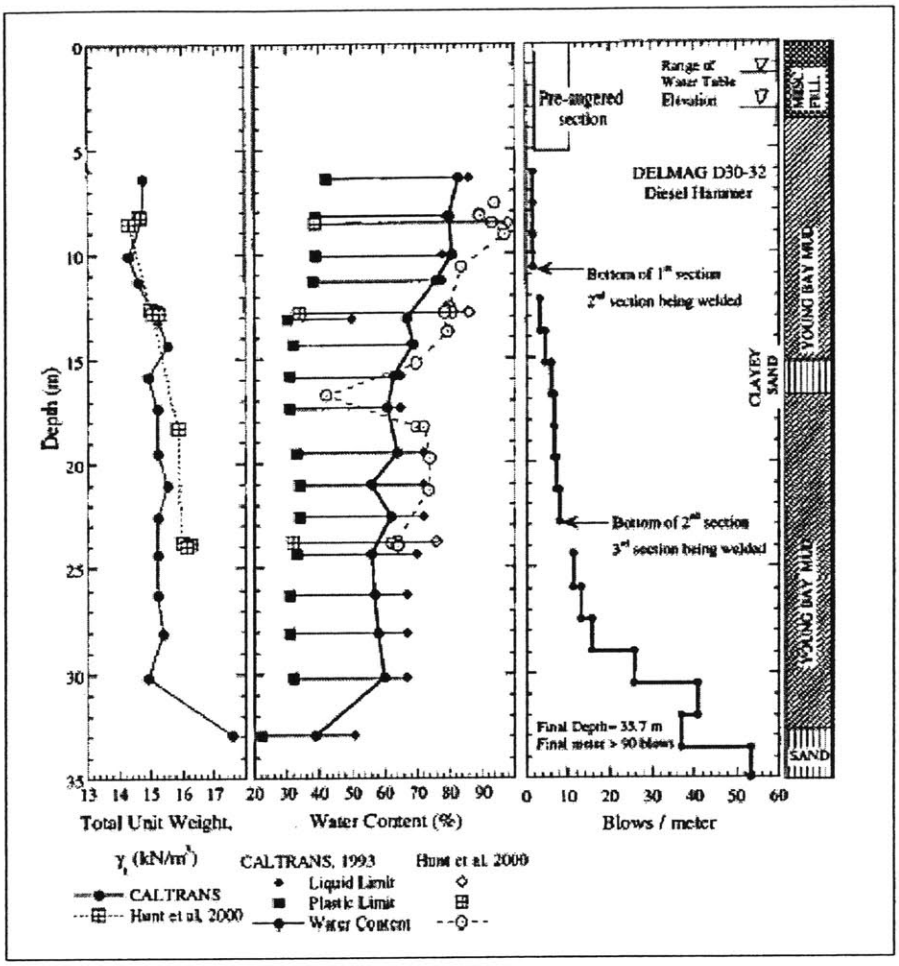

Figure 3-13 Summary of index tests results (Hunt et al 2000)

3.2.2 Constant rate of strain consolidation testing

Constant rate of strain consolidation tests were performed on pre and post- pile specimens. Fig. 3-14 presents standard e-log σ'_v compression curves from CRS testing on pre-pile and post-pile specimens from all target depths. All of these compression curves are nonlinear over the large stress range measured during the tests.

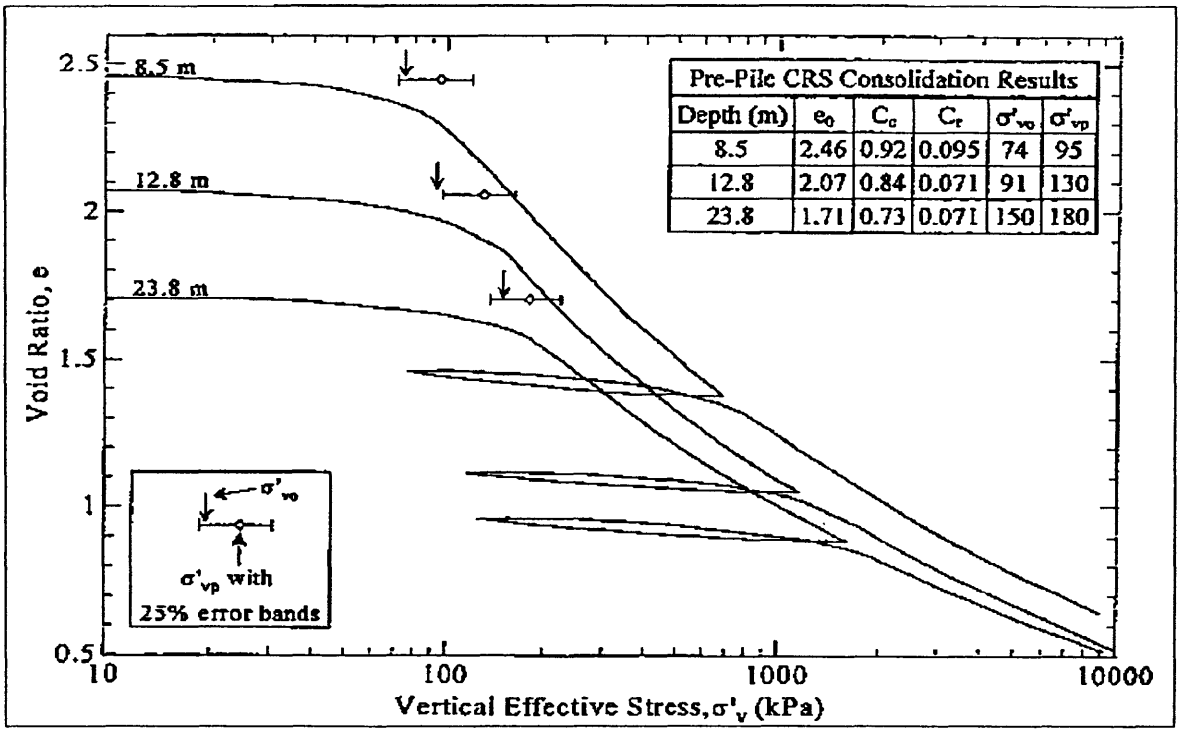

Figure 3-14 Constant rate of strain consolidation test on pre-pile specimens

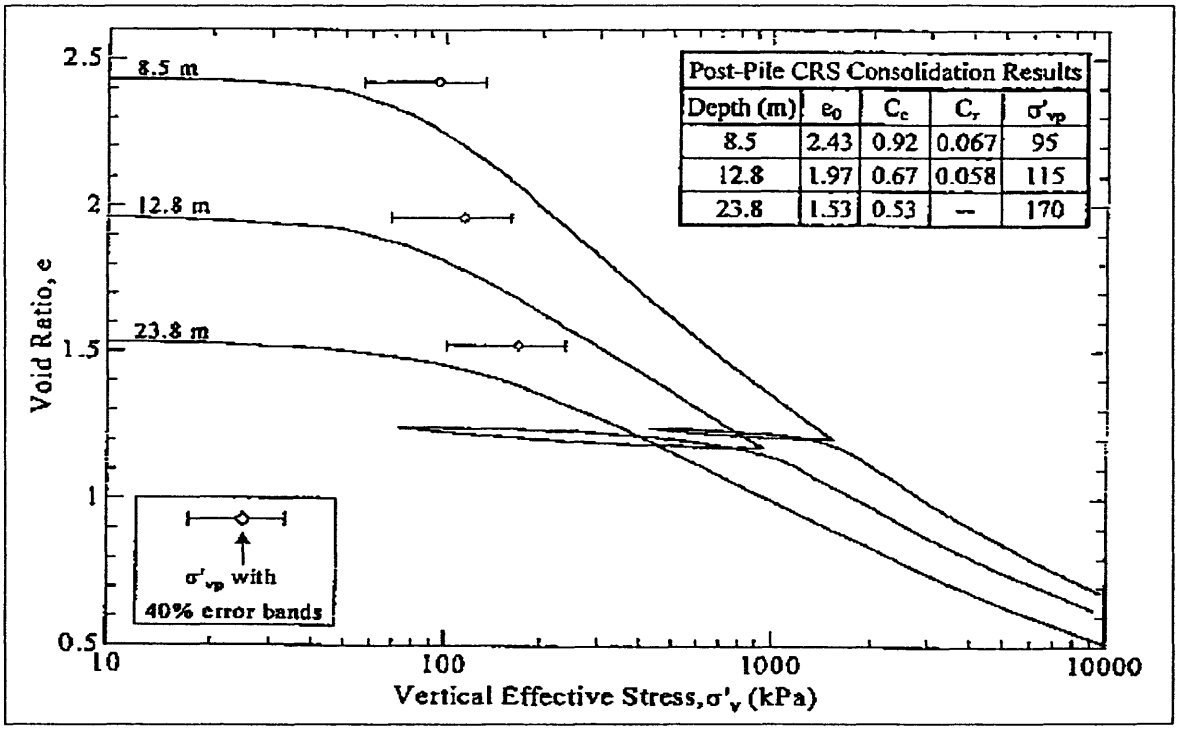

Figure 3-15 Constant rate of strain consolidation test on post-pile specimens

Values of initial effective stress reveal that the soil is lightly overconsolidated. The compression curves for the post-pile specimens show that values of C_c are shown to be equal to or lower than those measured in pre-pile tests. The values of the recompression index, C_r are slightly lower that in pre-pile tests.

The results show that the post-pile specimens begin at a lower void ratio than pre-pile specimens. Post-pile specimens exhibit a much longer transition period from recompression to virgin compression than pre-pile specimens. Post-pile *e*-log compression curves cross over and at high stresses become approximately parallel to pre-pile curves, though at slightly higher void ratios.

3.2.3 Triaxial radial consolidation testing

Radial consolidation tests were performed on pre- and post-pile specimens from a depth of 12.8 m. Two consolidation increments were applied in each test. The first was an isotropic increment from 25 to 120 kPa, followed by a 48 h recording period. This increment was equivalent to raising the mean effective stress of the pre-pile specimen through recompression and slightly beyond its in- situ maximum past pressure. The second increment was an isotropic increase from 120 to 220 kPa, followed by a 48 h recording period, and was targeted at the virgin compression stress range for the pre-pile specimen.

Figure 3-16 presents the measured axial strain versus square root of time during the first and second radial consolidation increment (25–120 kPa and 120–220 kPa respectively) for both pre- and post- pile specimens. Similar to the CRS test results, the post-pile

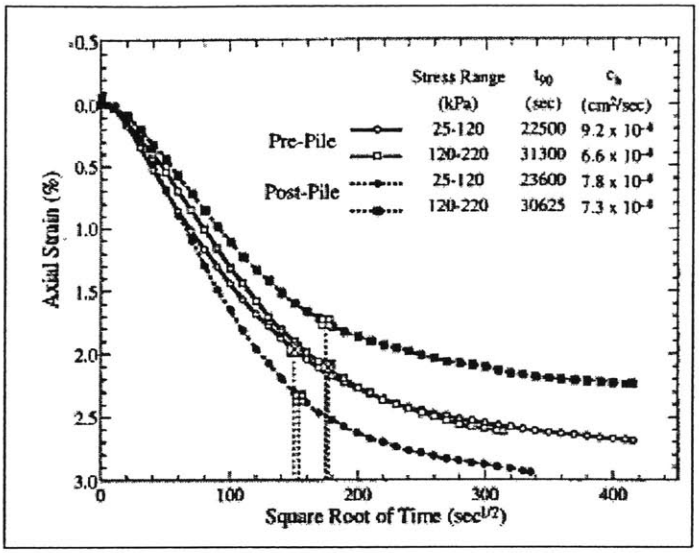

Figure 3-16 Results form triaxial radial isotropic consolidation tests

The post-pile specimen shows a softer response in the first radial consolidation increment. During the second consolidation increment, the pre-pile sample has entered the virgin compression range it strains more than the post-pile sample.

The initial virgin compression response of the pre-piles samples was softer than the post-pile samples that were still in the transition stage over the applied stress increment.

For the first increment, the horizontal layered pre-pile specimens shows a higher C_h value than the post-pile specimen which has been subjected to pile-induced distortion of its layering. For the second increment, the post-pile specimen now displays a higher value then the pre-pile specimen.

In the recompression regime, pre-pile specimens consolidate at a slightly faster rate than post-pile specimens, where as at higher stresses, post pile specimens consolidate at a somewhat slower rate than pre-pile specimens, primarily due to the gradual transition in the compression of post-pile specimens.

3.2.4 Triaxial strength testing

Triaxial strength testing was performed on pre- and post-pile specimens 15.25 cm in height and 7.25 cm in diameter. All specimens were consolidated anisotropically with a target K (σ'_h / σ'_v) of 0.62. This value corresponds to the coefficient of lateral earth pressure at rest for normally consolidated Bay Mud. Figure 3-17 presents the normalized deviatoric stress ($\sigma'_1 - \sigma'_2 / 2\sigma'_v$) and normalized pore pressure response versus axial strain plots for the normally consolidated tests.

The results show that when consolidated to approximate pre-pile in situ stresses, post-pile specimens show only slight increases in ultimate shear strength, but much higher ductility than equivalent pre-pile specimens. Test results indicate a complex response of post-pile specimens consolidated to near in-situ stresses. The initial stiff response may be a result of the imposed triaxial consolidation stresses, while the latter response may be the result of inherent and evolving anisotropy.

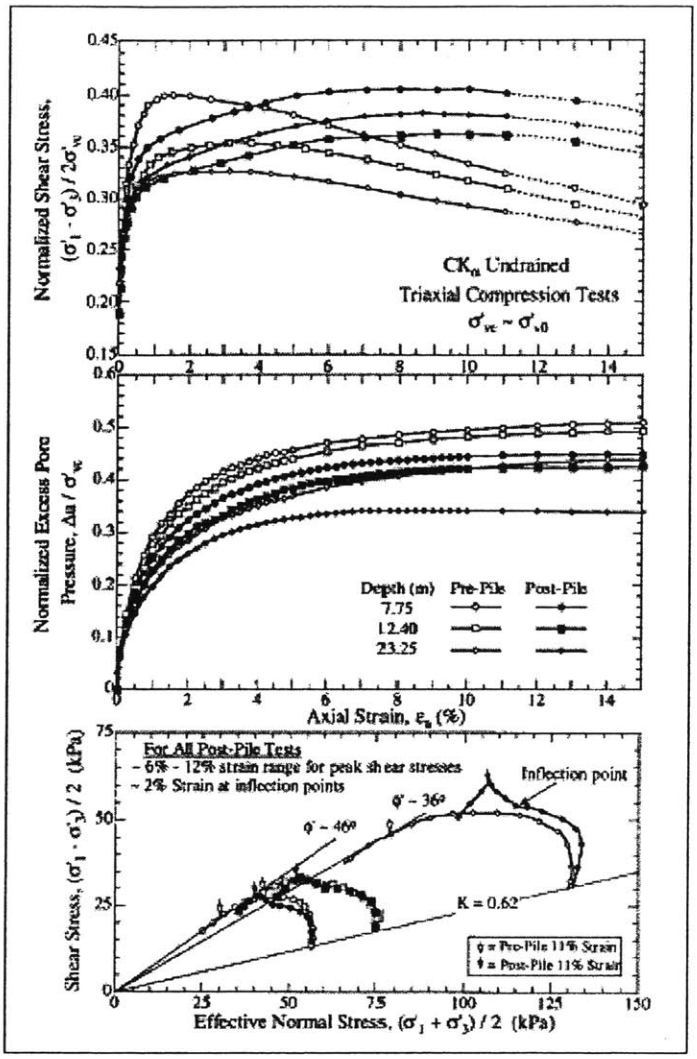

Figure 3-17 Stress-strain curves, pore pressure generation and stress paths for anisotropically consolidated triaxial tests to pre-pile in situ stress

Results for consolidation to three times pre-pile in-situ stresses are presented in Figure 3-18. At these higher consolidation stresses, all three post-pile specimens demonstrate slightly higher undrained strengths than their pre-pile counterparts. Failure strains continue to be higher for post-pile tests, but demonstrate less ductility than the post-pile specimens consolidated to approximate pre-pile stresses. It also shows that consolidation to approximately three times the in-situ vertical stress appears to erase most of the previous shear and consolidation stress history (i.e., pile driving). Post-pile failure strains are higher than pre-pile values, but demonstrate less ductility than the post-pile specimens consolidated to approximate pre-pile stresses.

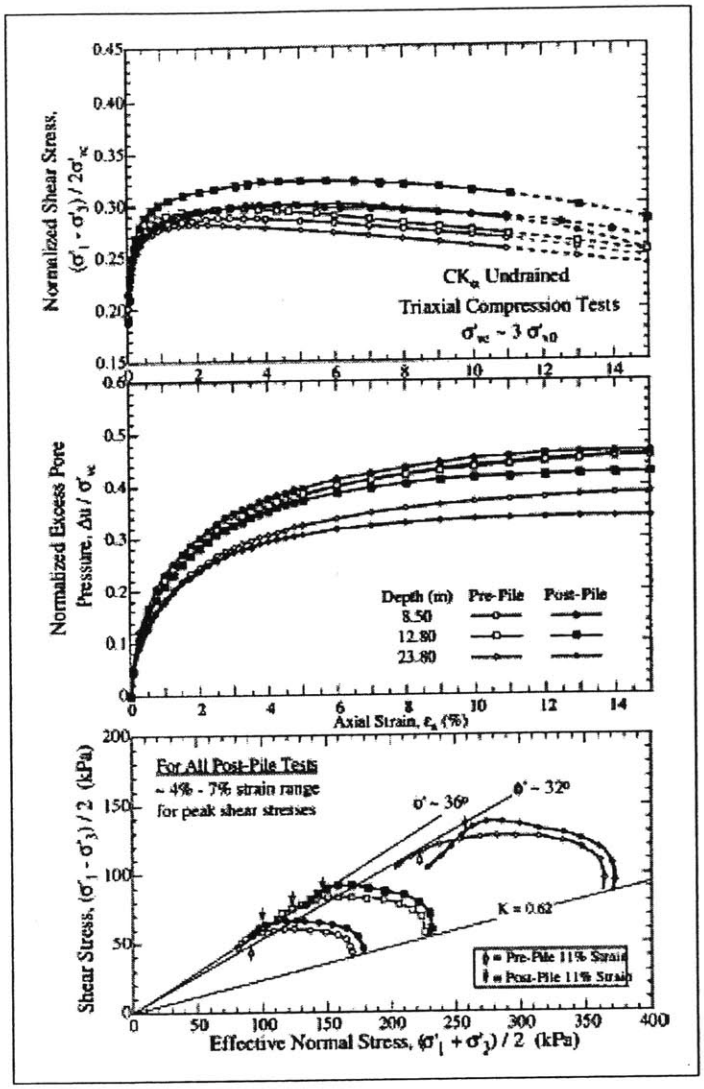

Figure 3-18 Stress-strain curves, pore pressure generation and stress paths for anisotropically consolidated triaxial tests to three times pre-pile in situ stress (SHANSEP type)

3.2.5 Direct simple shear

A total of six direct simple shear tests were performed on specimens from approximately 7.3 m depth. Three separate sets of tests were performed, each set consisting of a pre- and post-pile specimen, with constant height maintained throughout loading. The first set of tests was loaded monotonically at a rate of 10% strain per hour. The second set involved cyclic loading followed by monotonic loading to large strains. The third set of tests was performed on specimens that had been trimmed from samples extruded and lain sideways such that previously horizontal planes in the field were now oriented in a vertical direction. These specimens, referred to as transverse, were loaded monotonically at a rate of 10% strain per hour.

Fig. 3-19 shows the shear stress–strain and pore pressure generation plots for all six monotonic loading tests. Cyclic loading in the pre-pile specimen appears to have caused a slight reduction in strength compared to the ''monotonic only'' test. On the other hand, the transverse pre-pile specimens show a significant increase in strength. All three post-pile specimens present remarkably similar stress–strain curves, resulting in a higher ultimate strength than the normally oriented pre-pile specimens, and approximately equivalent strength to the pre-pile specimen with transverse orientation.

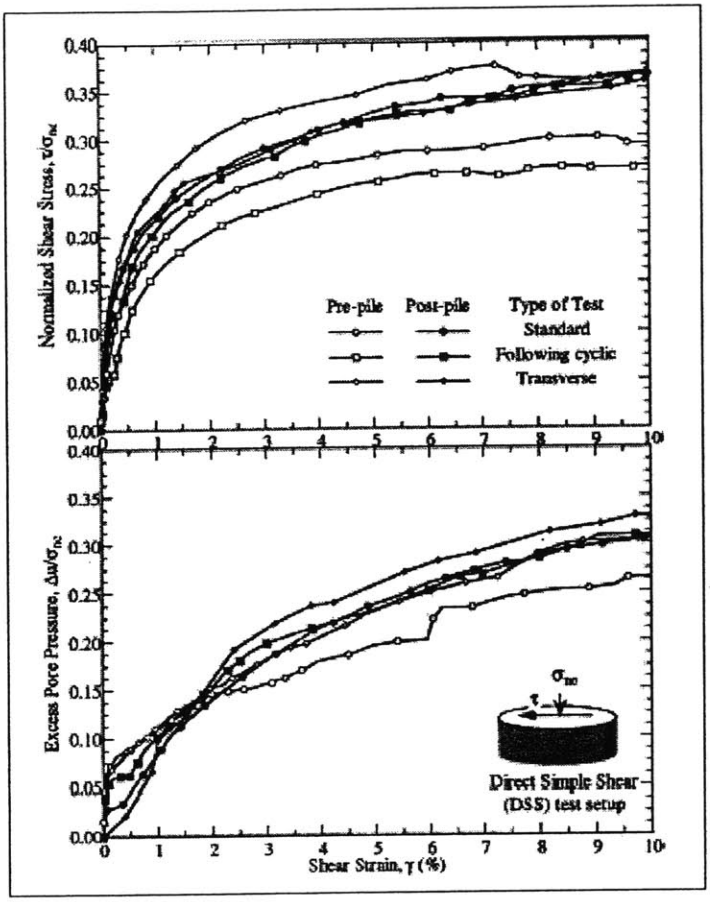

Figure 3-19 Shear stress-strain curves and pore pressure generated during monotonic direct simple tests

The results show that pre-pile shear strengths are dependent on specimen orientation, as transversely oriented specimens yield higher strengths than normally oriented specimens. In contrast, post-pile shear strengths appear to be nearly independent of normal versus transverse orientation, they have higher strengths than normally oriented pre-pile specimens, but are roughly equivalent to transversely oriented pre-pile specimens at large strains.

4 PREDICTION OF PILE BEHAVIOR IN BAY MUD

4.1 BACKGROUND

Hunts has modeled the stress variations during pile installation and subsequent pore pressure dissipation and he has compared the pore pressure, deformation and shear wave velocities with the field measurements. The results obtained by Hunt appear that cavity expansion may be a suitable tool for predicting stresses and deformation at some distance form the pile wall. However, pile response will be dictated most heavily by the stresses and soil properties in ties immediate vicinity and cavity expansion appears not to be well suited for this task. In addition, the cavity expansion predictions of pore pressure and stress adjacent to the pile wall influence the behavior of the model during the consolidation phase as pore pressures dissipated outward radially and the soil deforms inwards towards the pile. Thus it would seem that a more accurate representation of the pile induced strain field is necessary along with more advanced soil models that can capture the stain–softening response. Therefore, in this chapter, another approach which uses the strain path method and the advanced MIT-E3 soil model will be proposed to predict the change of pore pressure, stress and strain due to pile installation.

The approach used for the analysis is illustrated in the next section. The analysis involves the use of the strain path method with the combination of the MIT-E3 effective stresses soil model and non-linear finite element methods.

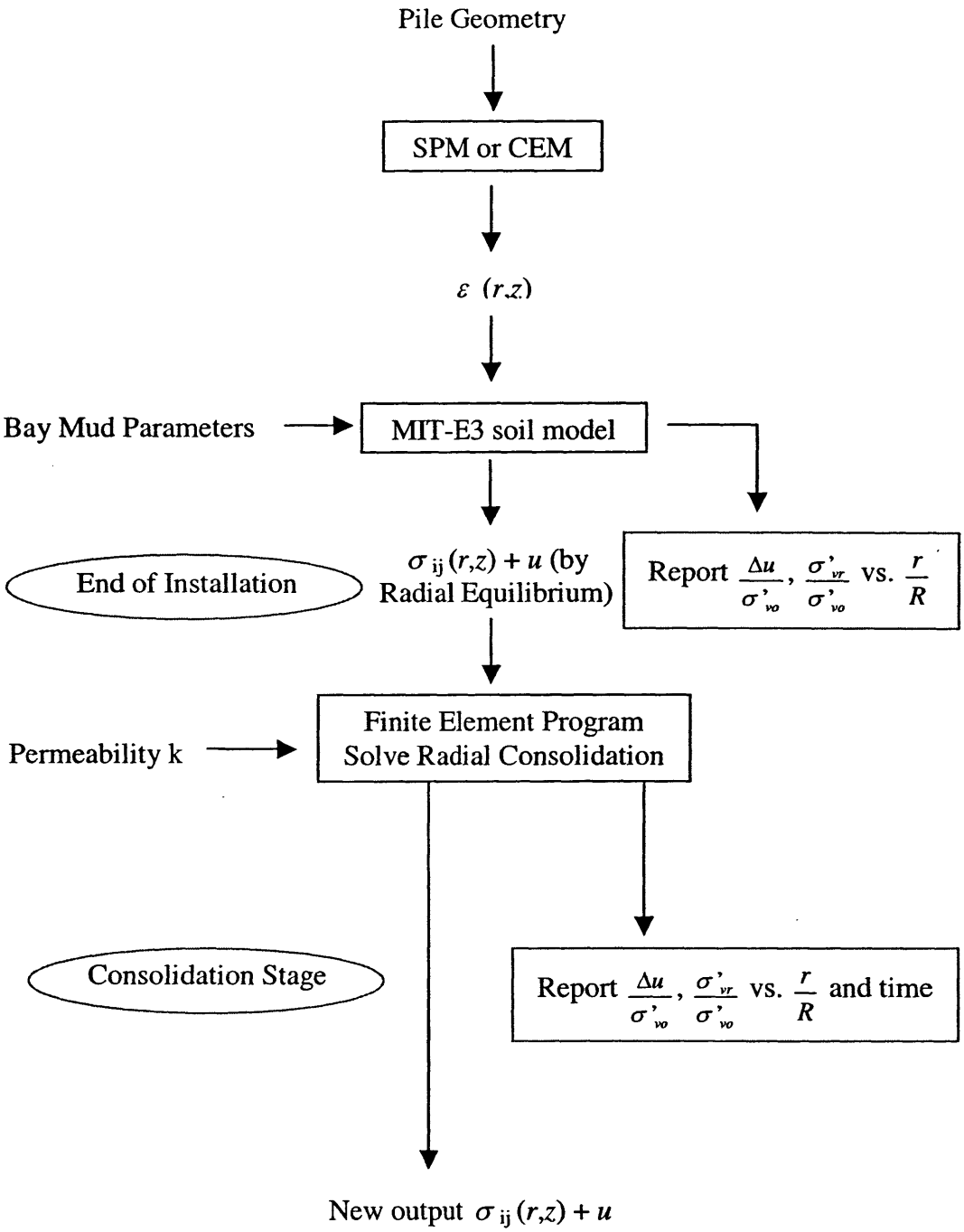

Figure 4-1 Flow chart of the proposed analysis

4.2 SELECTION OF MIT-E3 MODEL PARAMETERS

Site specific calibration of the MIT-E3 model requires selection of parameters listed in Table 4-1. The parameters listed in Table 4-1 were based on data from depth 12.8m. These parameters were selected with the help of Prof. Whittle. The methodology in parameter selection is as follows:

1. e_0 and λ were derived from the compression curve of the constant rate of strain consolidation test (CRSC) (Figure 3-14). With the assumption of a reference stress σ'_0 = 100 Pa and K = 0.61, i.e. with corresponding void ratio e_0 =1.9on the normal consolidation line. The value of λ can be obtained form the slope of the virgin compression curve.
2. Parameter C and n control the non-linearity in the volumetric response. These two parameters can be obtained via parametric studies of $\Delta\varepsilon_v$ versus OCR.
3. The *h* parameter describes the irrecoverable plastic strain that occurs after unloading/reloading cycle. An appropriate value of *h* must be obtained via parametric study. Although the parameter can affect reconsolidation around pile, there were no data available to provide a selection. Hence, h = 0.3 was chosen based on prior experience with clays of similar plasticity.
4. K_{ONC} is obtained form Hunt's data. It ranges from 0.60 to 0.62, hence, an average value of 0.61 is take.
5. $2G/K$ can be calculated from the equation

$$\frac{2G}{K} = \frac{3(1-2\upsilon')}{(1+\upsilon')}$$

Where υ'=0.3 is the elastic ratio at load reversal

6. ϕ'_{TC} and ϕ'_{TE} are the friction angles measured at the large strain in undrained triaxial compression and extension shear tests respectively. The value of ϕ'_{TC} is

based on SHANSEP type tests performed by Hunt (Figure 3-18) while ϕ'_{TE} was obtained using additional data supplied by Koutsottas (pes. comm.).

7. The c parameter defines the size of bounding surface (the semi axes ratio of the ellipse). This parameter can be obtained via the parametric studies of predicted undrained effective stress plots..
8. The S_t parameter essentially controls the post-peak shearing behavior and can be obtained via parametric study comparing the post-peak behavior of the predicted shearing behavior with that of the triaxial test.
9. The ω parameter controls the behavior at small strain levels during undrained triaxial shearing. The selected value ω=0.5 was chosen from shear stress-strain data presented by Hunt, and could be achieved if more detailed small strain stiffness data were to become available.
10. The γ parameter is related to the bounding plasticity. It can be determined by comparing the predicted undrained shearing behavior of consolidated clays with the triaxial test results. However, this data is not available from Hunt's thesis and again the parameter has been estimated from prior experience with similar clays.
11. κ_0 is the initial stiffness at load reversal point. It is related to G_{max} and K_{max}.

where $G_{max} = \frac{E'}{2(1+\nu')}$ and $K_{max} = \frac{E'}{3(1-2\nu')}$

The value of G_{max} can be measured from shear wave velocity v_s

$$G_{max} = \rho v_s^{\,2}$$

where ρ is the mass density $(1.5\times10^3 kg/m^3)$

v_s is the shear wave velocity $(85m/\sec)$

The value of K_{max} can be obtained from

$$\frac{G_{max}}{K_{max}} = \frac{3(1-2\upsilon')}{2(1+\upsilon')} = constant$$

Hence $\kappa_0 = \frac{(1+e_0)}{K_{max}}\sigma'_0\frac{G_{max}}{K_{max}}$

where e is the void ratio and $\sigma' = \frac{1}{3}(1 + 2K_0)\sigma'_v$

12. The ψ_0 parameter determines evolution and changes in size of yield surface. ψ_0 can be obtained via the parametric studies.

Table 4-1 presents the state variables used in the MIT-E3 soil model. The values in the bracket are obtained by prior research work.

Parameter	Depth of Interest 12.8m
e_0	1.90
λ	0.365
C	5.0
n	1.55
h	(0.3)
K_{0NC}	0.61
$2G/K$	0.923
ϕ'_{TC}	32°
ϕ'_{TE}	34°
c	0.95
S_t	2.5
ω	0.5
γ	(0.5)
κ_0	0.00734
ψ_0	(100)

( ) – No data. Value based on prior experience for Young Bay Mud

Table 4-1 MIT-E3 parameters

4.3 MIT-E3 MODEL PREDICTIONS

Figure 4-2, 4-3 and 4-4 show plots of the MIT-E3 model prediction used to compare with the results of undrained triaxial compression shear test (Figure 3-18). From the MIT-E3 prediction (figure 4-2), the peak value of the normalized deviatoric stress, q/σ'_{vo} (where $q = \sigma'_r - \sigma'_\theta$) is 0.59 which occurs at 1.5 % axial strain, ε_a while from the triaxial test (Figure 3-18), the peak value of q is also 0.59 which occurs at 3% axial strain, ε_a. Comparing at 10% axial strain, the predicted normalized deviatoric stress q/σ'_{vo} is 0.55 while the measured q/σ'_{vo} is 0.57.

From Figure 4-3, the predicted normalized pore pressure $\Delta u/\sigma'_{v0}$ at 10 % axial strain ε_a is 0.28 while the measured value from figure 3-18 is 0.41. The predicted values show good agreement with the measured data. In addition, with the strain softening behavior of Bay Mud, it shows the post-peak decreases in deviatoric stress and increases in pore pressure.

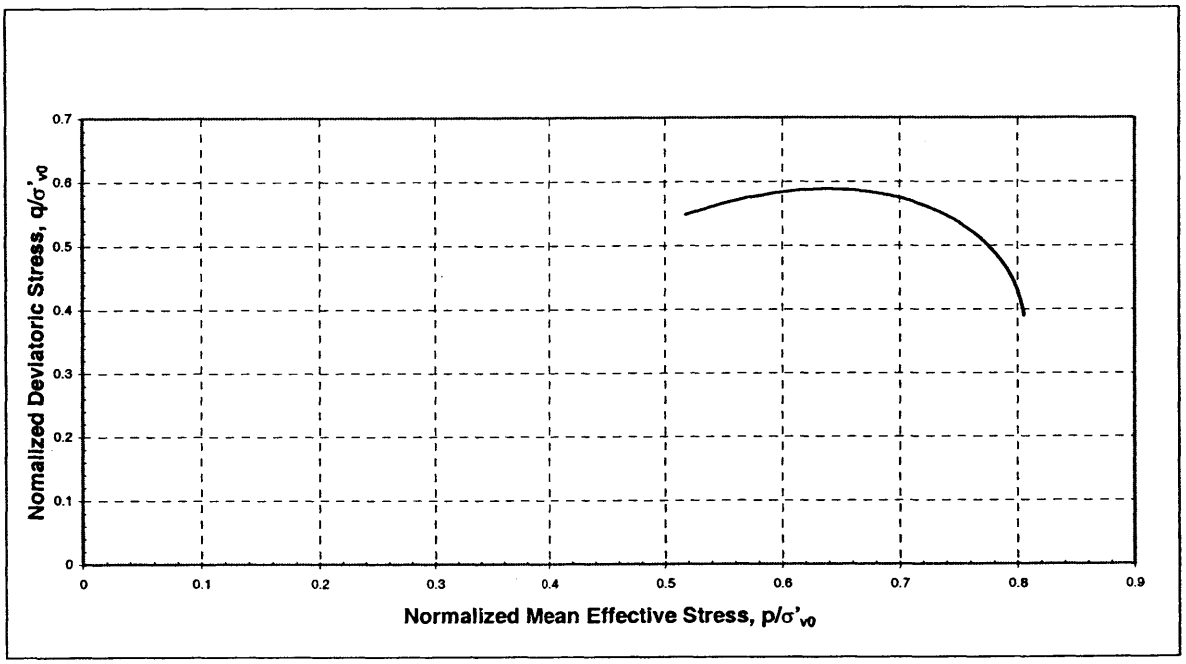

Figure 4-2 MIT-E3 model prediction of stress path for CK_0UC test on normally consolidated Buy Mud

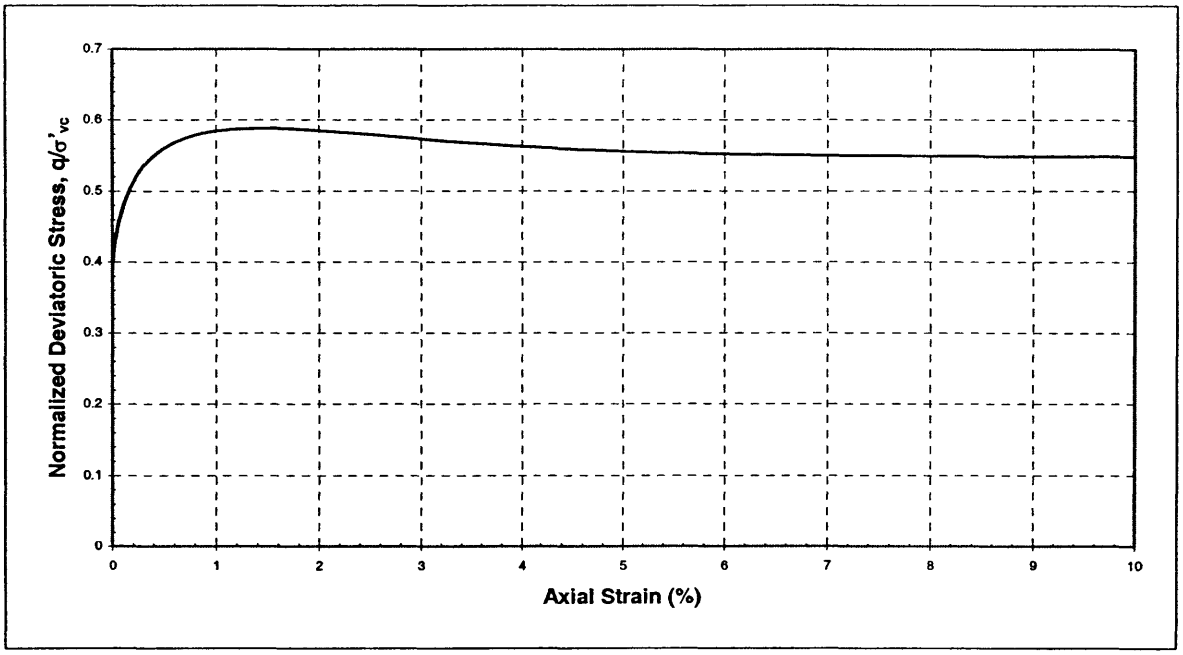

Figure 4-3 MIT-E3 model prediction of normalized deviatoric stress versus axial strain for CK_0UC test on normally consolidated Buy Mud

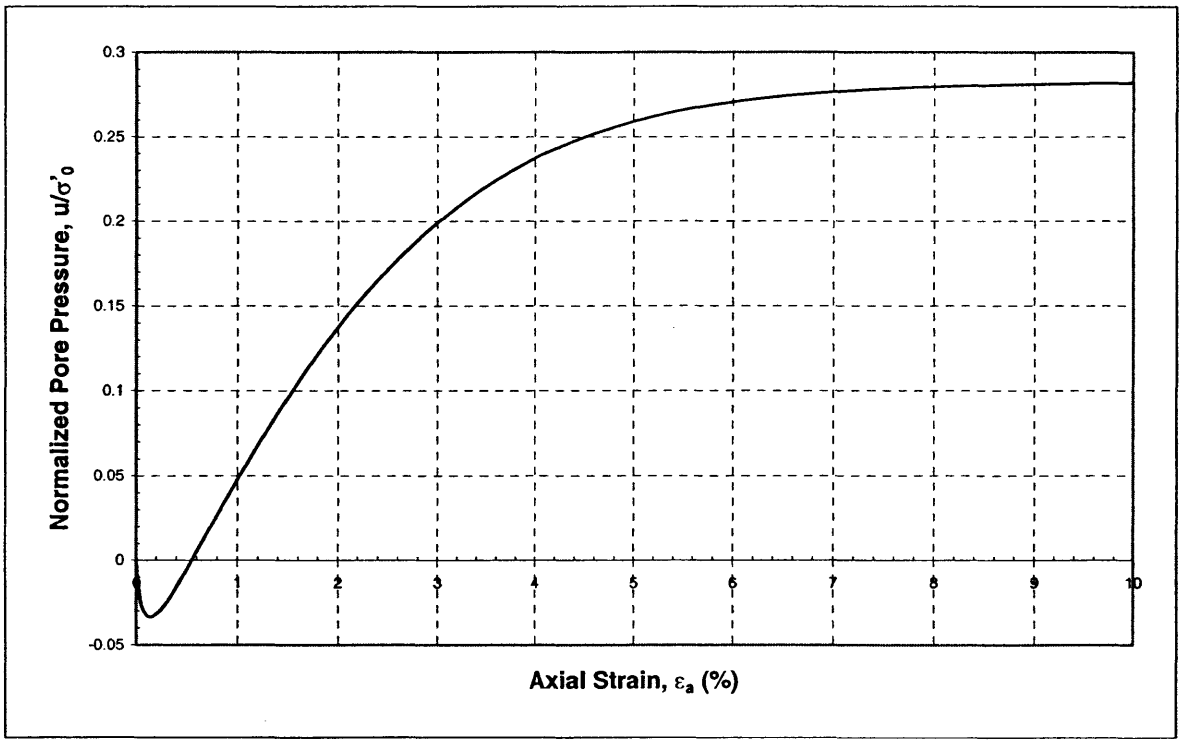

Figure 4-4 MIT-E3 model prediction1 of normalized deviatoric stress versus axial strain for CK_0UC test on normally consolidated Buy Mud

Figure 4-5 and 4-6 show plots of the MIT-E3 model prediction used to compare with the results of a monotonic simple direct shear test from 7.3 m depth (Figure 3-19). From the MIT-E3 predictions, the shape of predicted shear stress curve follows closely to that of the measured curves. Both of them appear to level off after approximately 6% strain. Comparing at 10% shear strain, the predicted normalized shear stress τ / σ'_{v0} is 0.26 (Figure 4-5) while the measured τ / σ'_{v0} is about 0.28.

Pore pressure predicted during monotonic loading is plotted in Figure 4-6. At approximately 2% strain, the curve shows a bending which corresponds to the yielding strain. The predicted normalized pore pressure $\Delta u / \sigma'_{v0}$ at 10 % shear strain γ is 0.23 while the measured $\Delta u / \sigma'_{v0}$ from Figure 3-19 is about 0.30. The predicted values show good agreement with the measured data.

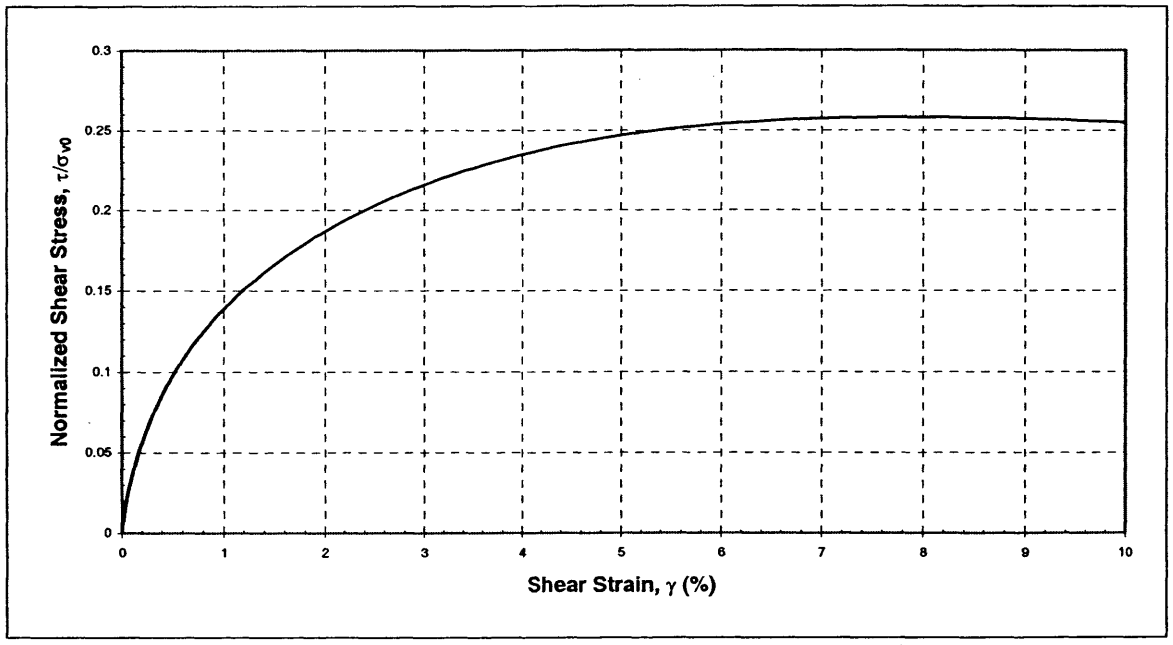

Figure 4-5 Predicted Shear Stress versus shear strain

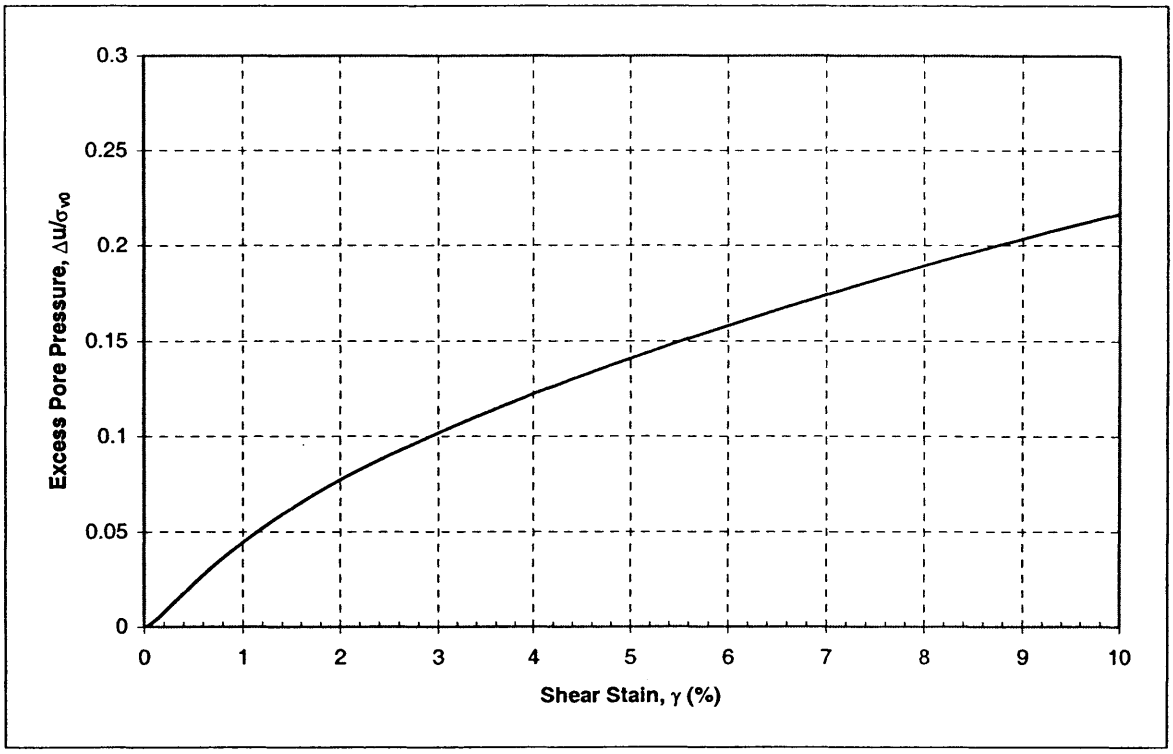

Figure 4-6 Predicted pore pressure versus shear strain

4.4 HYDRAULIC CONDUCTIVITY

Figure 4-7 presents predictions of pore pressure dissipation for piezocone tests. The pore pressure ratio $U = \Delta u/\Delta u_i$ is plotted as a function of the dimensionless time factor T

$$T = \frac{k\sigma'_p t}{\gamma_w R^2_{eq}} \text{ (equation in P.16)}$$

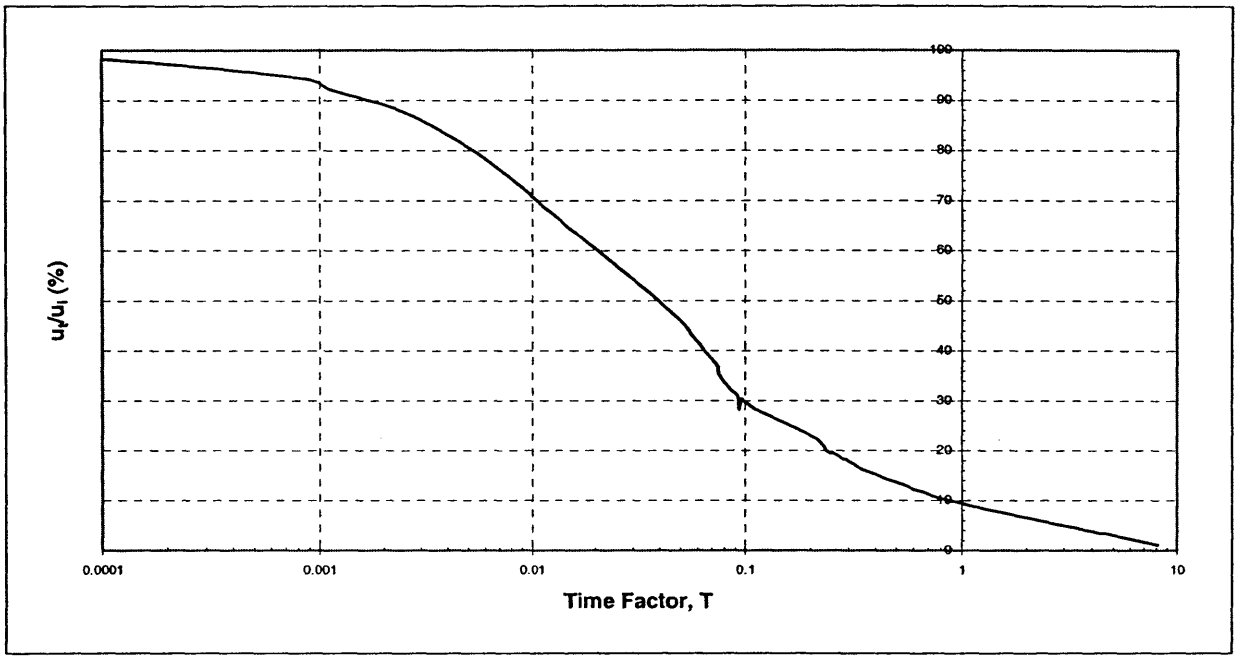

Figure 4-7 Predicted dissipation of pore pressure

Two piezocone dissipation tests were performed by Hunt (2000). The tests were performed in the upper and lower clay layers to estimate the required time for dissipation of penetration induced pore pressures from full scale pile installation. Figure 4-8 shows the results of the tests plotted as measured pore pressure versus log time scales. It is interesting to note that the two dissipation curves almost exactly overlap each other. It shows that the permeability of soil changes with depth.

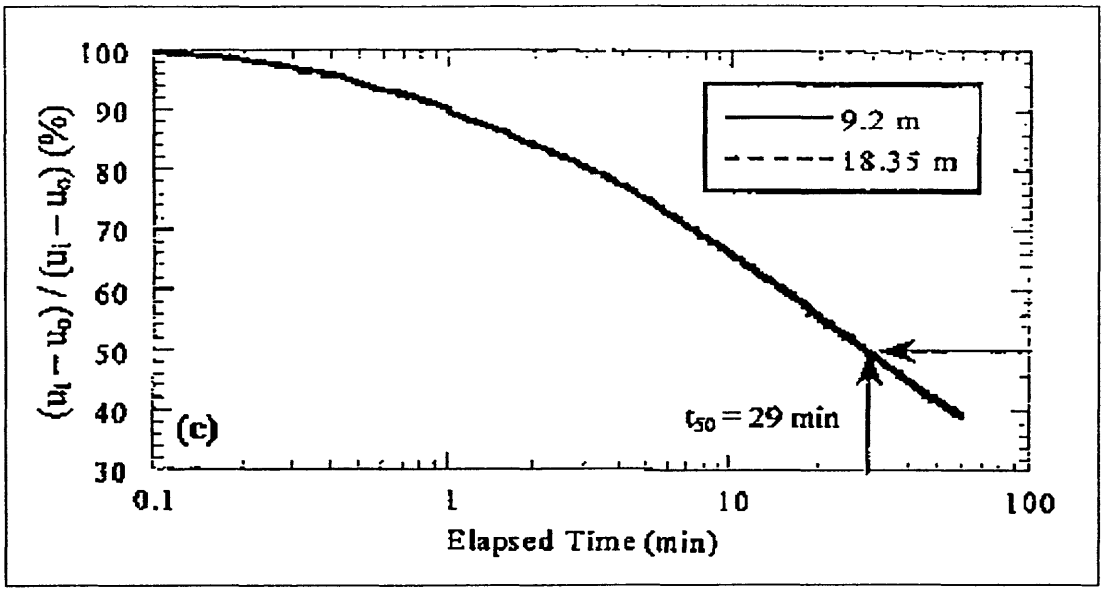

Figure 4-8 SCPTU-2 Dissipation tests

The permeability of soil can be obtained by making use of the results of the predicted and the measured pore water dissipation. As

$$T_{50} = \frac{kt_{50}\sigma'}{\gamma_w R^2}$$

$$k = \frac{\gamma_w R^2}{\sigma'} \frac{T_{50}}{t_{50}}$$

where $T_{50} = 0.04$ from Figure 4-2

t_{50} = 29 min from Figure 4-3

γ_w is unit weight of water (9.81 kN/m^3)

R is the radius of cone penetrometer (1.784 cm)

$$\sigma' = \frac{1}{3}(1 + 2K_0)\sigma'_{vo}$$

Hence the soil permeability can be estimated from the field data at given depth 9.2 m and 18.35 m, the permeability of soil is 7.0×10^{-8} m/min and 4.0×10^{-8} m/min respectively. Hence, the average value of soil permeability at depth 12.8 m is about 6.0×10^{-8} m/min. Hunt used an approximate value of 1×10^{-7} m/min which is relatively a good estimate. With this information, the input value of soil permeability required by the finite element can be confirmed.

4.5 PREDICTIONS OF PILE PERFORMANCE

4.5.1 Predictions of Pile Installation

In this section, predictions of radial effective stresses and pore pressures at various distances around the shaft will be presented. The stresses components are normalized by the in-situ vertical effective stresses σ'_{vo} while the radial dimensions, r, are normalized by the radius, R. The two principal parameters that are of interest in this analyses are normalized excess pore pressures $\frac{\Delta u}{\sigma'_{vo}}$ and the radial effective stress $\frac{\sigma'_{rr}}{\sigma'_{vo}}$.

Figure 4-9 shows the three principal effective stresses (σ'_r, σ'_θ and σ'_z) and the generated pore pressure (u) relative to the logarithm of the normalized radial distance form the pile center, r/R (R = pile radius). Initial stress values are seen to exist at large distances from the pile, with decreases in $\sigma'_r, \sigma'_\theta$ and σ'_z occurring at lesser distances. Soil within approximately $r/R = 4$ are at failure and show σ'_r as the major principal stress, σ'_θ as the minor principal stress and σ'_z as the intermediate principal stress. The radial stress σ'_r and tangential stress σ'_θ should have the same magnitude in the far field since the effect of pile installation becomes insignificant at large distance from pile.

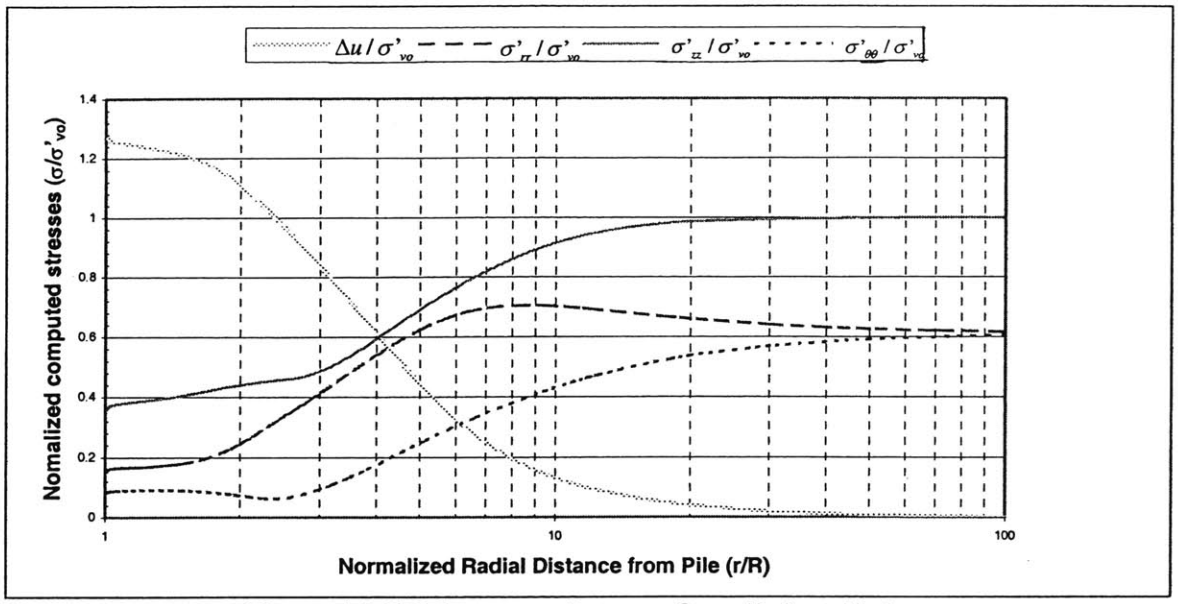

Figure 4-9 SPM computed stress after pile installation

For the pore pressure, from figure 4-9, it shows that pore pressure rise during pile installation, with the largest values occurring adjacent to the pile wall u_i/σ'_{vo}=1.28. Peak pore pressure at the soil-pile interface is greater than the in-situ overburden effective stress. Significant pore pressure increases have been predicted at distances exceeding ten-pile radius from the pile surface.

The results show that

1. The excess pore pressures at the shaft increase.
2. There is a large decrease in the radial effective stress close to the pile shaft.
3. The radial effective stress is similar in magnitude to the mean effective stress

4.5.2 Prediction of Set-Up

The principal parameters concerned in this part are radial effective stress acting on the pile shaft after full dissipation of excess pore pressures. Stresses after full dissipation of pre pressures are shown in Figure 4-10 and indicate significant increases in σ'_r and σ'_θ and partial recovery of σ'_z near the pile face. Physical constraints imposed by stationary pile surface have created a condition in which σ'_r remains the major principal

stress and σ'_θ and σ'_z are equal at the pile face. Again the radial stress σ'_r stays the same as the tangential stress σ'_θ at far field.

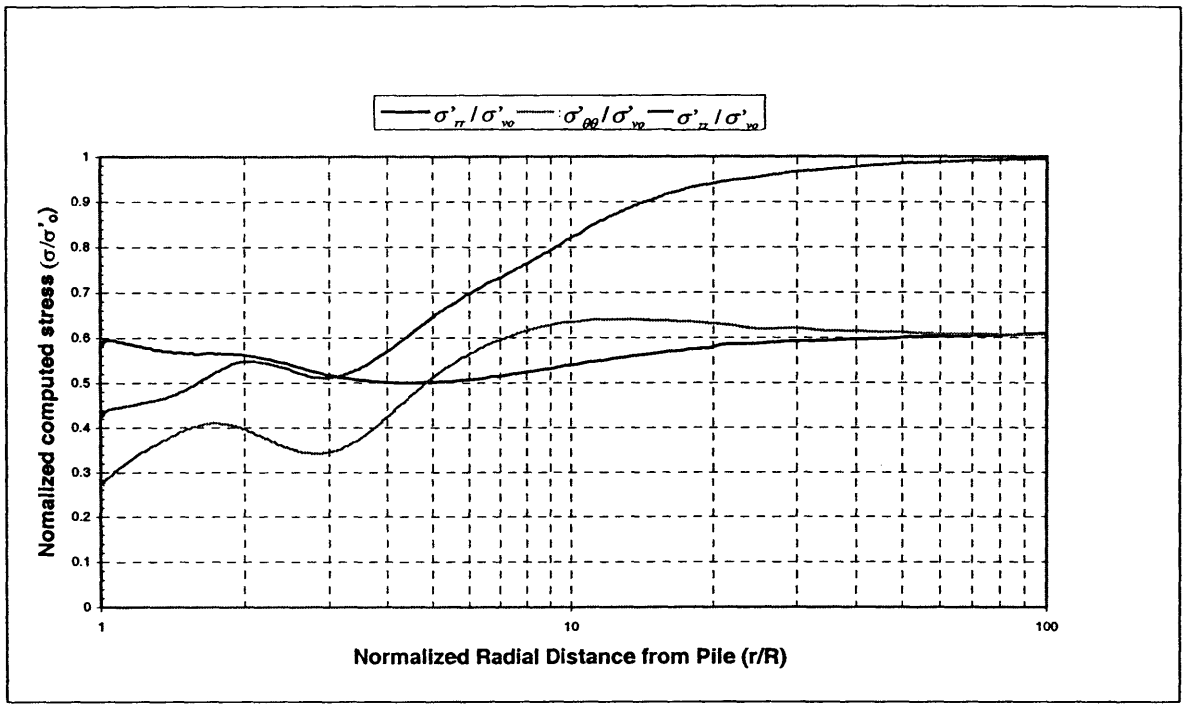

Figure 4-10 SPM computed stress after consolidation

The results show that

1. The predictions are generally in good agreement with the measured set-up data
2. The predicted set-up stresses are generally lower than other at the initial stage before the installation of pile
3. There is no excess pore pressure at the end of consolidation

4.5.3 Stress changes during installation and consolidation

Figure 4-11, 4-12 and 4-13 present plots of the variation during consolidation of σ'_r, σ'_θ and σ'_z respectively, versus the normalized radial distance form the pile. At the point adjacent to the pile face, there is a large increase in σ'_r and σ'_θ and with a lesser increase in σ'_z during consolidation. It shows that the effect of pile installation mainly occurs in horizontal direction than in the vertical direction. It is important to note that the value of stresses at far field should be the same during installation and consolidation as the effect of pile installation is insignificant away from pile.

It is expected that the stress increase as the pore pressure decrease during consolidation. However, it is worth noting that the effective radial stresses, σ'_r tend to decrease. It is because the pore pressure travels outward from the pile face pass through the outer area.

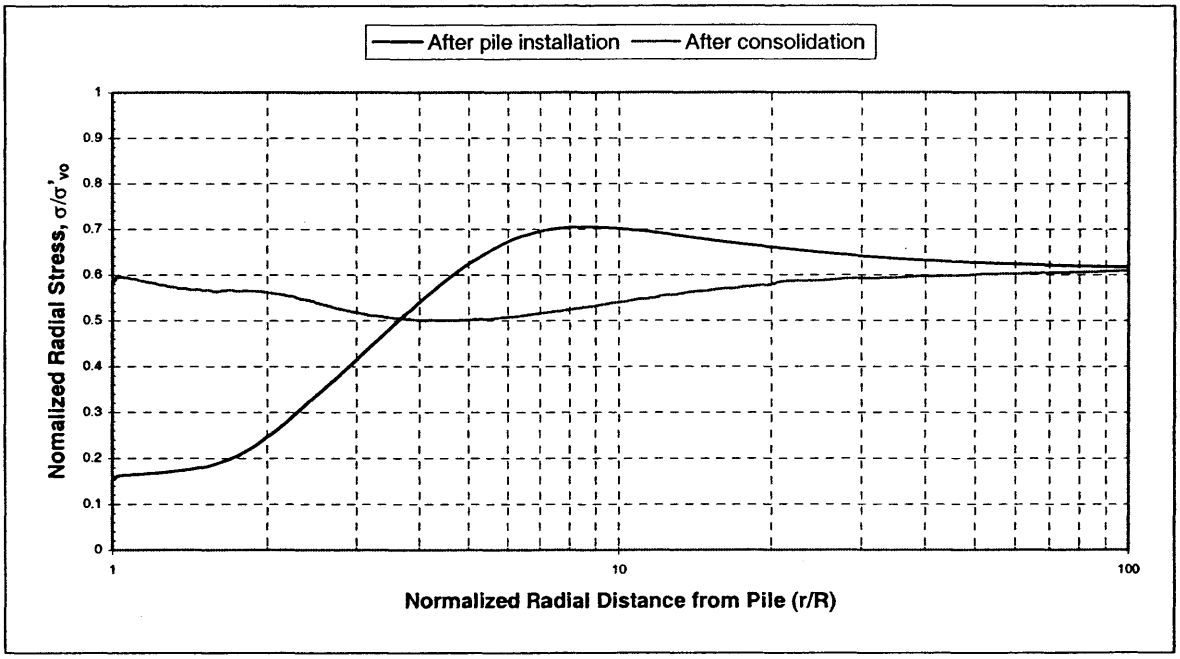

Figure 4-11 Effective radial stresses during post-pile consolidation

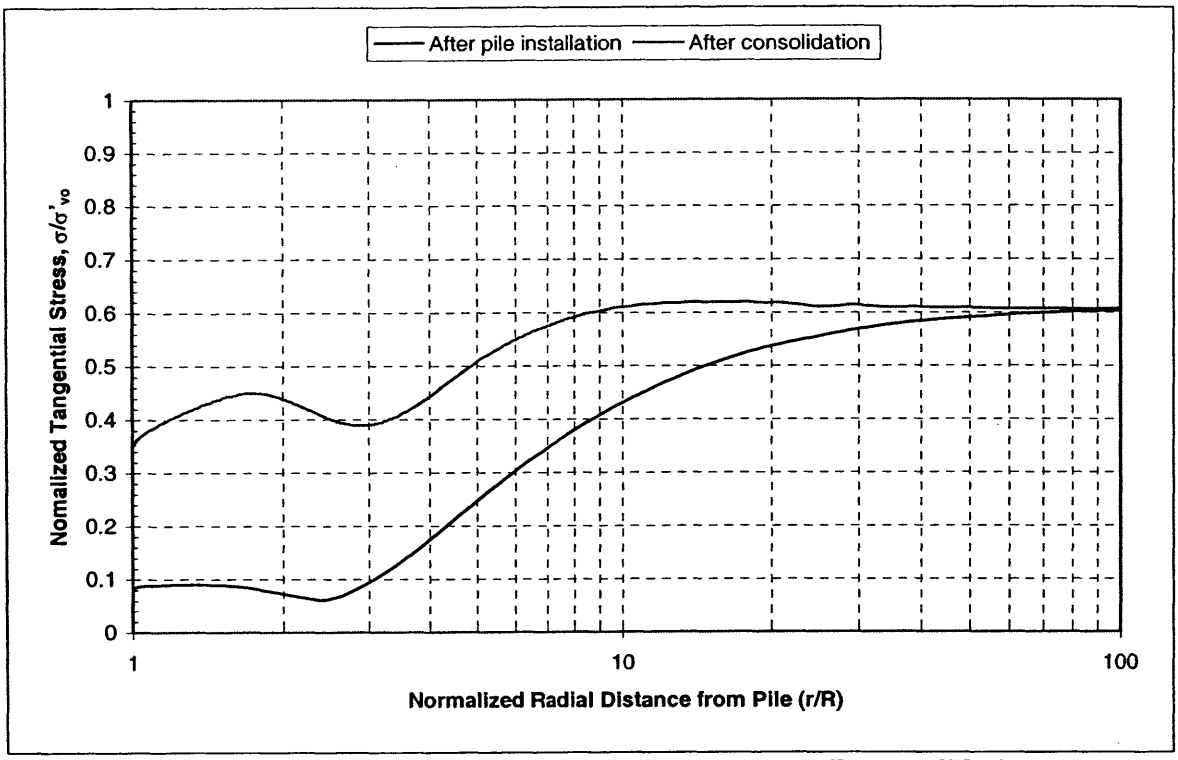

Figure 4-12 Effective tangential stresses during post-pile consolidation

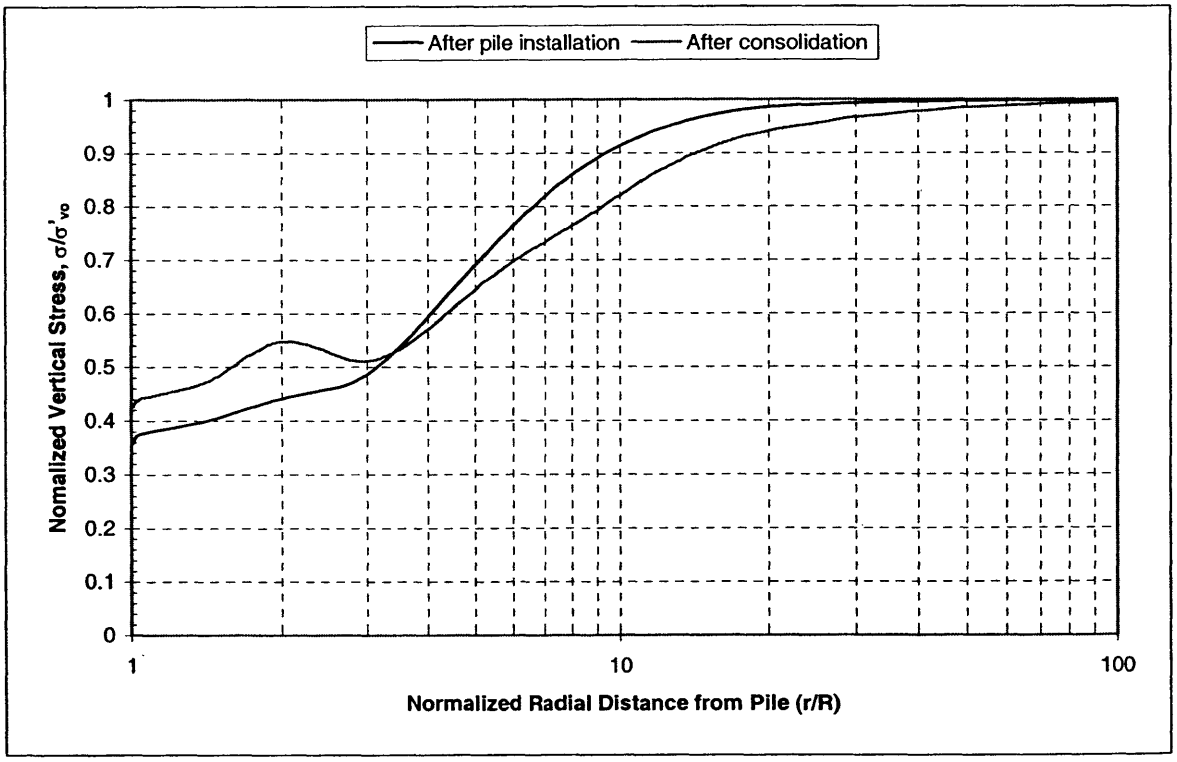

Figure 4-13 Effective vertical stresses during post-pile consolidation

Figure 4-14 shows the change of radial stresses, σ'_r and pore pressure, Δu versus log time factor, T. It agrees with the expectation that the radial stress increases when the excess pore pressure dissipates. The rate of dissipation increases at the beginning and decreases at the end of consolidation. The results also show that there is a net decrease of total radial stress, σ_r during consolidation.

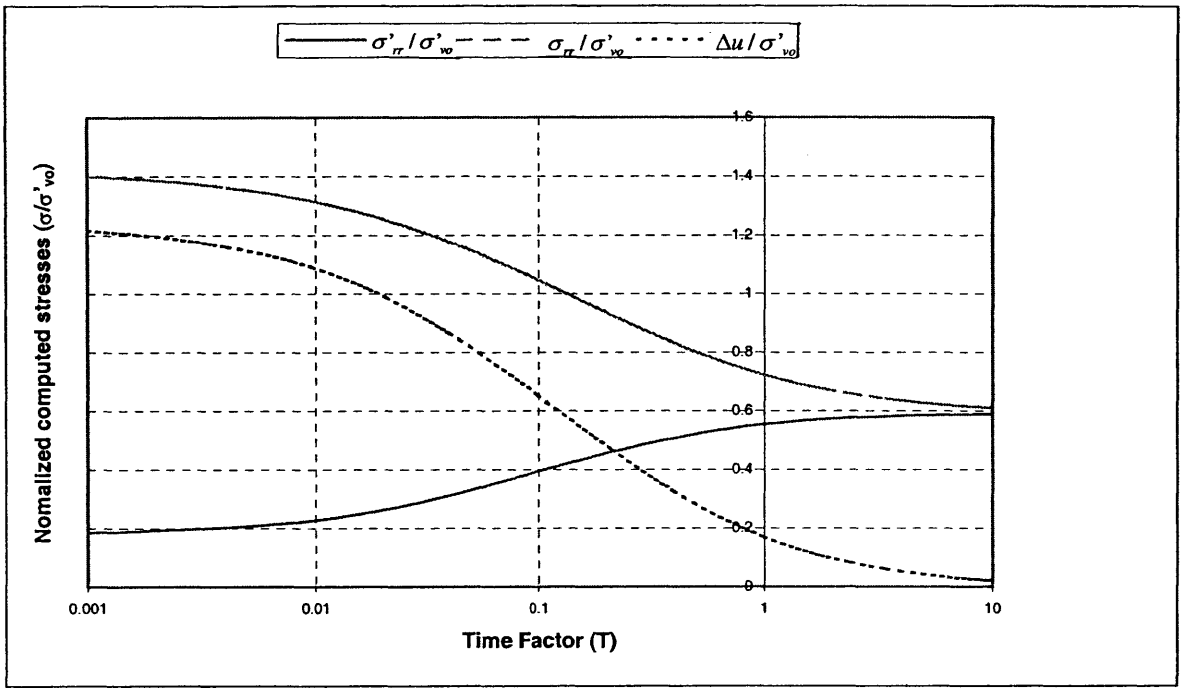

Figure 4-14 Change of stresses and pore pressure during consolidation

Further understanding of set-up behavior of pile can be obtained by plotting the excess pore pressure $\frac{\Delta u}{\Delta u_i}$, the set-up stress ratio $\frac{K}{K_c}$ (where $K = \frac{\sigma'_{rr}}{\sigma'_{v0}}$) and the total stress release ratio $\frac{H}{H_i}$ (where $H = \sigma_{rr} - u_0$) as shown in Figure 4-15.

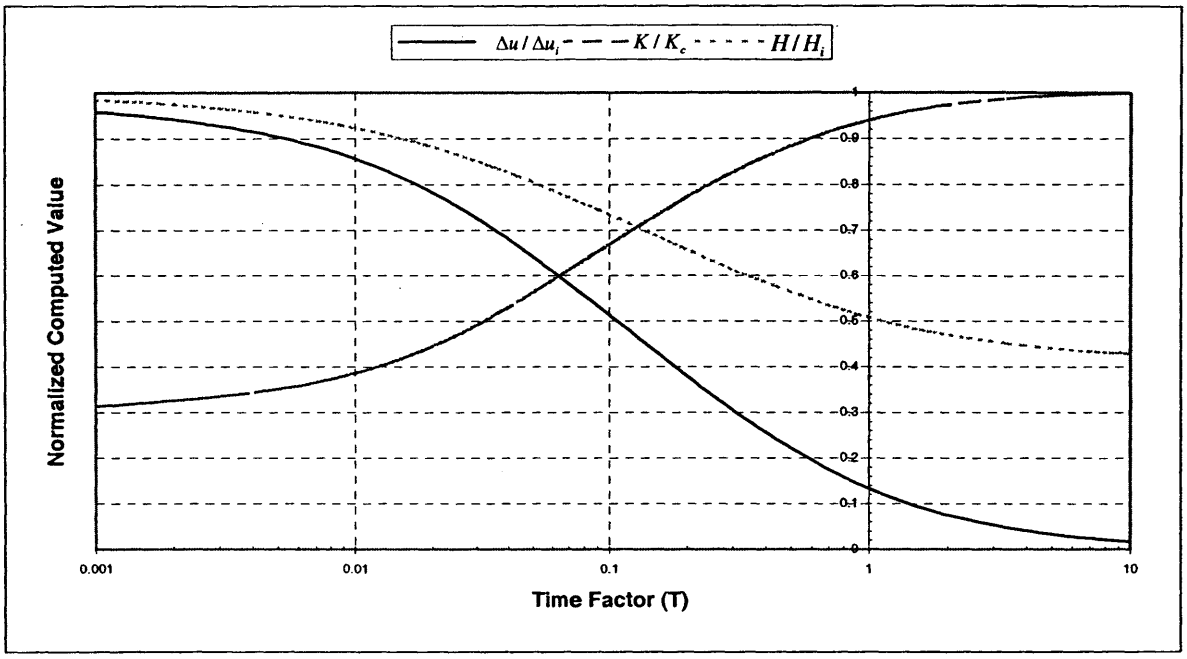

Figure 4-15 Change of soil behavior and pore pressure during consolidation

4.5.4 Strain and return deflection after consolidation

Figure 4-16 shows the SPM radial strain for R = 30.5 cm. This radial strain is obtained from the closed form solution. The results show that the maximum radial strain occurs at the point closet to the pile and the radial strain decreases exponential against radial distance from the pile.

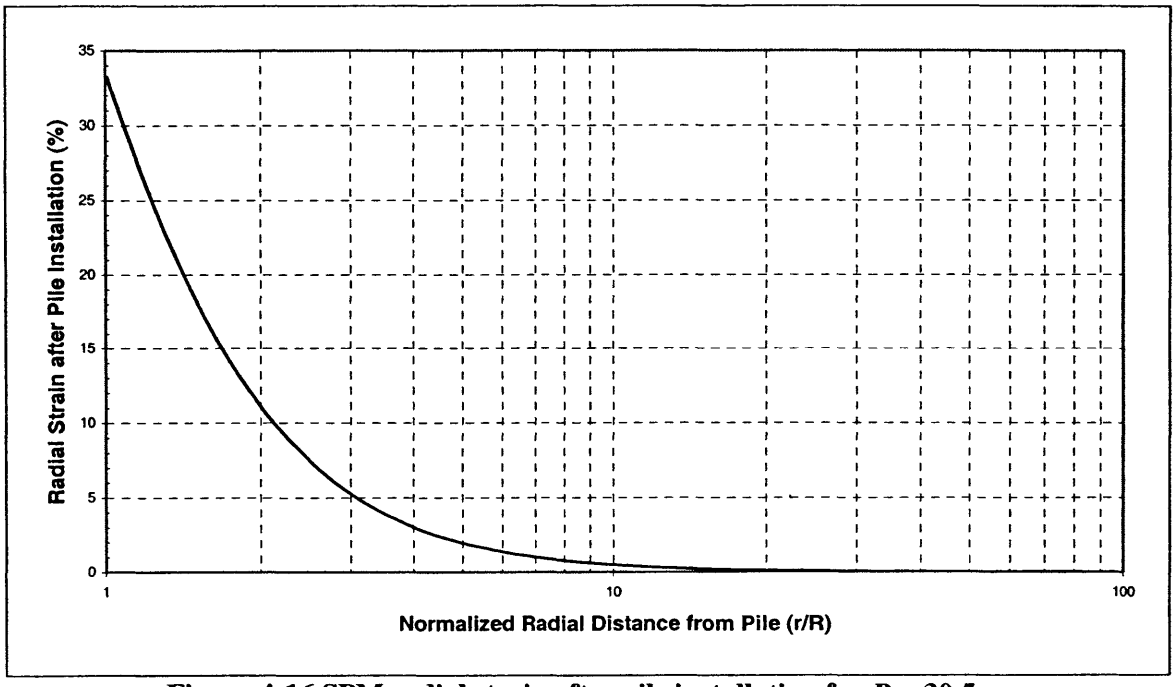

Figure 4-16 SPM radial strain after pile installation for R = 30.5cm

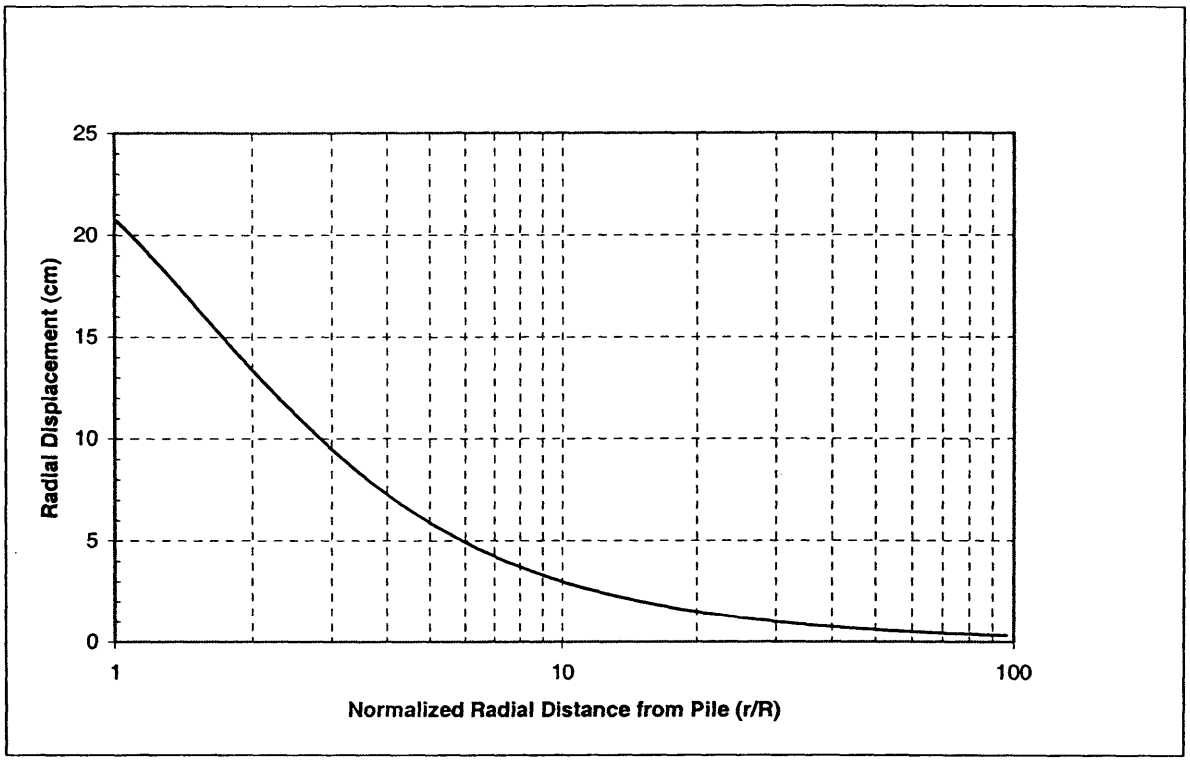

Figure 4-17 SPM radial displacement after pile installation for R = 30.5cm

Figure 4-18 shows the state of strain at the end of consolidation. It has been found that the radial strain on the pile surface is much larger than the vertical and tangential strain which agrees with argument that as pile is installed there will be a significant radial deformation in soil while the vertical deformation is relatively less. Besides, it shows that lateral deformations decrease with increasing distance from the pile. Again it shows that the effect on strain on far field is insignificant.

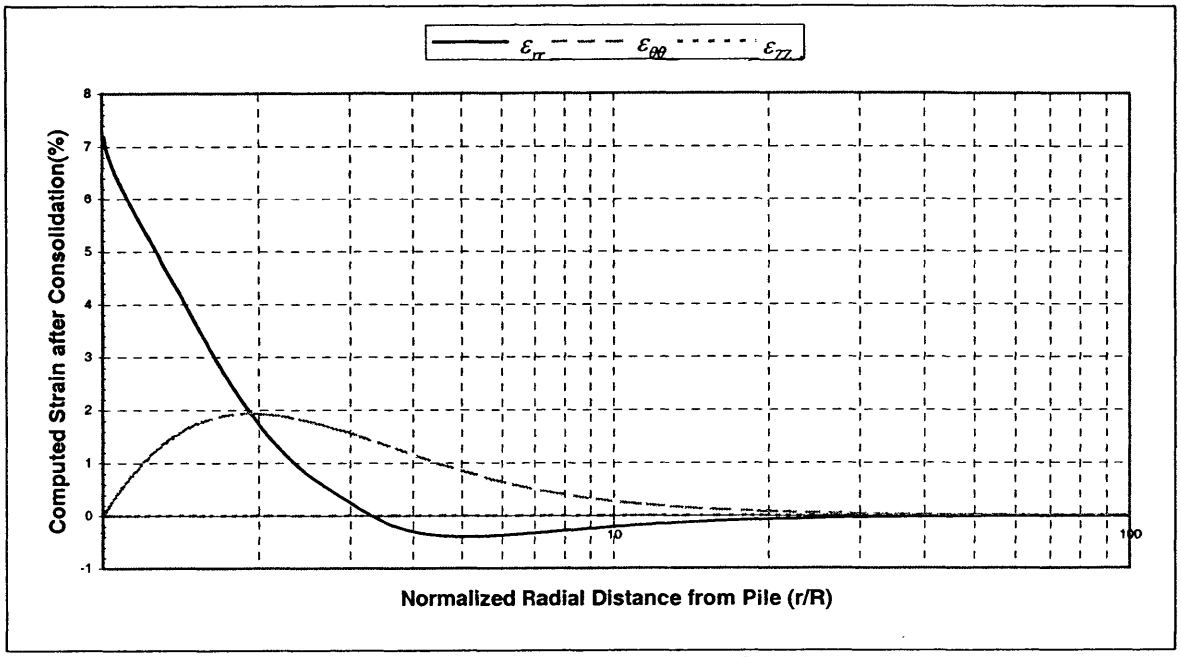

Figure 4-18 State of strain at the end of consolidation

Figure 4-19 shows the prediction of consolidation return deflection for analysis at 12.8m. The return deflection is the difference between the displacement after pile installation and displacement after consolidation. The peak return deflection occurs at approximately normalized radial distance 3.3.

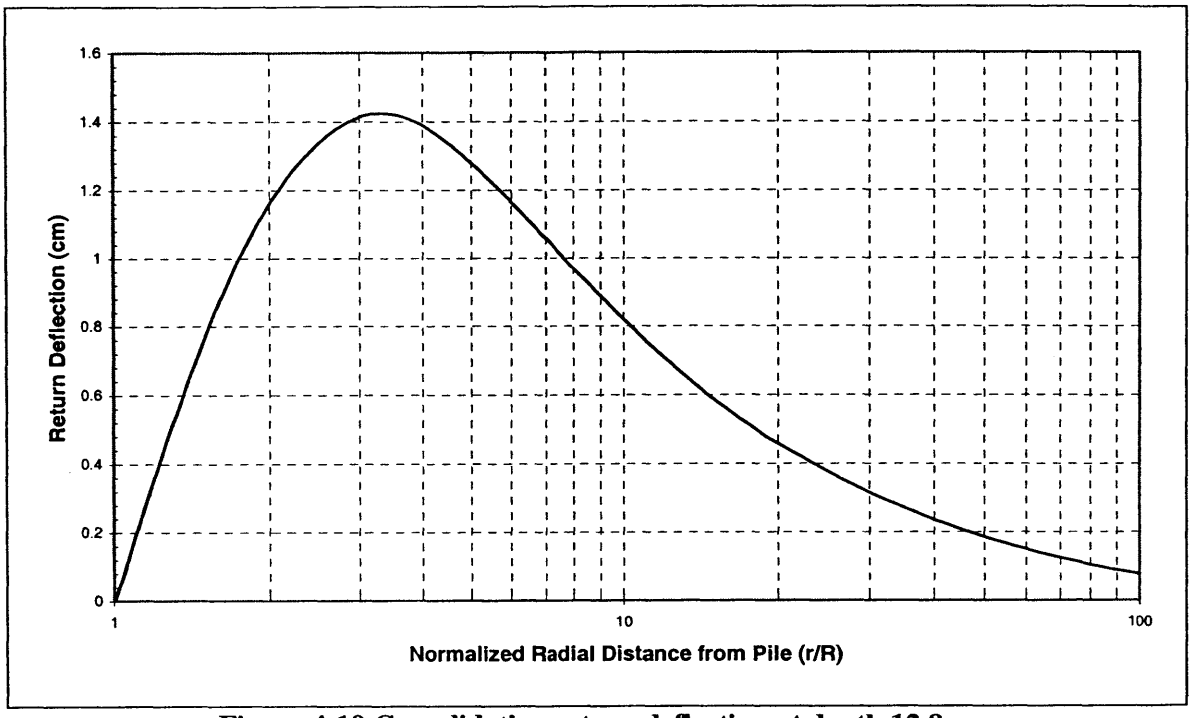

Figure 4-19 Consolidation return deflection at depth 12.8m

4.5.5 Prediction of consolidation at different distance to the pile

Predicted values of normalized excess pore pressure are presented in Figure 4-20. The radial distances of B-1, B-2, B-3, B-4 and B-5 are0.855 m, 1.465 m, 2.375 m, 1.065 m and 1.605 m respectively. It is apparent that significant pore pressures were generated at all radial distances (at different boreholes). In addition, the far borehole displays the slowest dissipation time. This can be explained by the radial dissipation path away from the pile, in which flow of pore water from the near borehole must pass by the far borehole, thus adding the pore pressure they have to dissipate.

From Figure 4-21, it shows that the borehole near to the pile all generated higher pore pressures than those at greater distance. Basically the dissipation time for generated pore pressure is highly dependent on the soil properties and the size of the pile.

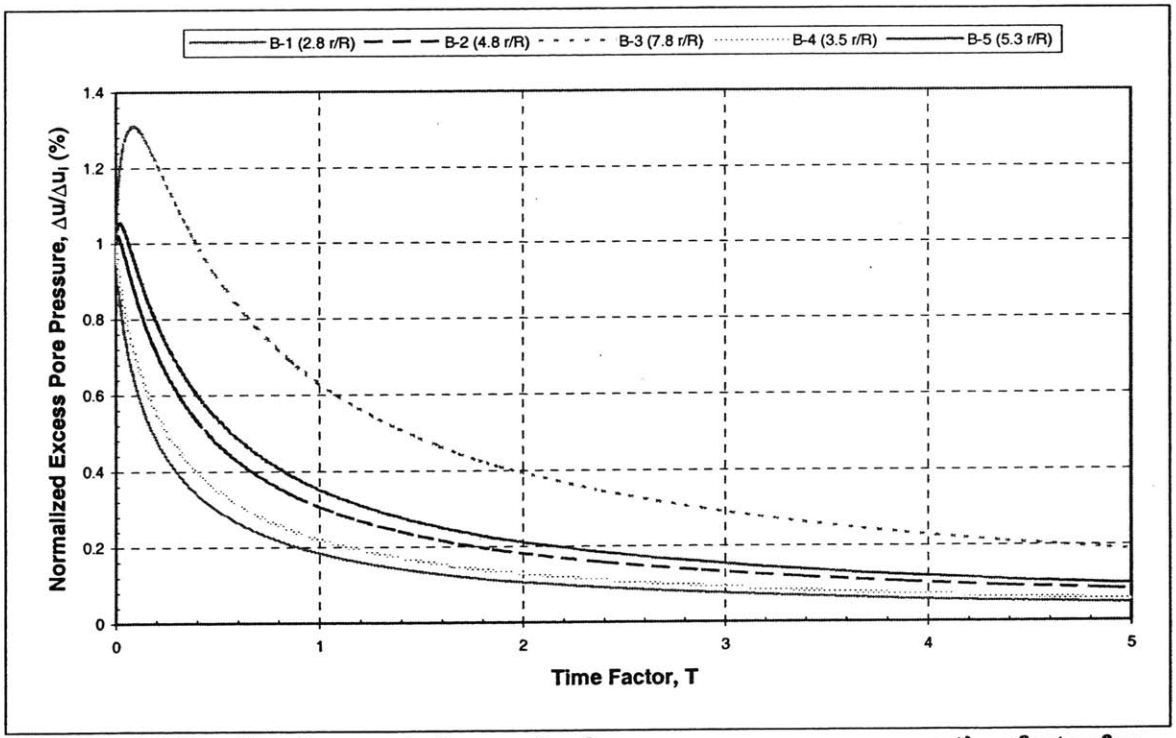

Figure 4-20 Predicted percent of normalized excess pore pressure versus time factor for boreholes B-1 to B-5

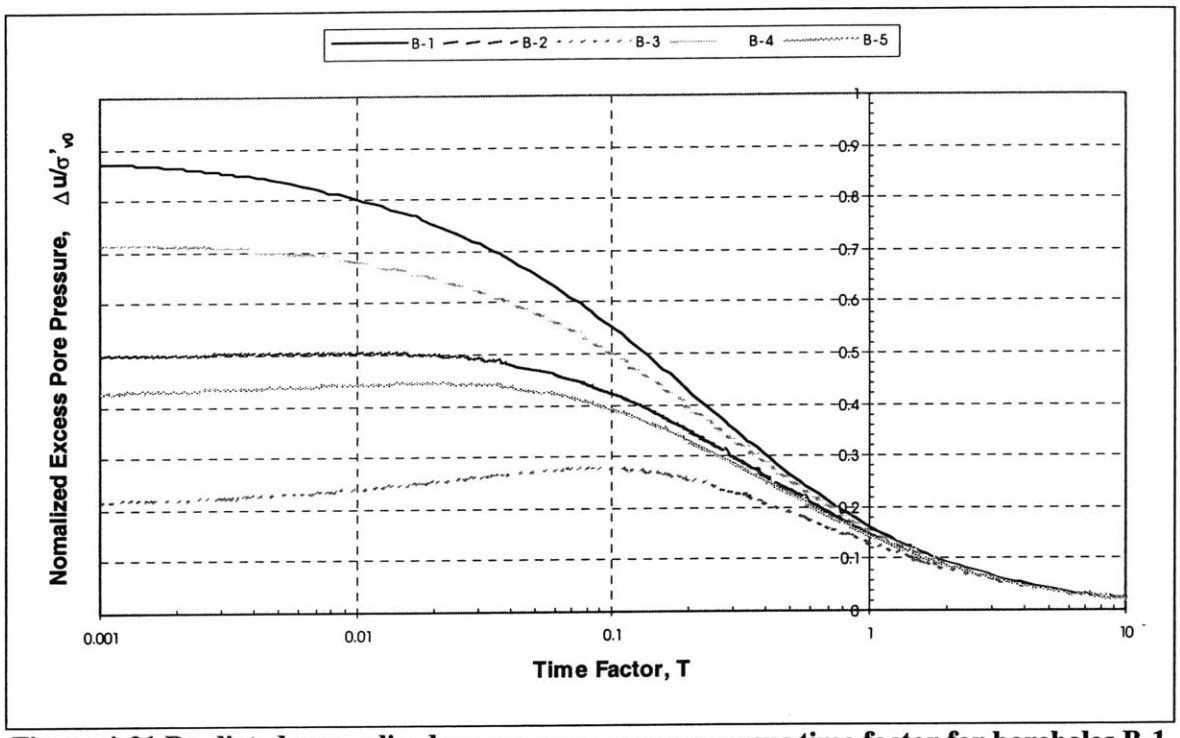

Figure 4-21 Predicted normalized excess pore pressure versus time factor for boreholes B-1 to B-5

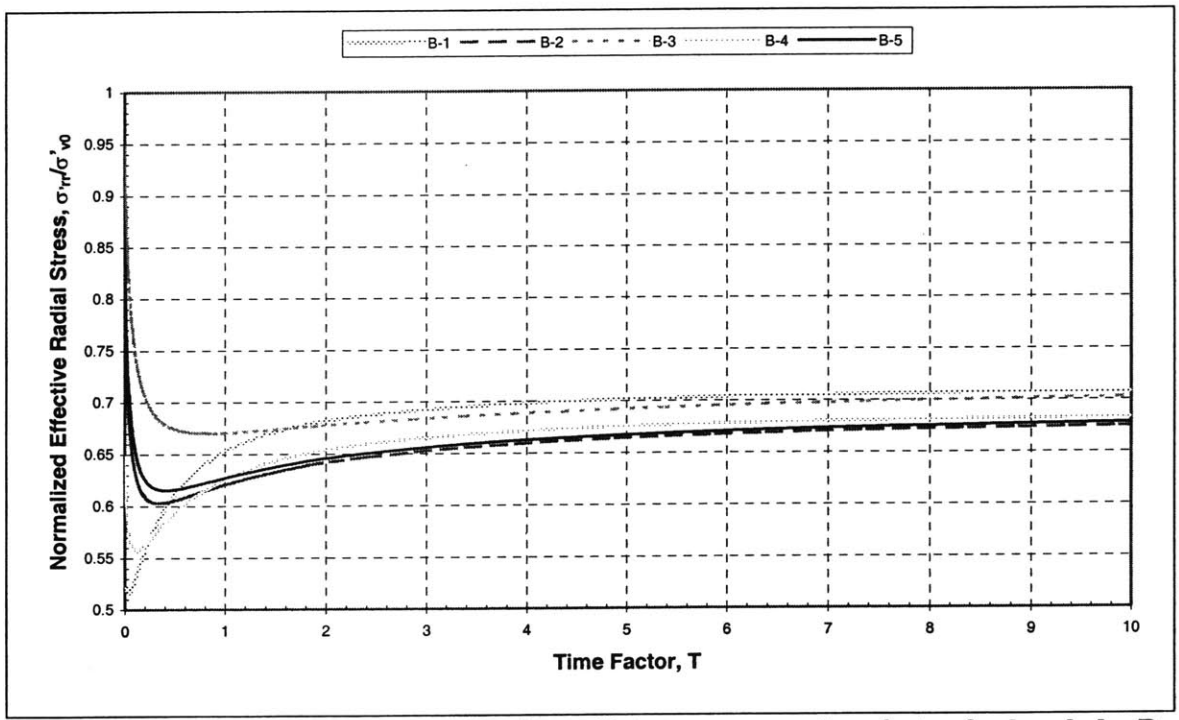

Figure 4-22 Predicted normalized effective radial stress versus time factor for boreholes B-1 to B-5

5 INTERPRETATIONS OF HUNTS DATA

This chapter considers the predictive capabilities and limitations of the proposed analysis by comparing the results with the field data measured by Hunt (2000).

5.1 COMPARISON OF PORE WATER PRESSURE

The measured normalized excess pore pressures are shown in Figure 5-1. Predictions of pore water pressure have lower values than the measured data. Hence, the SPM underpredicts the excess pore pressure. The prediction of pore pressure is mainly governed by the MIT-E3 parameter κ_0. Therefore, the reason of the discrepancies is mainly due to the inaccurate selection of parameter which dictates κ_0 i.e. v_s.

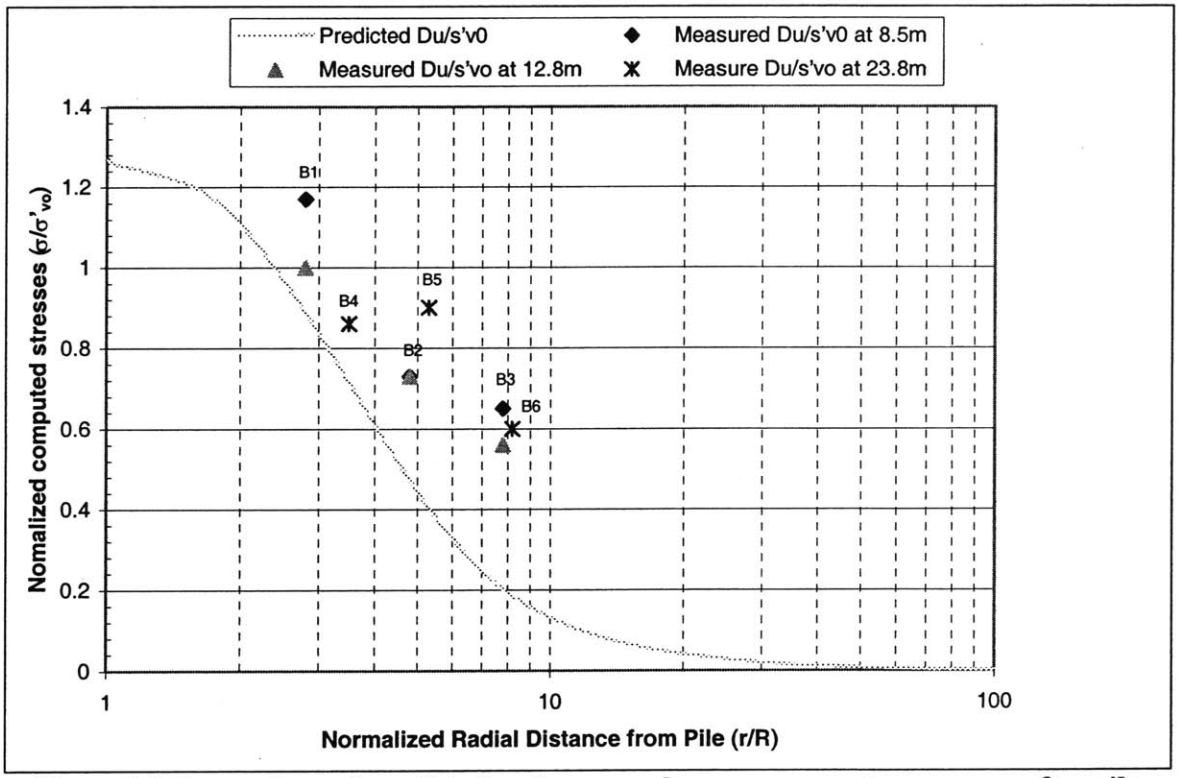

Figure 5-1 Comparison of predicted and measured excess pore water pressure after pile installation

5.2 COMPARISON OF DISSIPATION OF EXCESS PORE PRESSURE

Dissipation curves predicted from SPM with measured data superimposed at depth 8.5m, 12.8m and 23.8m are plotted in Figure5-2, 5-3 and 5-4 respectively. In figure 5-2, from the measured data, the approximate times for 80% dissipation of pore pressures at B-1 is 100 days while from the predicted data the time is approximately 75 days. Figure 5-2 shows excellent agreement between the predicted and the measured pore pressure dissipation at B-1 (r/R=2.8) while the predictions at B-2 (r/R=4.8) tend to overestimate the measured dissipation. The predictions for B-3 at (r/R=7.8) show, due to the radial increases in excess pore pressure during the first days after pile installation, there is flow of pore water from pile. These effects are not shown at all in the measurements. This may reflect other processes, such as drainage to the boreholes closer to the pile or other effects of the SPM idealization. In fact, it is surprising to find minimal apparent difference in measured dissipation behavior for B-2 and B-3. One can only conclude that the results in Figure 5-2 shows inconsistencies between the predicted and measured response at points far from the pile.

In Figure 5-3, the same trend of results can be seen as Figure 5-2 for which the prediction of pore water pressure of B-1 is very good but discrepancies occur for B-3. In Figure 5-4, as both B-4 and B-5 are relatively close to the pile, the predictions are relatively good. The prediction for B-6 is not provided here but it is expected that the prediction will follow the trend of B-3. Therefore, the SPM prediction can provide consistent accurate predictions at locations which are close to the pile ($2< r/R<5$) but the measured far field response is not accurately evaluated by the current SPM analyses.

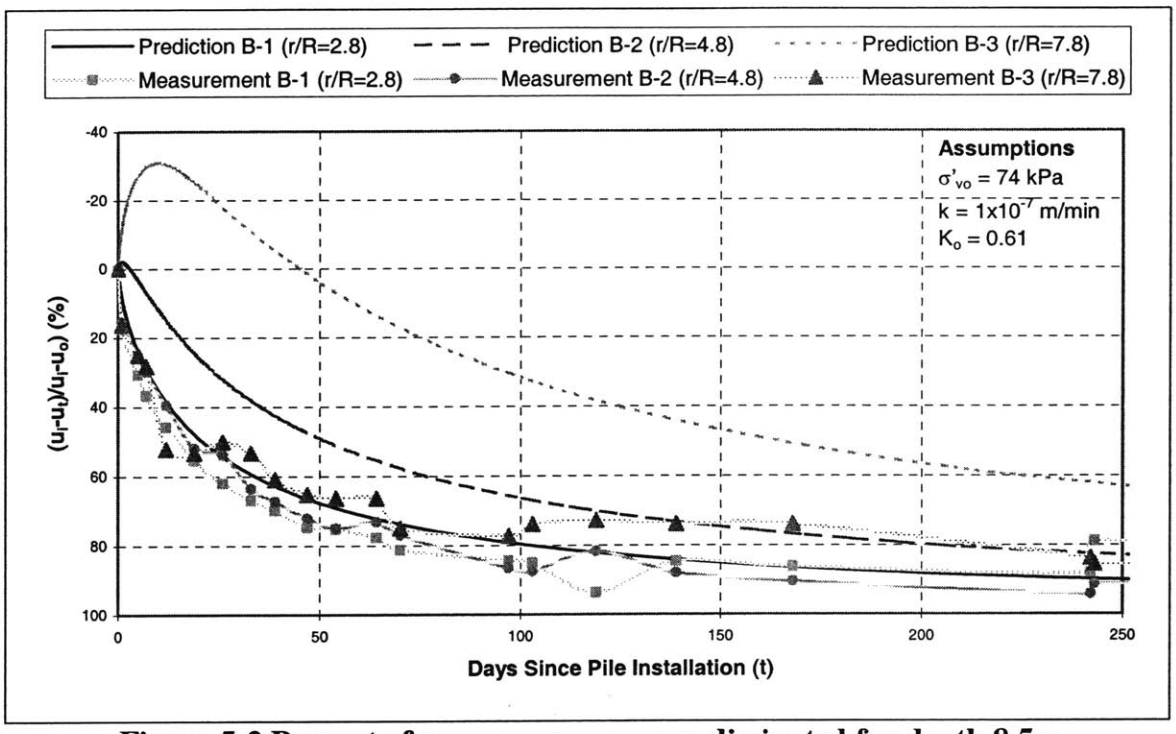

Figure 5-2 Percent of excess pore pressure dissipated for depth 8.5m

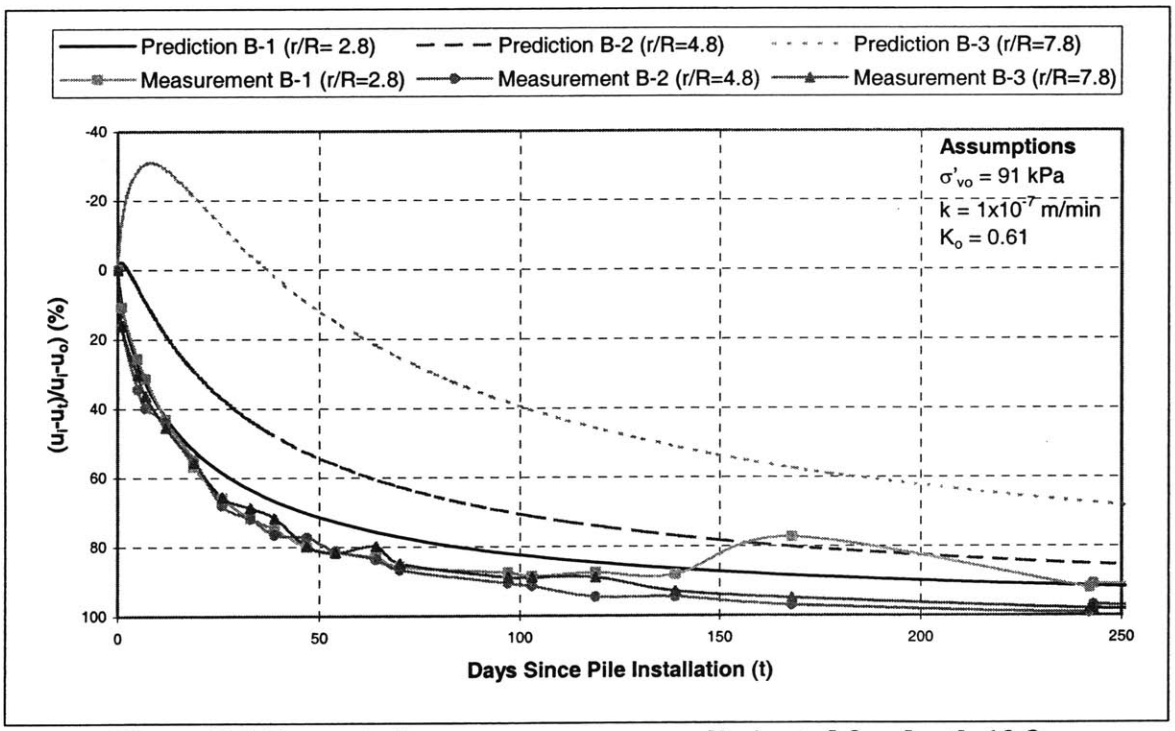

Figure 5-3 Percent of excess pore pressure dissipated for depth 12.8m

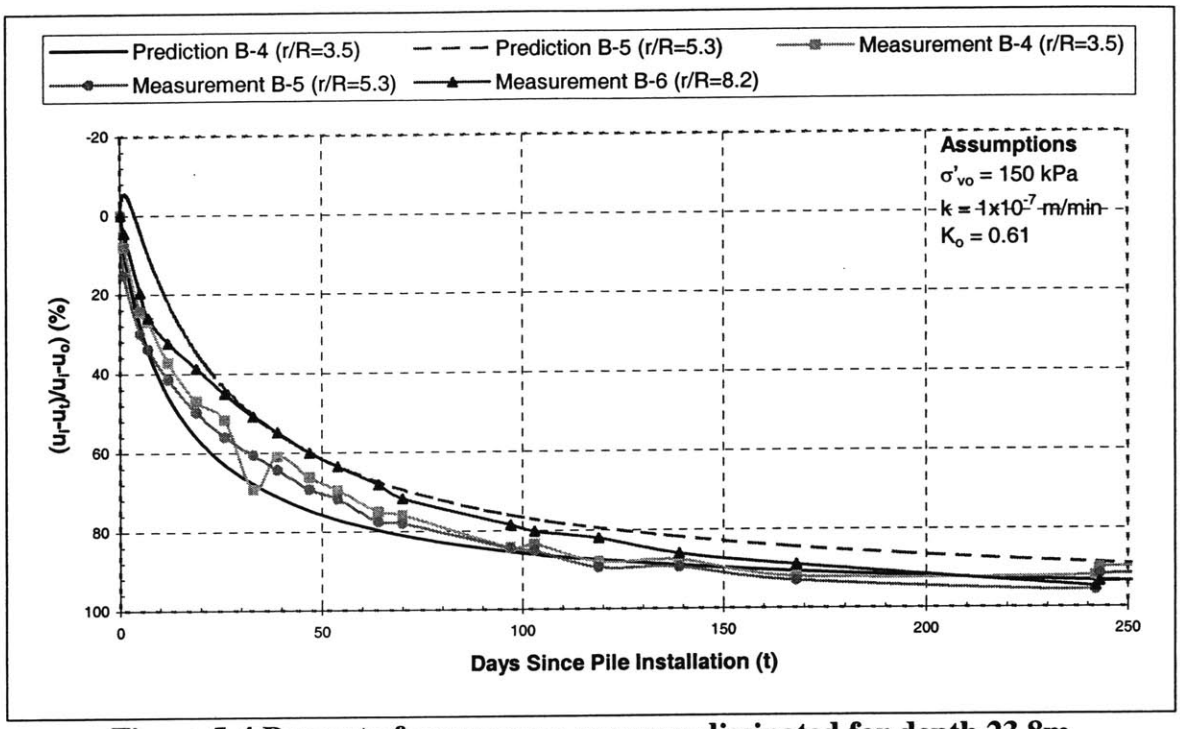

Figure 5-4 Percent of excess pore pressure dissipated for depth 23.8m

5.3 COMPARISON OF RETURN DEFLECTION

Figure 5-5 shows a comparison between predicted and measured consolidation return deflection around the pile shaft. The predicted value is based on depth 12.8m while the measured data represents the average and ±standard deviation for depths 10m to 16m. The graph indicates that the predicted peak return deflection is about 1.4cm at r/R 3.3 from pile which is within the range of the measured data. It has been found that the inclinometer data match the stain path method prediction reasonably. Large difference noticed for the other two measured data at B-5 and B-6 are likely due to the unexpected loading conditions during measurements.

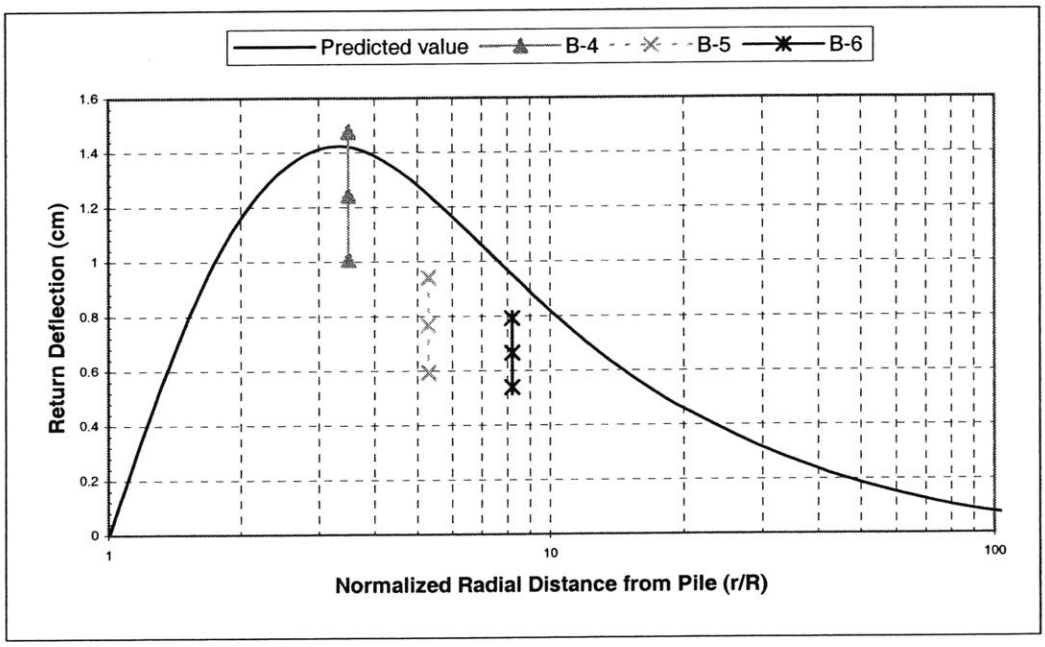

Figure 5-5 Consolidation return deflection around the pile shaft

5.4 COMPARISON OF SHEAR WAVE VELOCITY

Although direct prediction of shear wave velocity is not available from the SPM model, comparison can be made by considering the change in effective stress.

The value of shear wave velocity v_s can be measured from

$$G_{\max} = \rho v_s^2$$

$$v_s = \sqrt{\frac{G_{\max}}{\rho}}$$

where ρ is the mass density $(1.5 \times 10^3 kg/m^3)$

$G_{\max}$ is the maximum shear stiffness

From Figure 3-12, for B-4 it has been found that the shear wave velocity after consolidation (701 days) is about 500 m/s while the shear wave velocity after pile installation (5days) is approximately 300 m/s. Hence,

$$\frac{v_{s701}}{v_{s0}} = \frac{500}{300} = 1.67 \text{ and } \frac{G_{701}}{G_0} = 1.67^2 = 2.78$$

Since $\frac{G_{\max}}{K_{\max}} = \frac{3(1-2\upsilon')}{2(1+\upsilon')} = constant$ and $K_{\max} = (\frac{1+e}{\kappa_0})\sigma'$

where e is the void ratio

κ_0 is the initial stiffness at load reversal point

$$\sigma' = \frac{1}{3}(1+2K_0)\sigma'_v$$

The change of effective stress is approximately the same as G_{max} which means the effective stress after consolidation is 2.7 times of the effective stress after pile installation. However, from SPM predictions (see Figure 4-9 and 4-10) there is a net decreases in effective stress due to the pile installation. This result implies that measured changes in G_{max} are significantly different to theoretical predictions. It is actually very surprising to find an increase in G_{max} after pile installation. This data is unique (array installed pile tests) and can only be assessed in the light of future similar field experiments.

5.5 COMPARISON OF STRAIN PATH METHOD PREDICTIONS WITH CAVITY EXPANSION METHOD

This aim of this section is to interpretate the results obtained from CAMFE which was developed by hunt. Modified Cam-Clay (MCC) soil model and the Cavity Expansion Method (CEM) were incorporated in the CAMFE program to predict the stresses and deformation caused by installation. In this section, our data which was obtained by using the MIT-E3 model and Strain Path Methods (SPM) will be compared with Hunt's data.

Figure 5-6 shows predictions based on CEM and SPM in bilinear isotropic clay initially subjected to an isotropic stress. CEM predictions are represented by a straight line. The graph shows that at the pile wall the CEM prediction is more than twice the values indicated by the measurements while the SPM only slightly overpredicts measurements. Large discrepancies occur between the two predictions within the range $1<r/R<5$. It is due to strain path history and soil inelasticity effects neglected by cavity expansion. In $5<r/R<20$, minor differences exist between CEM and SPM predictions.

Baligh (1985) reports that the measurements of excess pore water in a variety of mostly soft to moderately overconsolidated clays (1<OCR<4) indicate three consistent aspects of significant:

1) Measurable values of Δu extend to a radial distance r/R=20
2) At the pile wall $\Delta u/\sigma_{vo} \cong 2.2$ (± 0.2)
3) Within the region $5<r/R<20$ measurements fall in a narrow band indicating that $\Delta u/\sigma_{vo}$ increased by 3.4 (± 0.6) per log cycle of log r/R

It seems that CEM prediction can only satisfy any two of these consistent aspect of Δu. However, SPM prediction can satisfy all three aspects of Δu around pile shafts and hence improve the deficiencies owned by CEM.

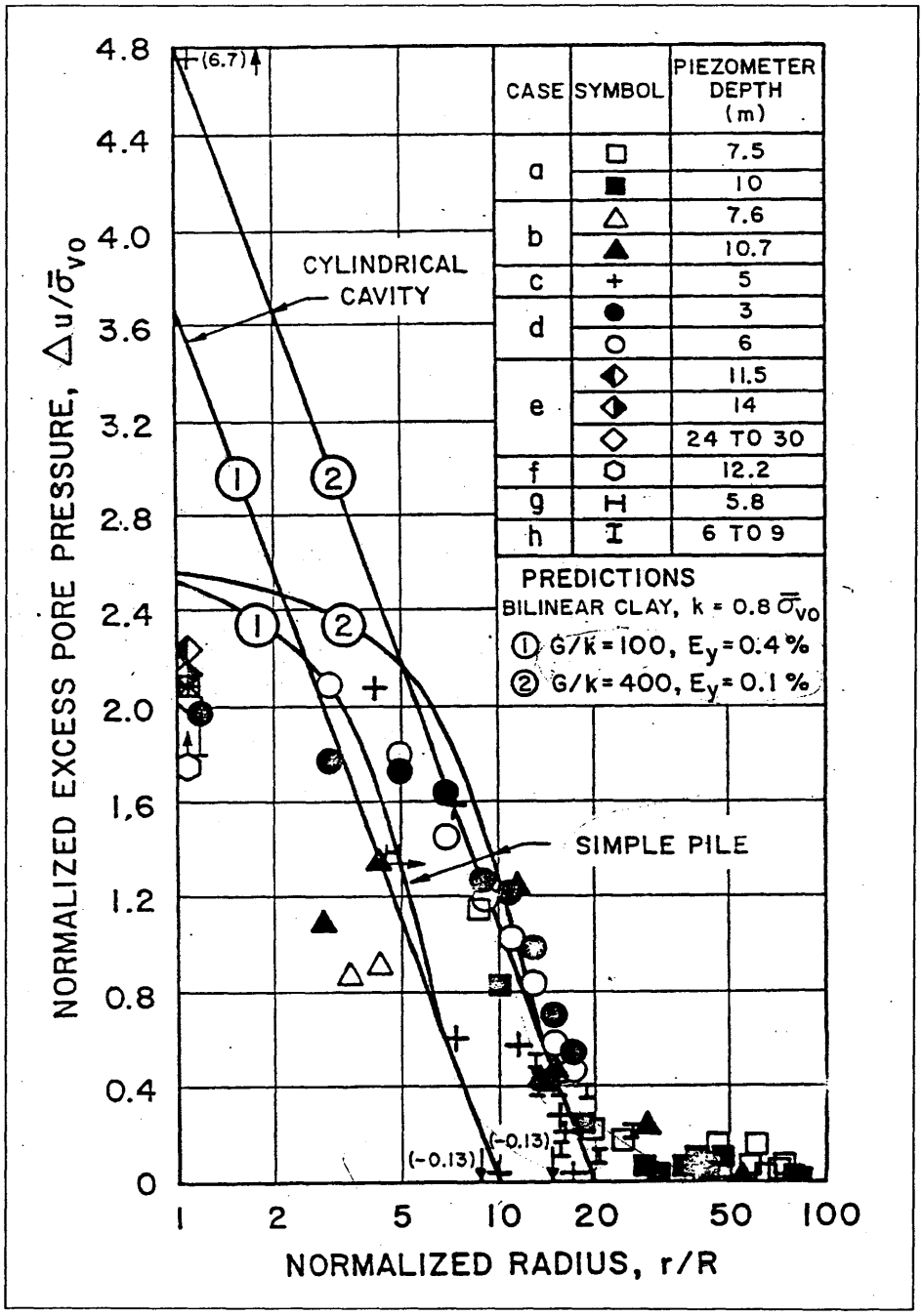

Figure 5-6 Distribution of excess pore pressures around pile shafts

Figure 5-7 shows the SPM predictions of stresses after pile installation. By comparing these results with the results obtained by Hunt which are computed by the CEM. (Figure 5-8), it has been found that the CEM analyses predict extremely high value of excess pore pressure than the SPM predictions. This result matches with the results obtained from Baligh (1985).

Besides, it is expected that radial effective stress should decreases while pore pressure increases. However, in Figure 5-8, it shows that the stresses at near field are even higher than that at far field which is not possible. In conclusion, it is believed that CEM can lead to unrealistic predictions in the neighborhood of shaft ($1<r/R<5$) and SPM appears to provide more reasonable predictions.

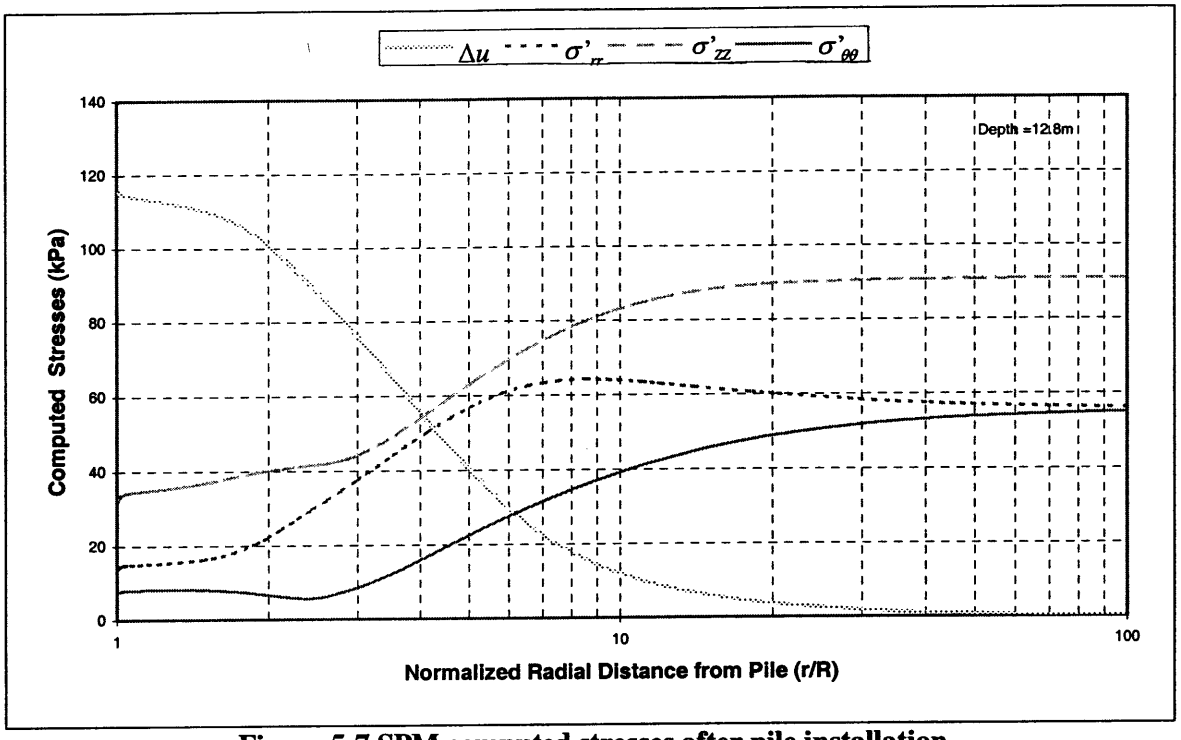

Figure 5-7 SPM computed stresses after pile installation

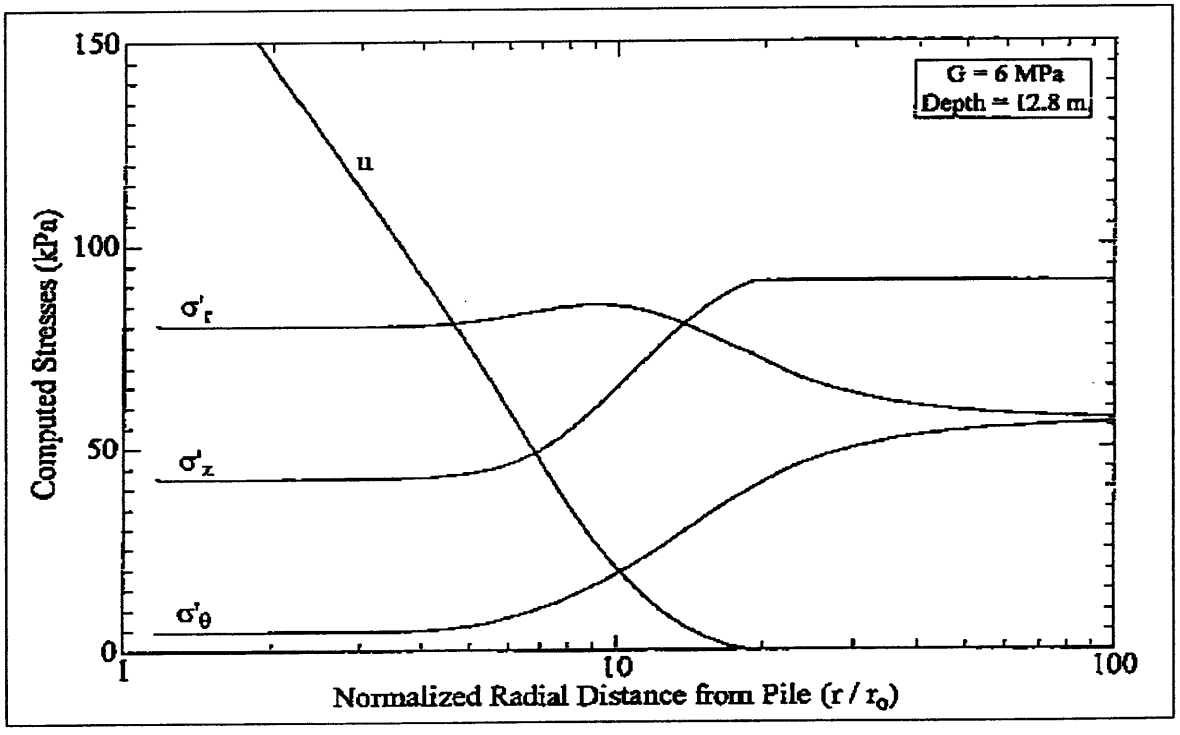

Figure 5-8 CEM computed stresses after pile installation

In order to illustrate the effects of CEM and SPM on stresses during consolidation, figure 5-9 shows the variation of $K\ (=\sigma'_h/\sigma'_{vo})$ at the wall of a closed-ended pile with the time factor, T (Predictions of CEM + MCC and predictions of SPM + MCC) obtained by Azzouz et. al. (1990) for a closed-endedd pile installed in highly plastic empire clay (at OCR=1.5). The results show that the method of simulating pile installation has a significant effect on predictions of the initial horizontal effective stress before consolidation. The SPM predicts a value of $K_i = 0.54$ that is much smaller than $K_i = 1.13$ predicted by CEM, but close to $K_i = 0.38$ measured by the PLS cell (Azzouz and Marrion, 1988). Compared to the SPM, the CEM predicts a much faster rate of increases in soil consolidation and buildup of σ'_h with time. This is mainly due to the large gradient of the installation excess pore pressures predicted by the CEM close to the pile shaft (which has been mentioned before). The CEM predicts higher values of σ'_h than the SPM throughout the soil consolidation process. Using the same soil model (MCC), the CEM predicts a final value, K_c=1.95 that is about 25% larger than that obtained by the SPM and is much higher than the value measured by the PLS cell.

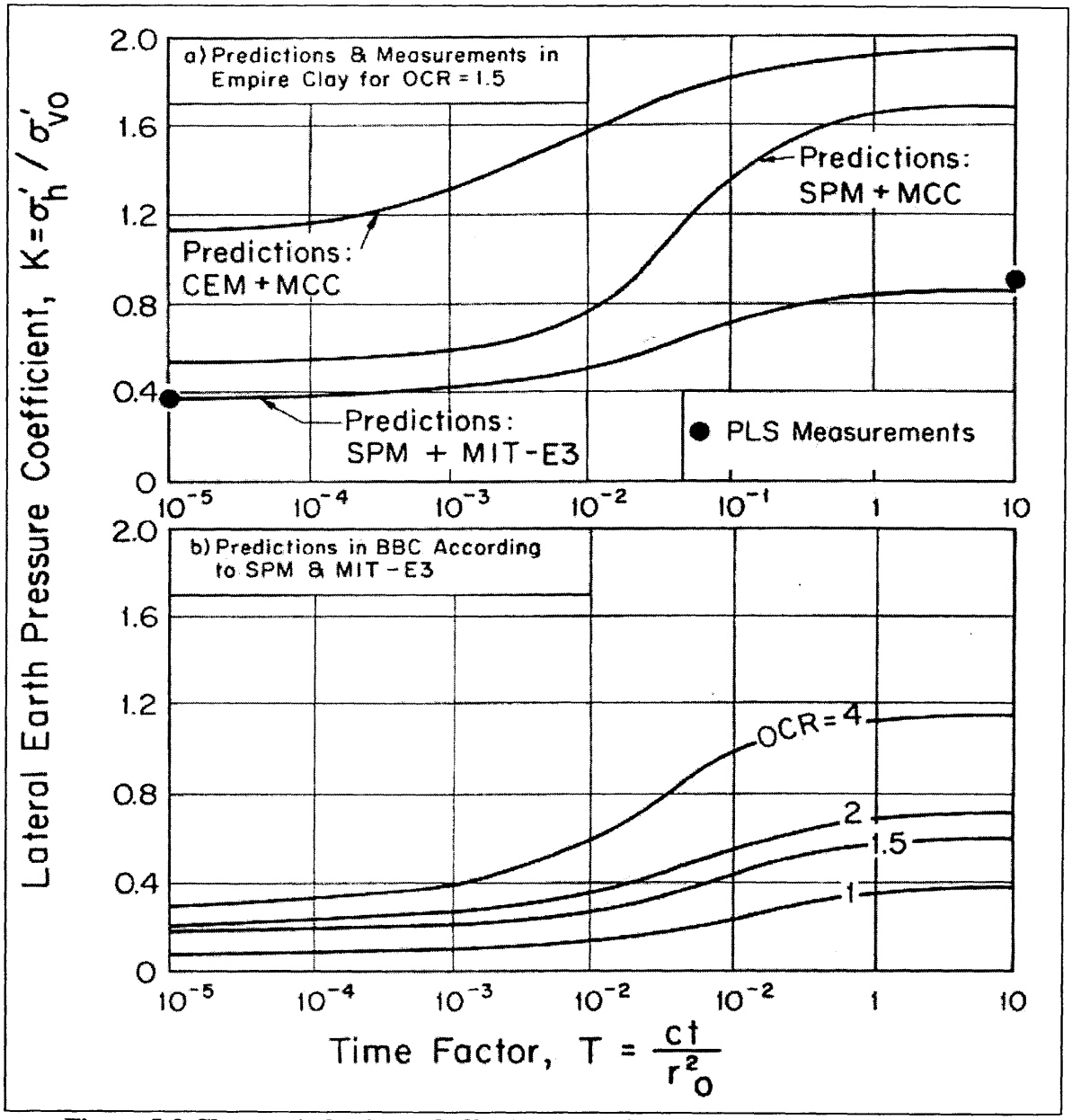

Figure 5-9 Changes in horizontal effective stress during consolidation at pile shaft

Figure 5-10 shows the SPM predictions of stresses after consolidation. By comparing the results obtained from SPM with the results obtained by CEM. (Figure 5-11), it has been found that the CEM analyses predicts higher values of σ'_r than the SPM predictions. This is because the CEM predicts a much faster rate of increases in soil consolidation and buildup of σ'_h. This result matches with the results obtained from Azzouz (1990). Hence, based on the findings of Azzouz, it shows that the SPM analyses can provide a better prediction than the CEM analyses. The results of our comparison match the results obtained by Baligh (1985) and Azzouz (1990).

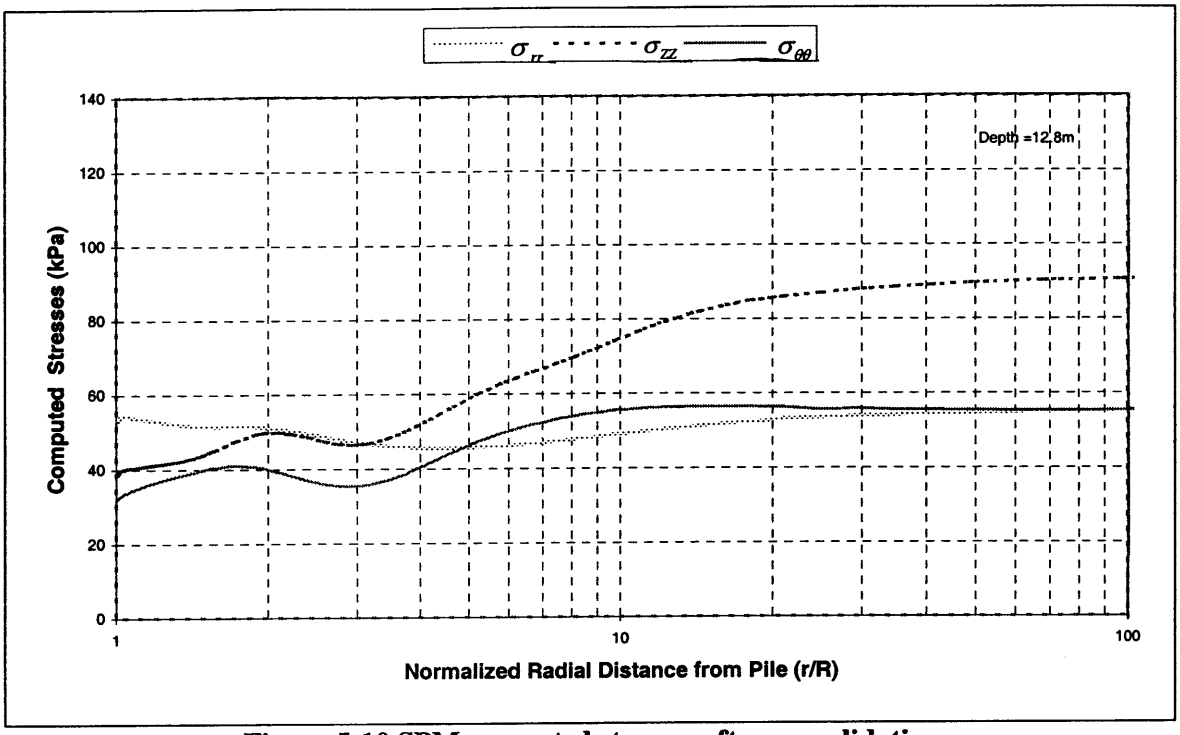

Figure 5-10 SPM computed stresses after consolidation

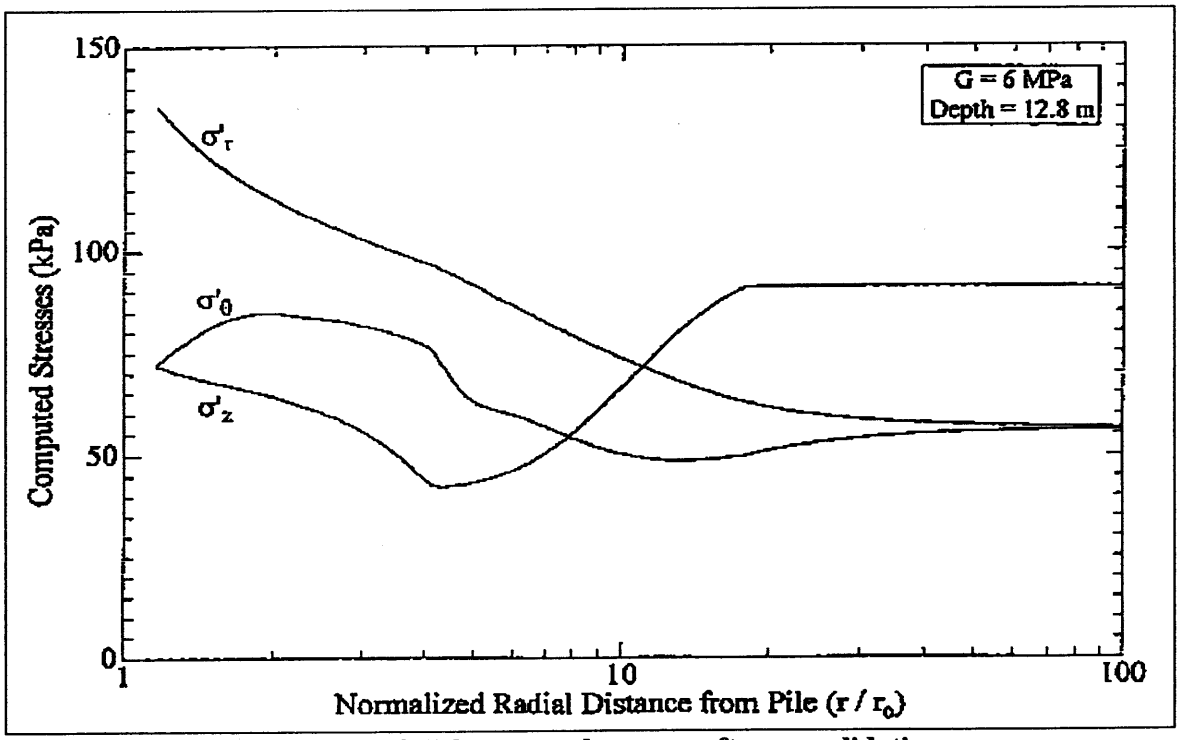

Figure 5-11 CEM computed stresses after consolidation

Figure 5-12 shows the consolidated return deflection predicted by CEM (whose value are shown on the right hand y-axis). The consolidated return deflection predicted by SPM is presented in Figure 4-19. The peak return deflection predicted by SPM is about 1.4cm which occurs at 3.3 radial distance from pile. However, for the CEM the value depends on the shear modulus, G. From the comparisons, it has been fount that here are some limitations of cylindrical cavity expansion since it does not properly reproduce strain paths near the pile wall. Together with the shortcomings of Modified Cam-Clay, which was formulated with a constant value of shear modulus, G and which cannot reproduce the post-peak strain-softening behavior of Young Bay Mud, it led to large discrepancies in the comparisons of the CEM and SPM.

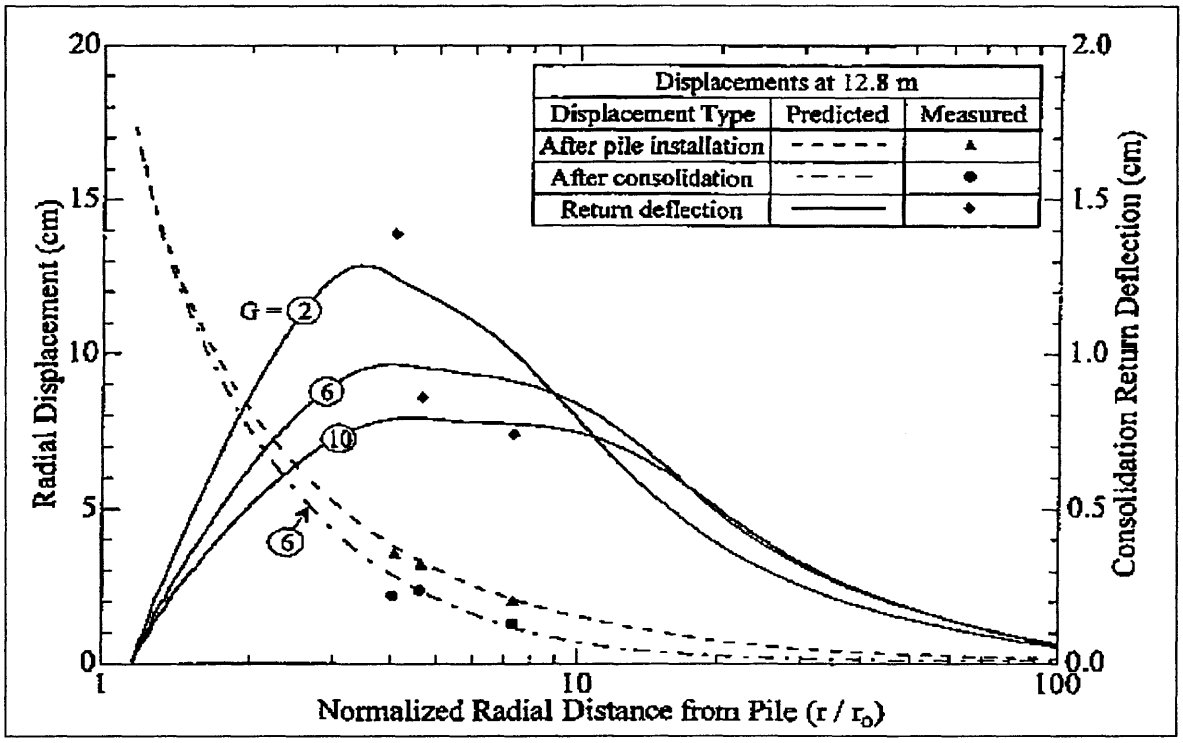

Figure 5-12 Radial displacements from pile installation and subsequent consolidation

6 SUMMARY CONCLUSIONS AND RECOMMENDATIONS

Large changes occur within clay after driving of a large diameter pile. The post driving stress and soil properties are not equivalent to their pre-pile values and they change over time after pile installation. Hence, it is important to investigate the response of soil in order to help modifying the foundation design due to the change of soil properties. This thesis re-interpreted the well-documented test data on the effects of driven pile installation in San Francisco Bay Mud. The effect of pile driving on static and dynamic properties of clay has been investigated by Hunt (2000). His research mainly based on a full-scale closed-ended pile (61cm diameter 35m long) driven into a deep deposit of San Francisco Young Bay Mud.

The results obtained from the field measurements were presented. Piezometers showed significant increases in pore pressure due to pile driving. Pore pressure within 1 pile diameter slightly even exceeded the initial vertical effective stress of the soil. These pore pressures dissipate with time and 80% consolidation for soils farther than one diameter away from the pile wall is achieved between 50 and 80 days. Inclinometers showed initial outward radial deformations. Subsequent measurements of lateral deflection show a return towards the pile as the excess pore pressure dissipates, with decreasing magnitude as a function of distance from the pile wall. Shear-wave velocity profiles at four radial distances were obtained as a function of time following pile driving using the suspension logging method. Following pile installation, the shear-wave velocity of the soil decreases due to a reduction in the effective stress and disturbance from pile-induced shear deformations, which are most severe immediately adjacent to the pile wall. During pore pressure dissipation, the shear-wave velocity increases primarily due to increases in effective stress. These measurements provide valuable information addressing changes in material properties of the foundation soil.

The laboratory testing program was performed on pre-pile and post-pile specimens. One-dimensional constant rate of consolidation tests were performed to determine the compressibility characteristics for this soil. Shear strength testing included anisotropically consolidated undrained triaxial tests were performed on specimens at two confinement levels to study the effect of fabric and evolving anisotropy. Direct simple shear testing was performed on specimens to observe changes in structure/fabric orientation of clay after pile installation.

Different analysis tools have been developed to model the strain induced during installation process. The most widely used methods are the Cavity Expansion Method (CEM) and the Strain Path Method (SPM). Previous experience reported by Whittle (1992, 1999) has shown that reasonable predictions of pile stresses and pore pressure can be achieved by using the SPM analyses in conjunction with the MIT-E3 soil model (Whittle et. al.) and non-linear radial consolidation. These methods have been validated using data from instrumented model piles. In contrast analyses with CEM methods overpredicts the radial stresses at the pile shaft (and also shaft capacity) (e.g. Azzong st al, 1990)

This thesis presents the application of SPM analyses in conjunction with the MIT-E3 model to re-interpret the tests reported by Hunt (2000). Site specific model input parameters were selected for MIT-E3 model using laboratory data presented by Hunt (2000) including one-dimensional CRS consolidation tests and SCK_0UC tests on normally consolidated Bay Mud (using SHANSEP consolidation). The model is clearly a better match to these laboratory data than the previous simulation reported by Hunt (2000) using the Modified Cam Clay (MCC) model.

For comparison of measured dissipation of excess pore pressure, the SPM prediction shows a very good prediction in near field but discrepancies occur further away from the pile. For the comparison of return deflection, the prediction at the peak value matches the measured data very well. However, there are discrepancies at the far field. Indirect comparison has been made with the shear wave measurements. However, no agreement

can be made with the measurements. Also neither CEM or SPM analyses seen capable of explaining the large net increase in shear wave velocity in the surrounding soil reported by Hunt (2000).

Based on the findings obtained from Baligh, it is believed that CEM can lead to unrealistic predictions in the neighborhood of shaft ($1<r/R<5$) and SPM appears to provide more reasonable predictions. The differences between the two approaches is basically due to strain path effects neglected by CEM that came into play because of inelastic behavior of the soil.

7 REFERENCES

1. Azzouz A.S., Baligh M.M. and Whittle A.J. (1990) *Shaft resistance of piles in clay* Journal of Geotechnical Engineering, Vol. 116, No.2, PP. 205-221.

2. Baligh M.M. (1985) *Fundamentals of deep penetration II: Pore pressures* Research Report R85-10, Order No.77, Department of Civil Engineering, Massachusetts Institute of Technology

3. Baligh M.M. (1985) *Strain Path Method.* ASCE Journal of Geotechnical Engineering, Vol. 111, No.9, PP. 1108-1136.

4. Baligh M.M. (1986) *Undrained deep penetration I: Shear stresses* Geotechnique 37, No. 4, 525-527

5. Bonaparte R. and Mitchell J.K. (1979) *The properties of San Francisco Bay Mud at Hamilton Air Force Base, California.* University of California, Berkeley, Department of Civil Engineering

6. Hunt C.E. (2000) *Effect of Pile installation on static and Dynamic Soil Properties* University of California, Berkeley, Department of Civil Engineering, Ph.D. Thesis

7. Hunt C.E., Pestana J.M., Bray J.D. and Riemer M.F. (2002) *Effect of Pile Driving on Static and Dynamic Properties of Soft Clay.* Journal of Geotechnical and Geoenvironmental Engineering, Vol. 128, No.1

8. Hwang J.H., Liang N. and Chen C.H. (2001) *Ground Response during Pile Driving.* Journal of Geotechnical and Geoenvironmental Engineering, Vol. 127, No.11

9. Payiatakis, S. and Davis J. (1998) *Structure Heave and Settlement Due to Pile driving – A Case History.* Effects of Construction on Structures. ASCE Geotechnical Engineering Special Publication, No.84, PP. 16-29

10. Pestana J.M., Hunt C.E. and Bray J.D. (2002) *Soil Deformation and Excess Pore Pressure Field around a Closed–Ended Pile.* Journal of Geotechnical and Geoenvironmental Engineering, Vol. 128, No.1

11. Rehkopf J.C. (2001) *Prediction and Measurement of ground Movements due to Pile Diving in Clay: A Case Study in East Boston.* Massachusetts Institute of Technology, M.Eng. Thesis.

12. Sagaseta C., Whittle A.J. (2001) *Prediction of Ground Movements due to Pile Driving in Clay.* Journal of Geotechnical and Geoenvironmental Engineering, Vol. 127, No.1, PP.55-66.

13. Sagaseta C., Whittle A.J. and Santagata M, (1997) *Deformation analysis of Shallow Penetration in Clay.* International Journal for Numerical and Analytical Methods in Geomechnaics, Vol. 21, PP. 687-719

14. Whittle A.J. (1996) *Assessment of an Effective Stress Analysis for Predicting the Performance of Driven Piles in Clays*

15. Whittle A.J. and (1994) *Formulation of MIT-E3 Constitutive Model for Overconsolidated clays.* ASCE Journal of Geotechnical Engineering, Vol. 120, No.1, PP. 1108-1136.

16. Whittle A.J. and Twarath Sutabutr (1996) *Prediction of Pile Set-up in Clay.*

17. Whittle A.J., DeGroot D.J., Ladd C.C. and Seah T-H (1994) *Model Prediction of the Anisotropic Behavior of Boston Blue Clay.* ASCE Journal of Geotechnical Engineering, Vol. 120, No.1, PP. 199-225.